Biomimetic Models of [NiFe] Hydrogenase for Electrocatalytic Hydrogen Evolution

PROEFSCHRIFT

ter verkrijging van

de graad van Doctor aan de Universiteit Leiden,

op gezag van Rector Magnificus Prof. mr. C. J. J. M. Stolker

volgens besluit van het College voor Promoties,

te verdedigen op dinsdag 10 oktober 2017

klokke 11:15 uur

door

Gamze Gezer

Geboren te Corlu, Turkey

in 1989

Samenstelling Promocommissie

Promotor	Prof. Dr. E. Bouwman
Co-promotor	Dr. D. G. H. Hetterscheid
Overige leden	Prof. Dr. R. J. M. Klein Gebbink (Utrecht University)
	Prof. Dr. M. T. M. Koper (Leiden University)
	Prof. Dr. H. S. Overkleeft (Leiden University)
	Dr. J. I. van der Vlught (University of Amsterdam)

ISBN: 978-94-6295-716-9

'*Victory is for those who can say 'Victory is mine'. Success is for those who can begin saying 'I will succeed' and say 'I have succeeded' in the end.'*

Mustafa Kemal Ataturk

dedicated to Muharrem, Eser

and Fatih Gezer

Table of Contents

List of Abbreviations

CPC	controlled-potential coulometry
CV	cyclic voltammetry
Cys	cysteine
d	doublet
DCM	dichloromethane
DMF	N,N-dimethylformamide
DMSO	dimethyl sulfoxide
ESI	electrospray ionization
FOWA	foot-of-the-wave analysis
FTIR	fourier transform infrared
GC	gas chromatography
Hacac	acetylacetone, 2,4-pentanedione
HCp	cyclopentadiene
HER	hydrogen evolution reaction
HOAc	acetic acid
HRMS	high resolution mass spectrometry
Htfa	trifluoroacetic acid
m	multiplet (NMR); medium (IR)
MeCN	acetonitrile
NMR	nuclear magnetic resonance
Phen	phenanthroline
PPh_3	triphenylphosphane
s	singlet (NMR); strong (IR)
Sec	selenocysteine
t	triplet
UV	ultraviolet
w	weak

Chapter 1

Introduction

Hydrogenases are enzymes which can catalyze the reversible oxidation of dihydrogen. Since H_2 gas might be used as a sustainable energy source, the structure and mechanism of hydrogenases have received the attention of many chemists. In this introductory chapter an overview is given of the different types of hydrogenases and their catalytic activities. Furthermore, structural and functional models of the active sites of the hydrogenases are described. The aim of the research described in this thesis concerns the synthesis and characterization of new complexes as mimics of [NiFe] hydrogenases. At the end of this chapter a short overview is given of the contents of thesis.

1.1 The Energy Challenge

The global daily energy consumption is increasing with the growing population, and providing an abundant, environmentally friendly and renewable energy source is one of the major challenges of contemporary research.[1,2] Molecular hydrogen (H_2) is a perfect candidate energy carrier as an alternative to fossil fuels. The "Hydrogen Economy" has been proposed to be the ultimate solution for future energy demands as dihydrogen is a 'clean' fuel producing only water upon combustion, and because it is chemically simple to store energy in the dihydrogen molecule.[3] Although platinum can be used as a very efficient and robust catalyst for dihydrogen production, it is an expensive metal and not a sustainable material due to its limited reserves on Earth.[4] In order to obtain cheap and efficient catalysts for dihydrogen production, earth abundant metals should be used. For the activation and production of dihydrogen gas, nature uses hydrogenase enzymes containing nickel and/or iron ions in their active sites; these enzymes regulate the electron and proton concentrations of the cell by dihydrogen uptake or evolution. In the past few decades, chemists have been trying to mimic the active sites of the hydrogenase enzymes in order to develop cheap and efficient electrocatalysts for dihydrogen evolution.[5]

1.2 Hydrogenases

1.2.1 General

Hydrogenases enzymes play an important role in the metabolism of bacteria, catalyzing the reversible oxidation of dihydrogen according to the reaction shown in eq. 1.[6]

$$2H^+ + 2e^- \rightleftarrows H_2 \qquad \text{Eq [1]}$$

Understanding of the hydrogenase enzymes is relevant for future energy applications since dihydrogen is a clean source of energy. In order to produce dihydrogen gas for the application in fuel cells, new catalysts may be developed by using biomimetic, functional models of hydrogenases.[7] Three types of hydrogenases are known, which are classified based on the metal center in the active site which are [FeFe], [Fe] and [NiFe] hydrogenases, as described in the following sections.

1.2.2 [FeFe] Hydrogenase

From the three classes of hydrogenases the [FeFe] hydrogenase and their model complexes have been studied most intensively.[3] These enzymes play a central role in microbial energy metabolism catalyzing the hydrogen evolution reaction (HER). The [FeFe] hydrogenase show the highest catalytic activity for proton reduction, but are also extremely sensitive to irreversible inactivation by dioxygen. The active site of the [FeFe] hydrogenase is buried deeply within the protein. The active site of [FeFe] hydrogenase contains a dinuclear iron center comprising the unusual CO, CN^- and an azadithiolate ligand, and is linked via a cysteine thiolate to an Fe_4S_4 cluster (Figure 1.1). Dihydrogen can enter and leave the active site through hydrophobic channels.[8,9] The active site of the [FeFe] hydrogenase contains a bridging azadithiolate ligand between the two iron centers. The central secondary amine group in this dithiolate ligand is believed to play a crucial role as a proton relay and might be part of the explanation of the extremely high activity of this hydrogenase enzyme.[3]

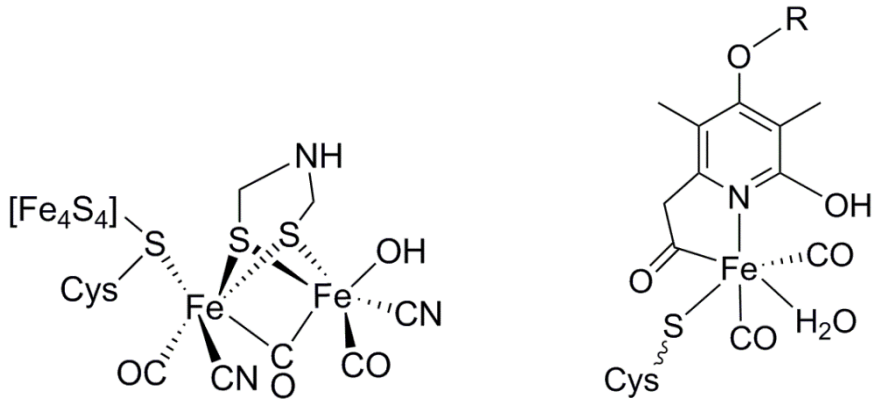

Figure 1.1: Schematic drawing of the active sites in [FeFe] hydrogenase (left) and [Fe] hydrogenase (right).

1.2.3 [Fe] Hydrogenase

Some methanogenic archaea bacteria contain a hydrogenase enzyme that does not contain a nickel center nor iron-sulfur clusters. These [Fe] hydrogenase contains a mononuclear iron catalytic center (Figure 1.1) and catalyzes the transfer of hydride groups. The absence of a nickel center in this hydrogenase is induced by the nickel-deficient environment in which the single-celled microorganisms grow.[8,9] In the hydrogenases containing a bimetallic active site iron-sulfur clusters function as channels to shuttle electrons from the active site to the electron accept or/donor protein partner. The [Fe] hydrogenase does not release electrons but rather

uses the coenzyme tetrahydromethanopterin as a hydride acceptor.[3,8] In contrast to the [FeFe] and [NiFe] hydrogenases the [Fe] hydrogenase does not catalyze the oxidation of H_2 to protons.[8]

1.2.4 [NiFe] Hydrogenase

The third class of hydrogenases comprises the [NiFe] hydrogenase containing a heterodimetallic Ni-Fe active site. Although this enzyme is mostly involved in the uptake of H_2, it is also able to catalyze the production of H_2.[9] The active site of [NiFe] hydrogenase contains a nickel center with four bonds to cysteine thiolates which is connected via two cysteine thiolate bridges to an iron center with CO and CN^- ligands (Figure 1.2).[10] The [NiFe] hydrogenases generally show lower activities in proton reduction than the [FeFe] hydrogenases, but they are much less sensitive for inactivation by dioxygen. Furthermore, generally they are able to recover from oxidative inactivation.[8]

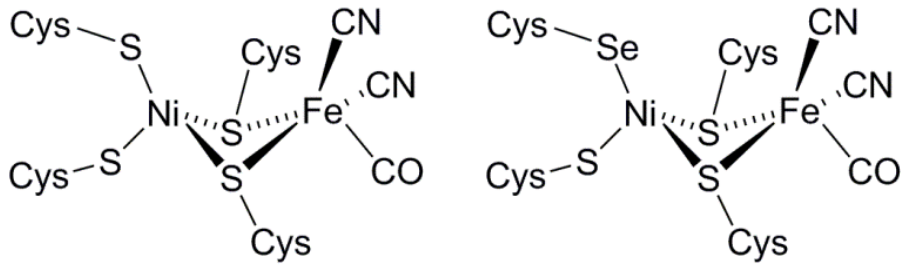

Figure 1.2: Schematic drawing of the active sites of [NiFe] hydrogenase (left) and [NiFeSe] hydrogenase (right).

The [NiFe] hydrogenase is built up from two subunits; a large subunit of 62.5 kDa containing the dinuclear active site and a small subunit of 28.8 kDa containing three iron-sulfur clusters distributed from the active site to the surface of the protein. These iron-sulfur clusters function as the electron shuttle pathway from the active site to a redox protein.[8] No consensus is apparent in literature concerning the exact catalytic mechanism of the [NiFe] hydrogenase.[3] One of the proposed mechanisms for the HER catalyzed by [NiFe] hydrogenase is depicted in Figure 1.3. The catalytic cycle starts from an initial epr-silent state called the Ni-SI state. Binding of a proton to the metal centers with a concurrent uptake of an electron results in a bridging hydride ligand between the iron and the nickel center. This Ni-C state then accepts an electron to reduce the Ni(III) center to Ni(II). A second proton can be brought in close

proximity to the bridging hydride via a cysteine ligand acting as a so-called proton relay. The proton and the hydride combine to evolve dihydrogen, with the regeneration of the Ni-SI state.[3,8]

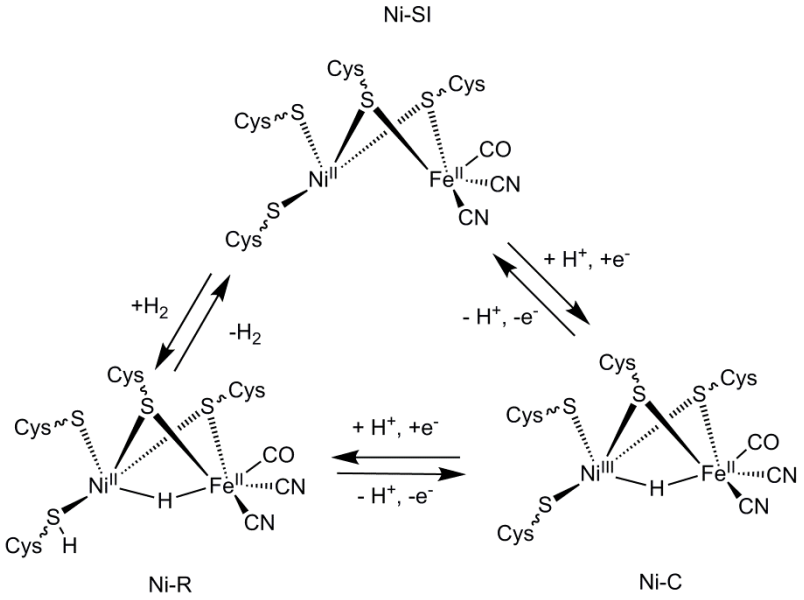

Figure 1.3: Postulated catalytic mechanism of the reversible HER catalysis by [NiFe] hydrogenases.[8]

1.2.5 [NiFeSe] Hydrogenase

The [NiFeSe] hydrogenase forms a subclass of the [NiFe] hydrogenase, in which one of the cysteines (Cys) in the active site of the enzyme is replaced by selenocysteine (Sec).[11] Selenocysteine is found in all three domains of life, however not many organisms use this aminoacid.[12] Generally, the Sec-containing redox proteins show higher catalytic activities than their Cys-containing homologues. The relevant properties of selenium that could explain this difference in activity are the higher nucleophilicity of selenium, the lower redox potentials of the Sec-homologues and the higher acidity of Sec; the pKa of Sec is 5.3 whereas that of Cys is 8.3. The increased acidity of Sec allows selenol groups to be active at lower pH ranges. Selenium is also a softer donor atom than sulfur, the polarizable volume of selenium is 3.8 $Å^3$ vs 2.9 $Å^3$ of sulfur.[13] Thus, due to the different electronic properties of selenium it is possible that the Sec ligand makes a better proton relay, and hence increases the activity of the enzyme as a whole.[3] A schematic representation of the active site of [NiFeSe] hydrogenase in the Ni-C state of the enzyme is shown in Figure 1.2.

1.3 Synthetic Models of the Active Site in [NiFe] Hydrogenase

1.3.1 Structural Models of [NiFe] Hydrogenase

After the determination of the first crystal structure of a hydrogenase enzyme, chemists used the insight gained from the active site as inspirations for the design of new molecular catalyst for proton reduction. By using either the biomimetic approach or the bio-inspired approach, several organometallic complexes have been designed and synthesized.[5] Whereas many structural and functional models for the active site in [FeFe] hydrogenase have been reported, synthetic models of the active site of the [NiFe] hydrogenase are less prevalent.[15]

The first structural model for the heterodinuclear active site in [NiFe] hydrogenase was reported by Darensbourg and coworkers,[16] and comprised a Ni(II) complex of a tetradentate N_2S_2 ligand, of which one of the thiolate sulfurs formed a bridge to an $Fe(CO)_4$ group. In this compound the Ni-Fe distance is 3.76 Å, which is significantly longer than that found in the biological system (2.6-2.9 Å).[16] Pohl and coworkers reported the first example of an Ni-Fe complex with two thiolate bridges between the metal centers, resulting in an Ni-Fe distance of 2.8 Å, which is in the range found in the biological system (Figure 1.4).[17]

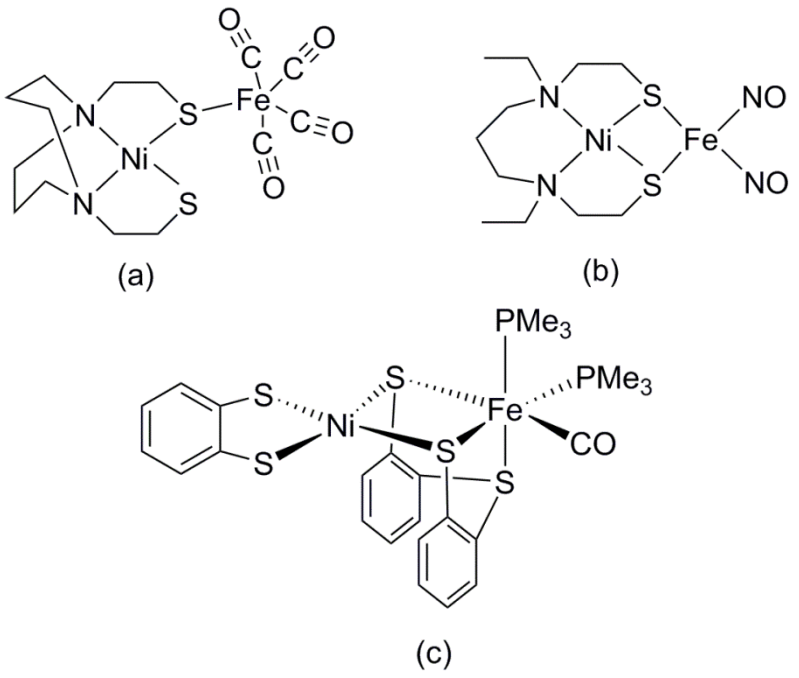

Figure 1.4: Structural models for the active site in [NiFe] hydrogenase reported by Darensbourg et al. (a),[16] Pohl et al. (b),[17] and Sellmann et al (c).[18]

In 2002 Sellmann and coworkers reported the first structural mimic comprising an NiS_4 coordination sphere with a low-spin Ni(II) center bridged by two thiolate donor atoms of a tridentate ligand to a low-spin Fe(II)-carbonyl moiety (Figure 1.4c).[18]

Although several structural models were reported with different ligand environments, none of them have been reported as catalysts either for H_2 oxidation or for proton reduction to H_2 until 2006.[10,19-21]

1.3.2 Functional Models of [NiFe] Hydrogenase

In 2004 Sellmann and coworkers reported a trinuclear Ni_2Fe complex as the first functional model of [NiFe] hydrogenase, although the catalytic activity is not clearly described (Figure 1.5).[22] The activity of this compound for proton reduction was observed using a solution of HBF_4 in dichloromethane, which resulted in oxidation of the complex with the formation of H_2 as identified by ^1H NMR.[22] The group of Schröder reported a functional model of [NiFe] hydrogenase in 2006. The trinuclear complex contained one nickel ion in a tetradentate ligand bridging to two iron centers that are each additionally bound to three carbonyl ligands in a six-coordinate, distorted octahedral geometry (Fig.1.5).[23] This compound was reported to catalyze the reduction of protons from a solution of trifluoroacetic acid (Htfa) in dichloromethane to form H_2 with an activity of 6 turnovers per hour at a potential of −1.64 V *vs* $Fc^{+/0}$. However, the compound appeared to be stable only for 1 h.[23]

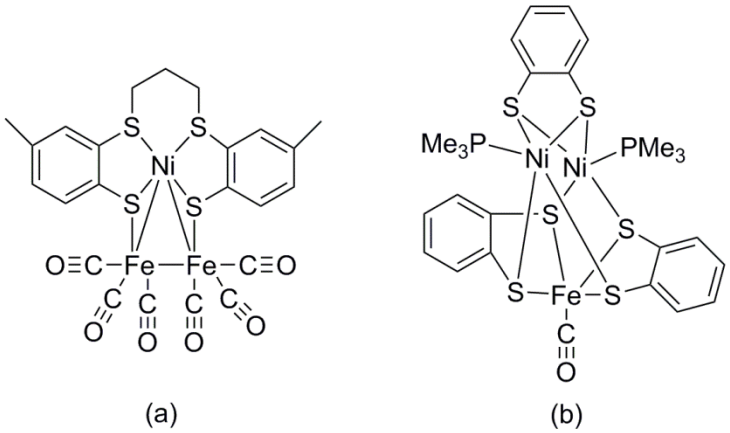

Figure 1.5: First functional models for [NiFe] hydrogenases reported by the group of Schröder (a)[23] and Sellmann et al. (b).[22]

In 2009 the group of Rauchfuss reported the compound [(dppe)Ni(μ-H)(μ-pdt)$Fe(CO)_3$] (dppe = 1,2-bis(diphenylphosphanyl)ethane; pdt = 1,3-propanedithiolate) and derivatives of this

complex by substituting CO ligands for phosphorous-based ligands (Fig. 1.6a).[24] This compound was found to be an active catalyst for proton reduction upon addition of Htfa to a dichloromethane solution as indicated by electrochemical measurements, but no quantitative results were reported.[24] In 2010 Artero and Fontecave reported the use of the compound [Ni(xbSmS)], described by the group of Bouwman in 2002, to create a NiFe species in which the iron center is substituted with a Cp^- ligand and a carbonyl group. This complex was reported to catalyze the HER in a solution of Htfa in DMF: in a 4 h experiment 20 turnovers were achieved (Fig. 1.6b).[25]

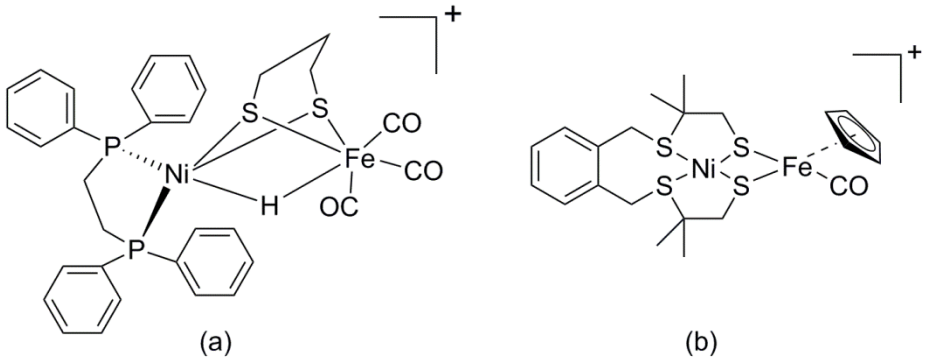

Figure 1.6: Examples of reported complexes as functional mimics of the [NiFe] hydrogenase active site.[24,25]

After these early examples of functional models, many new investigations have been reported that were aimed at understanding of the catalytic mechanism [NiFe] hydrogenase and the development cheap, high efficient catalysts.[26,27] Although a variety of model compounds have been reported until now, only few of them efficiently catalyze the hydrogen evolution reaction as functional mimics of hydrogenases.[28-33] All complexes have structural similarities with [NiFe] hydrogenase comprising either an NiS_4 or an NiS_2N_2 environment further bound to various iron centers. Two of these complexes are shown in Figure 1.7, being NiFe complexes with different nickel environments (NiS_4 and NiS_2N_2) bound to the $FeCp^*CO$ moiety (HCp^* = pentamethylcyclopentadiene). The complex comprising an NiS_4 environment appeared to have better catalytic activity in proton reduction than the complex with an NiS_2N_2 environment in the presence of HBF_4 in acetonitrile solution according to the results of electrochemical studies.[33] These differences in catalytic activity of highly similar compounds show the importance of further studies to model systems with different ligand environments. Until now the geometry of the metal centers, ligand flexibility and environment have been found to play an important role in the efficiency of electrocatalytic proton reduction.

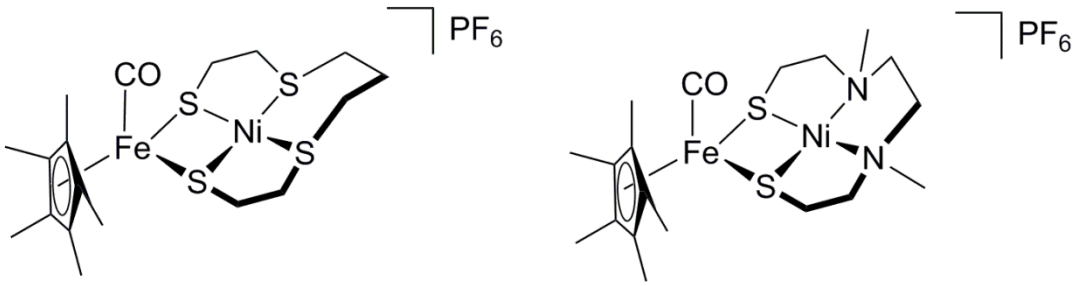

Figure 1.7: Two models of [NiFe] hydrogenases with NiS_4 and NiS_2N_2 environment.[33]

The structural and functional models for [NiFe] hydrogenase are not limited to [NiFe] species. In the further development of structural and functional mimics for the active site in [NiFe] hydrogenase, dinuclear [NiRu] compounds were also prepared.[8,34-37] The choice of replacing iron by ruthenium in mimicking the active site of the [NiFe] hydrogenase is based on the fact that many ruthenium complexes are active (homogeneous) catalysts in hydrogenation and hydrogen transfer reactions. Most significant is the fact that Ru(II) ions are able to accept both hard and soft ligands such as hydride and dihydrogen, which makes its suitable for replicating the function of the iron center in the active site of the [NiFe] hydrogenase.[8] In 2006 the group of Fontecave reported a bioinspired [NiFe] hydrogenase mimic that was prepared by combining the nickel complex [Ni(xbSmS)] with a $[Ru(CO)_2(Cl)_2]$ moiety to obtain the dinuclear NiRu complex shown in Figure 1.8a.[38,39] Following this approach another [NiRu] compound was reported comprising a ruthenium center with a Cp^- ligand (HCp = cyclopentadiene) and a variety of monodentate ligands (Figure 1.8b).[35] By using the compound $[Ni(xbSmS)RuCp(dmso)]PF_6$ as an electrocatalyst for the hydrogen evolution reaction in DMF, the overpotential of the reaction was reduced by180 mV (which is 660 mV) vs Ag/AgCl electrode compared to previously reported complexes with different ligands on ruthenium center ($[Ni(xbSmS)Ru(CO)_2Cl_2]$ and $[Ni(xbSmS)Ru(p\text{-}cymene)Cl]^+$).[35]

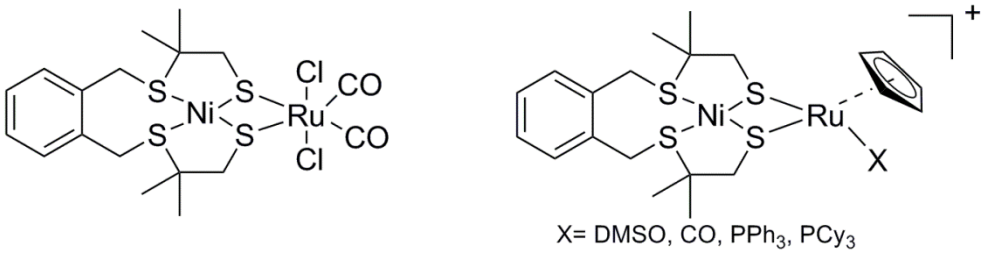

(a) (b)

Figure 1.8: Examples of [NiRu] complexes as bio-inspired models for the active site in [NiFe] hydrogenase.[35,38]

In 2011, DuBois and coworkers reported a highly efficient electrocatalyst for proton reduction based on a mononuclear nickel compound comprising the ligand 1,3,6-triphenyl-1-aza-3,6-diphosphacycloheptane (Figure 1.9a). This electrocatalyst catalyzes the production of dihydrogen with a turnover frequency of 33,000 s^{-1} in acetonitrile in the presence of protonated dimethylformamide and even 106,000 s^{-1} in the presence of 1.2 M water in acetonitrile.[40] The mechanistic investigations revealed that the pendant amines situated above and below the plane of coordination play a crucial role as protons relays.[40]

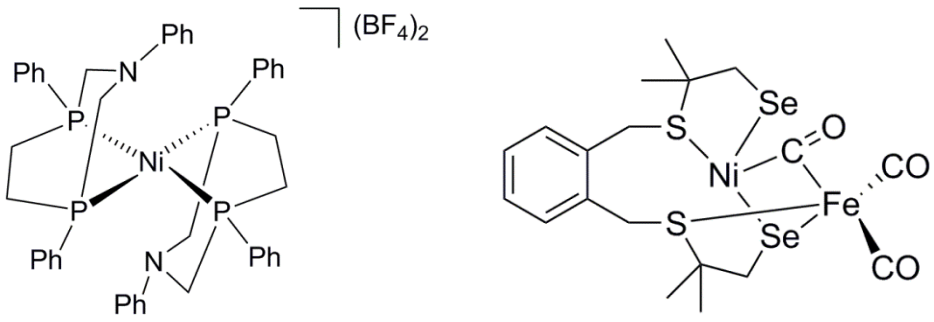

(a) (b)

Figure 1.9: The mononuclear nickel electrocatalyst for proton reduction reported by the group of DuBois (a)[40] and first structural model of [NiFeSe] hydrogenase reported by the group of Reisner (b).[11]

While many synthetic models were developed for the active site in [NiFe] hydrogenase, the group of Reisner focused their attention on mimics for the [NiFeSe] hydrogenase. The first approach in mimicking the [NiFeSe] hydrogenase active site was reported in 2014.[41] A mononuclear nickel compound containing a tetradentate dithioether-diselenolate ligand was reported as a mimic of the nickel part of the active site. Later the same group described a structural mimic of the [NiFeSe] hydrogenase active site containing both nickel and an iron center (Figure 1.9b).[11] The nickel part of this compound is based on the [Ni(xbSmS)] complex in which the terminal sulfurs of the S_4-ligand were replaced by selenium to obtain [Ni(xbSmSe)]. The iron part constitutes an iron(II) center with three CO ligands, of which one is bridging between the nickel and iron center. This model is the first structural model for the active site in [NiFeSe] hydrogenase.[11]

1.4 Aim and Outline of This Thesis

The aim of the research described in this thesis concerns the synthesis and characterization of new Ni, NiFe and NiRu complexes as structural and functional mimics of the active site in [NiFe] hydrogenase for electrocatalytic proton reduction.

In Chapter 2 the synthesis and characterization are described of new nickel complexes of two tetradentate S_2Se_2 ligands and the corresponding NiFe complexes obtained after reaction with $[FeCp(CO)_2]I$ as mimics of the active site in [NiFeSe] hydrogenase. The electrochemical and electrocatalytic properties towards proton reduction have been investigated and are also reported.

In Chapter 3 two NiRu complexes are reported as mimics of [NiFe] and [NiFeSe] hydrogenases. The NiRu complexes described in this chapter were obtained by the reaction of the nickel complexes [Ni(xbSmS)] and [Ni(xbSmSe)] with $[RuCp(PPh_3)_2Cl]$. The ligands only differ in the presence of either two thiolates or two selenolate groups in an attempt to get insight in the role of the selenolate group in the activation of protons by the isostructural [NiRu] compounds. The electrochemical properties of the complexes and their activities as electrocatalyst in the hydrogen evolution reaction are compared.

In Chapter 4 the synthesis and characterization is reported of a number of new nickel dithiolate/diselenolate complexes. These compounds appeared to be unstable in light. The light-induced C-S / C-Se bond cleavage that occurs in these compounds is described. This reactivity is relevant for the understanding of the the mechanism of methyl-coenzyme M reductase (MCR).

In Chapter 5 the reaction of [Ni(xbSmS)] and [Ni(xbSmSe)] with the compound cis-$[Ru(phen)_2(Cl)_2]$ is described. The electrochemical properties of the resulting trinuclear [NiRu] complexes are described, and their activity as electrocatalysts for proton reduction is compared.

Finally, in Chapter 6 a summary is presented of the findings described in this thesis, followed by general conclusions and an outlook for further research.

1.5 References

1. J. Turner, G. Sverdrup, M. K. Mann, P.-C. Maness, B. Kroposki, M. Ghirardi, R. J. Evans, D. Blake, *Int. J. Energy Res.*, 2008, **32**, 379.
2. W. Lubitz, B. Tumas, *Chem. Rev.,* 2007, **107**, 3900.
3. C. Tard, C. Pickett, *Chem. Rev.*, 2009, **109**, 2245.
4. M. Wang, L. Chen and L. Sun, *Energy Environ. Sci.*, 2012, **5**, 6763.

5. P. Chenevier, L. Mugherli, S. Darbe, L. Darchy, S. DiManno, P. D. Tran, F. Valentino, M. Iannello, A. Volbeda, C. Cavazza , V. Artero, . *R. Chim.*, 2013, **16**, 491.
6. D. Sellmann, F. Lauderbach and F. W. Heinemann, *Eur. J. Inorg. Chem.*, 2005, 371.
7. H. Ogata, W. Lubitz and Y. Higuchi, *Dalton Trans.*, 2009, 7577.
8. T. R. Simmons, G. Berggren, M. Bacchi, M. Fontecave , V. Artero, *Coord. Chem. Rev.*, 2014, 270.
9. L. De Gioia, 2013, *Bioinorganic Fundamentals and Applications: Metals in Natural Living Systems and Metals in Toxicology and Medicine;* Elsevier, 2013; Vol. 3., 343.
10. S. Canaguier, V. Artero, M. Fontecave, *Dalton Trans.*, 2008, 315.
11. C. Wombwell and E. Reisner, *Chem. Eur. J.*, 2015, **21**, 8096.
12. C. S. A. Baltazar, M. C. Marques, C. M. Soares, A. M. DeLacy, I. A. C. Pereira, P. M. Matias, *Eur. J. Inorg. Chem.,* 2011, 948.
13. D. Steinmann, T. Nauser, W. H. Koppenol, *J. Org. Chem.*, 2010, **75**, 6696.
14. E. Bouwman, J. Reedijk, *Coord. Chem. Rev.*, 2005, **249**, 1555.
15. G. M. Chambers, M. T. Huynh, Y. Li, S. Hammes-Schiffer, T. B. Rauchfuss, E. Reijerse, W. Lubitz, *Inorg. Chem.*, 2016, **55**, 419.
16. C. H. Lai, J. H. Reibenspies and M. Y. Darensbourg, *Angew. Chem., Int. Ed.*, 1996, **35**, 2390.
17. F. Osterloh, W. Saak, D. Haase, S. Pohl, *Chem. Commun.*, 1997, 979.
18. D. Sellmann, F. Geipel, F. Lauderbach, F. W. Heinemann, *Angew. Chem., Int. Ed.*, 2002, **41**, 632.
19. M. C. Smith, J. E. Barclay, S. P. Cramer, S. C. Davies, W. W. Gu, D. L. Hughes, S. Longhurst and D. J. Evans, *Dalton Trans.*, 2002, 3410.
20. J. A. W. Verhagen, M. Lutz, A. L. Spek , E. Bouwman, *Eur. J. Inorg. Chem.*, 2003, 3968.
21. Z. L. Li, Y. Ohki and K. Tatsumi, *J. Am. Chem. Soc.*, 2005, **127**, 8950.
22. D. Sellmann, F. Lauderbach, F. Geipel, F. W. Heinemann, M. Moll, *Angew. Chem. Int. Ed.*, 2004, **43**, 3141.
23. A. Perra, E. S. Davies, J. R. Hyde, Q. Wang, J. McMaster and M. Schröder, *Chem. Commun.*, 2006, 1103.
24. B.E. Barton, M. Whaley, T. B. Rauchfuss, D. L. Gray, *J. Am. Chem. Soc.*, 2009, 6942.
25. S. Canaguier, M. Field, Y. Oudart, J. Pecaut, M. Fontecave, V. Artero, *Chem. Commun.,* 2010, **46**, 5876.
26. D. Schilter, J. M. Camara, M. T. Huynh, S. Hammes-Schiffer and T. B. Rauchfuss, *Chem. Rev.*, 2016, **116**, 8693.
27. S. Ogo, *Coord. Chem. Rev.*, 2017, **334**, 43.
28. T. Kishima, T. Matsumoto, H. Nakai, S. Hayami, T. Ohta and S. Ogo, *Angew. Chem. Int. Ed.*, 2016, **55**, 724.
29. P. A. Summers, J. A. Calladine, F. Ghiotto, J. Dawson, X.-Z. Sun, M. L. Hamilton, M. Towrie, E. S. Davies, J. McMaster, M. W. George and M. Schröder, *Inorg. Chem.*, 2016, **55**, 527.
30. L.-C. Song, M. Cao and Y.-X. Wang, *Dalton Trans.*, 2015, **44**, 6797.

31. C. U. Perotto, G. Marshall, G. J. Jones, E. S. Davies, W. Lewis, J. McMaster and M. Schröder, *Chem. Commun.*, 2015, **51**, 16988.
32. L.-C. Song, X.-Y. Yang, M. Cao, X.-Y Gao, B.-B. Liu, L. Zhu and F. Jiang, *Chem. Commun.*, 2017, **53**, 3818.
33. D. Yang, Y. Li, L. Su, B. Wang and J. Qu, *Eur. J. Inorg. Chem.*, 2015, 2965.
34. Y. Oudart, V. Artero, J. Pécaut, C. Lebrun and M. Fontecave, *Eur. J. Inorg. Chem.*, 2007, 2613.
35. S. Canaguier, L. Vaccaro, V. Artero, R. Ostermann, J. Pécaut, M. J. Field and M. Fontecave, *Chem. Eur. J.*, 2009, **15**, 9350.
36. Y. Oudart, V. Artero, L. Norel, C. Train, J. Pécaut and M. Fontecave, *J. Organomet. Chem.*, 2009, **694**, 2866.
37. G. M. Chambers, R. Angamuthu, D. L. Gray and T. B. Rauchfuss, *Organometallics*, 2013, **32**, 6324.
38. Y. Oudart, V. Artero, J. Pecaut, M. Fontecave, *Inorg. Chem.*, 2006, **45**, 4334.
39. J. A. W. Verhagen, D. D. Ellis, M. Lutz, A. L. Spek , E. Bouwman, *Dalton Trans.*, 2002, 1275.
40. M. L. Helm, M. P. Stewart, R. M. Bullock, M. R. DuBois, D. L. DuBois, *Science,* 2011, **333**, 863.
41. C. Wombwell, E. Reisner, *Dalton Trans*, 2014, **43**, 4483.

Chapter 2

Electrocatalytic Proton Reduction by a Model for [NiFeSe] Hydrogenases

Abstract

Two new heterodinuclear nickel-iron complexes [Ni(pbSmSe)FeCpCO]PF_6 and [Ni(xbSmSe)FeCpCO]PF_6 were synthesized as mimics of the [NiFeSe] hydrogenase active site (HCp = cyclopentadiene; H_2pbSmSe = 1,9-diselenol-3,7-dithia-2,2,8,8-tetramethylnonane; H_2xbSmSe = 1,2,-bis(2-thiabutyl-3,3-dimethyl-4-selenol)benzene). The compounds were characterized by single crystal X-ray diffraction and cyclic voltammetry. X-ray structure determinations showed that in both NiFe complexes the nickel(II) center is in a square-planar S_2Se_2 environment; the two selenolate donors are bridging to the iron(II) center that is further coordinated to an η^5-cyclopentadienyl group and a carbon monoxide ligand. Electrochemical studies showed that the complex [Ni(pbSmSe)FeCpCO]PF_6 is an electrocatalyst for the production of H_2 in DMF in the presence of acetic acid at −2.1 V vs. Fc^+/Fc; a foot-of-the-wave (FOW) analysis of the catalytic currents yielded an estimation of k_{obs} of 24 s^{-1}.

This chapter has been published: G. Gezer, D. Durán Jiménez, M. A. Siegler, and E. Bouwman, *Dalton Trans.*, 2017, **46**, 7506.

2.1 Introduction

Hydrogenase enzymes, catalyzing the reversible oxidation of dihydrogen, play an important role in the metabolism of bacteria.[1] In the past decades, hydrogenases have attracted the attention of synthetic chemists, since dihydrogen gas may be used as a sustainable source of energy. In order to produce dihydrogen gas for the application in fuel cells, new efficient electrocatalysts for the hydrogen-evolving reaction (HER) may be developed by using biomimetic, functional models of hydrogenases.[2]

Three types of hydrogenases are known, which are classified based on the metal center in the active site. The [FeFe] hydrogenases contain a dinuclear iron center linked to an Fe_4S_4 cluster, comprising CO, CN^- and a dithiolate ligand. These [FeFe] hydrogenases catalyze both H_2 evolution and uptake, but their predominant activity is in H_2 evolution. However, the [FeFe] hydrogenases generally are highly air sensitive. The [Fe] hydrogenases have a mononuclear iron catalytic center and do not contain Fe-S clusters. These enzymes catalyze the transfer of hydride groups and H_2 activation.[3] The third class of hydrogenases comprises the [NiFe] hydrogenases containing a heterodimetallic Ni-Fe active site with a nickel center bound to four cysteine thiolates with two of the cysteines bridging between the nickel and an iron center (Figure 2.1a).[4] Although this enzyme is mostly involved in the uptake of H_2, it is also able to catalyze the production of H_2.[3] The [NiFeSe] hydrogenases form a subclass of the [NiFe] hydrogenases, in which one of the non-bridging cysteines (Cys) in the active site of the enzyme is replaced by selenocysteine (Sec) (Figure 2.1b).[5] [NiFeSe] hydrogenases show interesting properties for H_2 production such as their high catalytic rates and their activity at low overpotentials; as they are less air-sensitive they produce H_2 even in the presence of low concentrations of O_2.[6] Compared to their cysteine homologues the [NiFeSe] hydrogenases have higher catalytic activity in the hydrogen evolution reaction.[3,7] This difference in activity may be explained by the differences in the physical properties of selenium compared to those of sulfur, such as its higher acidity and higher nucleophilicity, in addition to the lower redox potential of the selenocysteine redox couple. The pKa of Sec is 5.3 whereas the pKa of Cys is 8.3, which may help in the rapid exchange of protons. Selenium is also a softer donor atom than sulfur; the polarizable volume of selenium is 3.8 Å in comparison to 2.9 Å for sulfur. Although these different properties can be the potential causes for the higher catalytic activity of the [NiFeSe] hydrogenases, the exact role of selenocysteine in the [NiFeSe] hydrogenases is still not completely clear.[8,9]

In the past decades a large number of structural and functional models for the active site in [NiFe] hydrogenases have been reported with overpotentials for proton reduction as low as 50 mV. From these studies, it was found that the addition of a cyclopentadienyl (Cp^-) ligand resulted in increased catalytic rates and stability of the catalyts.[10-14] Apart from these models, a number of mononuclear Ni/Co/Fe complexes and several heterodimetallic [NiRu] complexes have been reported as functional models of the [NiFe] hydrogenases active site.[15-19] Two heterodinuclear compounds related to our work described in this Chapter have been reported by Artero and Schröder, comprising NiS_4 centers bound to a {FeCpCO} group (Figure 2.2a-b).[11,20] However, so far only one heterodimetallic nickel-iron complex was reported comprising a selenolate ligand coordinated to the nickel center, as a potential model of the active site in [NiFeSe] hydrogenases (Figure 2.2c).[7] In this Chapter, we describe the synthesis and characterization of two new heterodimetallic nickel-iron complexes (Figure 2.3) as mimics of the [NiFeSe] hydrogenase active site. The electrochemical properties and electrocatalytic activity for H_2 production of these NiFe complexes are reported.

(a) (b)

Figure 2.1: Schematic representation of the active site in (a) [NiFe] and (b) [NiFeSe] hydrogenases.[4,5]

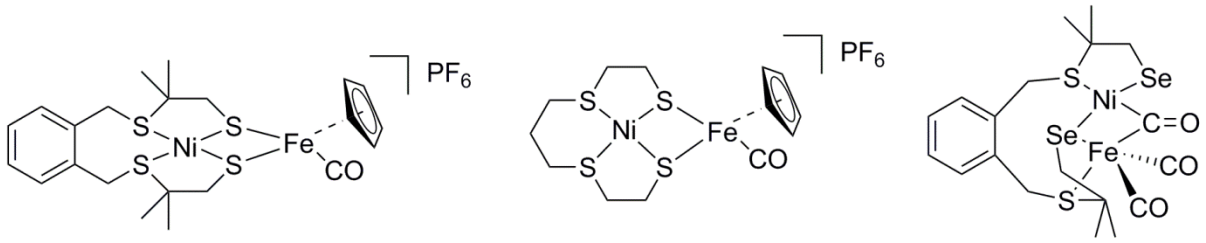

(a) (b) (c)

Figure 2.2: Schematic drawings of the [NiFe] hydrogenase models reported by Artero (a)[11] and Schröder (b),[20] and the first structural model of [NiFeSe] hydrogenases reported by Reisner (c).[7]

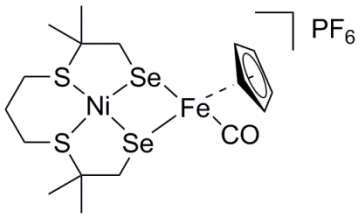

[Ni(pbSmSe)FeCpCO]PF_6

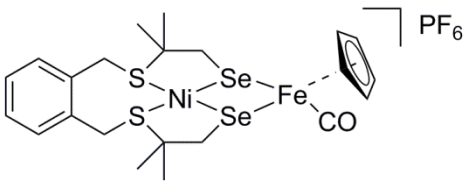

[Ni(xbSmSe)FeCpCO]PF_6

Figure 2.3: Schematic drawing of the heterodimetallic compounds described in this Chapter.

2.2 Results

2.2.1 Synthesis and Characterization

The novel heterodinuclear compounds [Ni(pbSmSe)FeCpCO]PF_6 **(5)** and [Ni(xbSmSe)FeCpCO]PF_6 **(6)** were synthesized following the procedure shown in Scheme 2.1. The two different selenouronium ligands precursors were synthesized based on reported procedures. The compounds 1,9-dichloro-3,7-dithia-2,2,8,8-tetramethylnonane and bis(3-chloro-2,2-methyl-1-thiapropyl)-o-xylene were treated with two equivalents of selenourea in ethanol to give the selenouronium ligand precursors **(1)** and **(2)** as white powders in high purities in 86% and 90% yield, respectively. The ligand precursor **(2)** has been reported earlier.[7] The compounds [Ni(pbSmSe)] **(3)** and [Ni(xbSmSe)] **(4)** were synthesized by heating the selenouronium ligand precursors in refluxing ethanol with [$Ni(acac)_2$] in the presence of NMe_4OH. The compounds [Ni(pbSmSe)] **(3)** and [Ni(xbSmSe)] **(4)** were obtained as green solids in 64% and 83% yield, respectively. The compounds were characterized with ^1H and ^{13}C NMR spectroscopy, mass spectrometry, elemental analysis and single crystal X-ray crystallography for compound **(3)**; the X-ray structure of compound **(4)** has been reported.[7] The nickel compounds **(3)** and **(4)** give rise to sharp resonances in the ^1H NMR spectra indicating that the nickel(II) centers in these compounds are in low-spin, square-planar geometries, which are retained in solution. The clear NMR spectra are in contrast with those of the corresponding sulfur-based compounds [Ni(pbSmS)][21] and [Ni(xbSmS)],[22] which generally show broad signals. Such broadening of the NMR signals is ascribed to fluxional behavior of the ligand surrounding the nickel ion; as a result part of the time the nickel centers are in more or less tetrahedral geometries giving rise to the paramagnetic high-spin state. Reaction of the mononuclear nickel complexes **(3)** and **(4)** with one equivalent of commercially available [$FeCp(CO)_2I$] in dichloromethane provided the corresponding [Ni(L)FeCpCO]I complexes; subsequently the counter anion was exchanged by the addition

of NH_4PF_6 in acetonitrile resulting in the compounds [Ni(pbSmSe)FeCpCO](PF_6) **(5)** and [Ni(xbSmSe)FeCpCO](PF_6) **(6)**. These heterodinuclear complexes were characterized with NMR and FTIR spectroscopy, mass spectrometry, elemental analysis and single crystal X-ray crystallography. The ^{1}H NMR spectra of the NiFe complexes recorded in dichloromethane are weak and poorly resolved, but show the expected signals of the cyclopentadienyl, aromatic and methyl protons. However, the methylene groups which are in close proximity to nickel center are not clearly discernible. Several attempts have been undertaken to obtain better quality ^{1}H NMR spectra of the NiFe complexes. Spectra were recorded in another solvent (DMSO) and were recorded at different temperatures, but unfortunately to no avail. Again, the broadening of these signals might be explained by tetrahedral distortions of the square-planar geometry, resulting in a fraction of the nickel centers to be in the high-spin state. In contrast to the mononuclear compounds this distortion is not fluxional, but immobilized by the bridging of the two selenolate donor atoms between the Ni(II) and Fe(II) centers (see below). In addition, the results of the mass analysis and IR spectra (see below) indicate that a dynamic equilibrium may exist of compounds that are the result of a disproportionation reaction of **(5)** or **(6)** $[Ni(L)FeCpCO]^+$ to form $[Ni(L)FeCp]^+$ and $[Ni(L)FeCp(CO)_2]^+$, which would also give rise to broad signals.

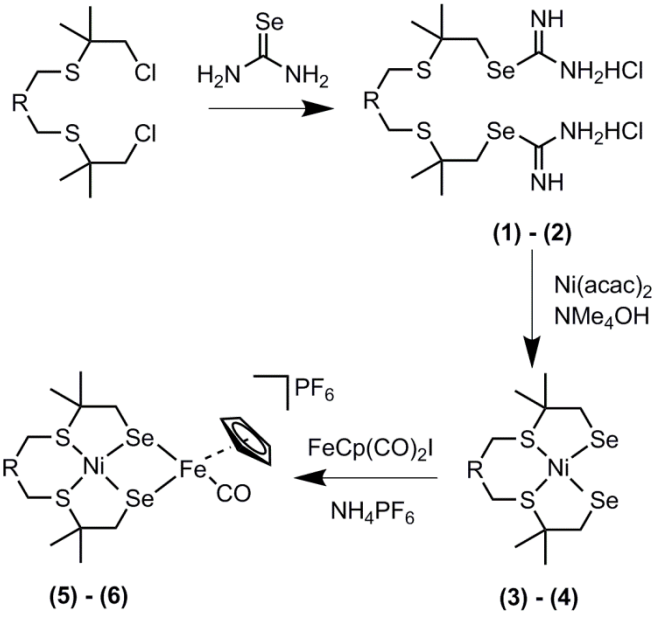

R: CH_2 for 1-3-5; R: C_6H_4 for 2-4-6

Scheme 2.1: Synthesis scheme of the selenouronium salts **(1)** and **(2)**, the mononuclear Ni complexes **(3)** and **(4)** and the heterodinuclear NiFe complexes **(5)** and **(6).**

2.2.2 Description of the Structures

Single crystals of **(3)** suitable for X-ray structure determination were obtained by vapor diffusion of pentane into a dichloromethane solution of the complex; crystallographic and refinement data are provided in Table AII.1. A projection of the molecular structure is given Figure 2.4 and selected bond distances and angles are listed in Table 2.1. Complex **(3)** crystallizes in the space group $P2_1$; the asymmetric unit contains one molecule of the mononuclear compound [Ni(pbSmSe)]. The Ni(II) center is in a square-planar geometry by the coordination of two selenolate and two thioether donor atoms. The Ni-Se bond distances are 2.2898(6) and 2.2910(6) Å; as expected for the larger ionic radius of Se these distances are longer than the Ni-S bond distances of 2.180(8) Å in the thiolate analog [Ni(pbSmS)].[21] As a result, the Ni-S thioether bond distances at 2.1707(10) and 2.1608(11) Å are slightly shorter than those of 2.1711(3) and 2.1668(3) Å in [Ni(pbSmS)].[21] The square-planar geometry reveals a slight tetrahedral distortion with a dihedral angle of 8.91°, defined by the planes S1-Ni1-S2 and Se1-Ni1-Se2, which is slightly larger than in the thiolate analog having a dihedral angle of 5.17°.[21] This larger tetrahedral distortion in the solid state of the selenolate compound is rather surprising, as the NMR spectra of the thiolate compound are broadened due to the fluxionality of the ligand, which results in the nickel ion in the low-spin square-planar structure to be in equilibrium with a nickel center in a more tetrahedral high-spin state. In contrast, the NMR spectra show the selenolate compound to be clearly low-spin and diamagnetic, which may indicate that the tetrahedral distortion in the solid state is merely due to packing effects.

Single crystals of the complexes **(5)** and **(6)** were obtained by vapor diffusion of diethyl ether into dichloromethane solutions of the complexes; crystallographic and refinement data are provided in Table AII.1. Projections of the molecular structures of the heterodinuclear complexes are shown in Figure 2.5; selected bond distances and angles are listed in Table 2.1. Complex **(5)** crystallizes in the space group $R\bar{3}$ and the crystal lattice contains some amount of significantly disordered solvents molecules. Complex **(6)** crystallizes in the space group $P2_1/c$; the coordination spheres around Ni1 and the CO coordinated to Fe1 are found to be slightly disordered over two orientations. The nickel(II) ions in the complexes **(5)** and **(6)** are in square-planar geometries bound to two thioether and two selenolate donor atoms. In both compounds the two Se donor atoms are bridging to the Fe(II) ion, resulting in a Ni-Se-Fe-Se 'butterfly' core with a 'hinge' angle (defined by the angle between the planes through $NiSe_2$

and $FeSe_2$) of 120.87° for **(5)** and 108.36° for **(6)**. The Fe(II) ion in both complexes is further coordinated to a symmetrically bound η^5-cyclopentadienyl ligand and a CO ligand. The Ni-Se distances of 2.2837(5) and 2.2933(5) Å in [Ni(xbSmSe)FeCpCO]PF_6 are longer than the corresponding Ni-S thiolate distances of 2.1670(9) and 2.1717(8) Å found in [Ni(xbSmS)FeCpCO]BF_4,[11] as a result of the larger ionic radius of the selenolate donor atom. For both NiFe complexes the square-planar geometry of the nickel centers is slightly distorted, with dihedral angles of 7.39° and 12.63° for complexes **(5)** and **(6)** respectively. This distortion seems to be caused by the bridging of both selenolate atoms between the Ni(II) and Fe(II) centers, resulting in larger S-Ni-Se and significantly smaller Se-Ni-Se angles. In both complexes the molecule of CO is directed towards the Ni center with a Ni-C(O) distance of 3.1 Å for complex **(5)** and 2.9 Å for complex **(6).** The major difference between the two heterodinuclear compounds is the relative orientation of the {FeCpCO} group. Whereas in complex **(5)** the {FeCpCO} group and the bridge between the sulfur atoms are on the same side of the Ni square plane, in complex **(6)** they are on opposite sides.

Table 2.1: Selected bond lengths (Å) and angles (°) for the complexes **(3)**, **(5)** and **(6)**

Distances (Å)	**(3)**	**(5)**	**(6)**
Ni1-Se1	2.2898(6)	2.2768(8)	2.2837(5)
Ni1-Se2	2.2910(6)	2.2978(7)	2.2933(5)
Ni1-S1	2.1608(11)	2.1996(11)	2.1835(7)
Ni1-S2	2.1707(10)	2.1817(12)	2.1820(8)
Fe1-Se1		2.3859(7)	2.4043(5)
Fe1-Se2		2.4018(8)	2.3923(5)
Fe1-Cp(centroid)		1.71(4)	1.70(3)
Fe1-C12/C22		1.741(4)	1.773(3)
Angles (°)	**(3)**	**(5)**	**(6)**
S1-Ni1-Se1	89.79(3)	92.75(4)	91.31(2)
S2-Ni1-Se2	90.79(3)	93.00(4)	91.74(2)
Se1-Ni1-Se2	87.62(2)	82.52(3)	80.550(17)
S1-Ni1-S2	91.80(4)	91.27(4)	95.02(3)
S2-Ni1-Se1	170.94(4)	173.92(4)	167.66(3)
S1-Ni1-Se2	177.40(4)	172.33(4)	169.19(3)
Se1-Fe1-Se2		78.11(2)	76.174(15)
Ni1-Se1-Fe1		85.40(3)	
Ni1-Se2-Fe1		84.58(3)	

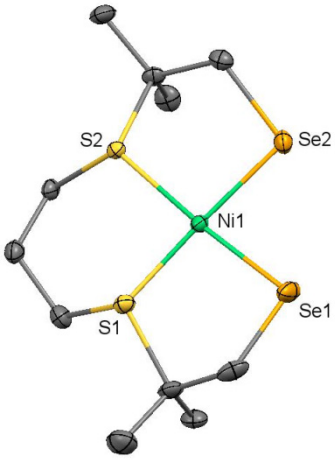

Figure 2.4: Displacement ellipsoid plot (50% probability level) of **(3)** at 110(2) K. Hydrogen atoms are omitted for clarity.

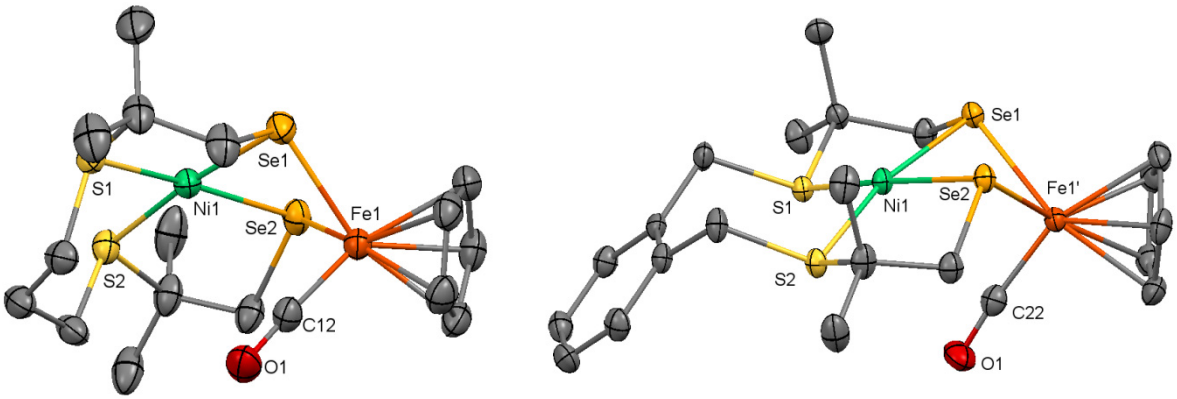

(a) (b)

Figure 2.5: Displacement ellipsoids plots (50% probability level) of the cationic complex in (a) **(5)** and (b) **(6)** at 110(2) K. Hydrogen atoms, PF_6^- anions, lattice solvent molecules, and disorder (in **(6)**) are omitted for clarity.

2.2.3 IR Spectroscopy of the NiFe Complexes

The carbonyl stretching bands in the solid state IR spectra of compound **(5)** appear at 1918 (m), 1987 (s) and 2035 (s) cm^{-1}, whereas the IR spectrum of compound **(6)** reveals one strong band at 1923 cm^{-1} in addition two weaker bands at 1989 and 2037 cm^{-1} (Figure AII.6-7). Based on its structure complex **(5)** should show only a single CO band. Indeed, the compound $[Ni(xbSmS)FeCpCO]BF_4$ has been reported to show a single carbonyl stretching band in the IR spectrum at 1939 cm^{-1}.[11] However, the compound $[Ni(xbSmS)FeCp(CO)_2]BF_4$, showing two CO stretching bands at 2008 and 2054 cm^{-1}, was reported to be an intermediate in the

formation of [Ni(xbSmS)FeCpCO]BF_4. Interestingly, the mass spectra recorded of crystals of compound **(5)** show three major fragments: two of them are assigned to the expected monocationic compound $[M-PF_6]^+$ and the compound after loss of the CO ligand $[M-(PF_6)-(CO)]^+$. Unexpectedly, also a fragment that can be assigned to the monocationic compound with two CO ligands ($[M-(PF_6)+(CO)]^+$) is observed. This fragment might be the result of disproportionation of $[Ni(pbSmSe)FeCpCO]^+$ to form $[Ni(pbSmSe)FeCp]^+$ and $[Ni(pbSmSe)FeCp(CO)_2]^+$, the former compound would contain a 16-electron Fe^{II} center, whereas the second species would be asymmetrically bridged by only one of the selenolate atoms. In contrast, whereas the IR of compound **(6)** indicates that a product containing two molecules of CO bound to iron may be present, the mass spectrum of **(6)** does not show a peak that can be assigned to a fragment $[M-(PF_6)+(CO)]^+$. We therefore have to conclude that whereas for compound **(6)** the product with one CO ligand bound to iron is the most stable one, for compound **(5)** a mixture of $[Ni(pbSmSe)FeCpCO](PF_6)$ and $[Ni(pbSmSe)FeCp(CO)_2](PF_6)$ is obtained, from which a single crystal of the monocarbonyl complex was picked. Because of the small mass difference of one molecule of CO the elemental analysis is not conclusive.

Similar values of IR stretching bands have been reported for the carbonyl ligands in the active sites of the [NiFe] and [NiFeSe] hydrogenases as well as for another structural model of [NiFeSe] hydrogenases.[7] The relatively lower energy of the CO stretching frequencies in the selenolate compounds has been attributed to an increase of electron density at the Fe center, as the selenolate donor atoms are more electron-donating than thiolate donor atoms.[7]

2.2.4 Electrochemical Analyses

The electrochemical properties of the nickel and nickel-iron complexes were investigated using cyclic voltammetry; the relevant data are presented in Table 2.2. For the mononuclear complex **(3)** one reversible reduction wave is observed with an E_{pc} at −2.1 V *vs*. Fc^+/Fc at a scan rate of 200 mV s^{-1} in DMF (Figure 2.6a), which is tentatively ascribed to the Ni^{II}/Ni^{I} redox couple. In contrast, the corresponding thiolate-containing compound [Ni(pbSmS)] has been reported to show two irreversible waves at −1.05 V and −1.5 V *vs*. Fc^+/Fc at a scan rate of 100 mV s^{-1} in dichloromethane solution.[21] We could not readily find an explanation for the large difference of nearly 1 V between the observed reduction potential of **(3)** and the values reported for the corresponding thiolate-containing compound [Ni(pbSmSe)]. Therefore a CV of complex **(3)** was also recorded in dichloromethane solution (Figure AII.3). Although the reduction of **(3)** appeared to be irreversible in dichloromethane, the reduction potential of **(3)**

was found to be similar in both dichloromethane and in DMF solution. For the nickel complex **(4)** one irreversible wave is observed with an E_{pc} at −1.99 V *vs*. Fc^+/Fc at a scan rate of 200 mV s^{-1} in DMF (Figure 2.6b), similar to the irreversible electrochemical behavior reported for the analogous thiolate compound [Ni(xbSmS)] at −2.03 V *vs*. Fc^+/Fc in DMF solution.[11] The slightly less negative reduction potential for the nickel center in compound **(4)** relative to that in **(3)** may tentatively be ascribed to larger flexibility of the 7-membered chelate ring of the xylyl backbone, facilitating a change in redox state of the nickel center. We do not have an explanation for the differences in reversibility of the reduction wave of the nickel centers in **(3)** and **(4)**, nor for the observation that the reduction wave for **(3)** is reversible in DMF, whereas it is irreversible in DCM. Furthermore, we cannot give a reason for the apparent 1 V difference in the reduction potentials of [Ni(pbSmSe)] **(3)** and [Ni(pbSmS)], especially as the difference in reduction potentials for the xylene-bridged compounds [Ni(xbSmS)] and [Ni(xbSmSe)] **(4)** is negligible.

The same electrochemical conditions with a scan rate of 200 mV s^{-1} were also used to study the electrochemical behavior of the NiFe complexes **(5)** and **(6)** in DMF solutions. For complex **(5)** one quasi-reversible wave is observed with an E_{pc} at −2.1 V *vs*. Fc^+/Fc (Figure 2.7a) with an i_{pc} that is nearly two times higher than the i_{pa}. For complex **(6)** one quasi-reversible wave is observed with an E_{pc} at −1.99 V *vs* Fc^+/Fc (Figure 2.7b). At first sight it thus seems that the presence of the cyclopentadienyl-iron moiety does not influence the reduction potential of the nickel(II) ion. In addition for both complexes one small wave is observed at around −1.4 V *vs* Fc^+/Fc.

In order to better understand the electrochemical properties of the nickel-iron complexes, the electrochemical behavior of $[FeCp(CO)_2I]$ was also examined (Figure AII.4). For this compound one irreversible reduction is observed with an E_{pc} at −2.05 V *vs*. Fc^+/Fc at a scan rate of 200 mV s^{-1} in DMF, which is tentatively ascribed to the Fe^{II}/Fe^{I} redox couple. Similar to the nickel-iron complexes, an additional small wave is observed at −1.3 V *vs* Fc^+/Fc. This feature thus indicates that the small wave around −1.4 V *vs* Fc^+/Fc in the voltammograms of the nickel-iron complexes is related to the presence of the [FeCp(CO)I] moiety. It seems that the quasi-reversible reduction of complex **(5)** with an E_{pc} at −2.1 V *vs*. Fc^+/Fc is an overlap of the reduction of the nickel ion in **(3)** (E_{pc} at −2.1 V *vs*. Fc^+/Fc) with the reduction wave of iron center in $[FeCp(CO)_2I]$ (at −2.05 V *vs*. Fc^+/Fc). Upon closer inspection of the reduction wave for compound **(5)**, it looks as if this wave indeed reveals a shoulder around −2.0 V. This overlap of two redox events may also explain why the

reversibility of this reductive peak changed from reversible in the mononuclear complex [Ni(pbSmSe)] to quasi-reversible in the heterodinuclear compound **(5)**. In comparison, the complex [Ni(xbSmS)FeCpCO]BF_4 has been reported to show one reversible redox couple at −1.43 V *vs*. Fc^+/Fc and one irreversible wave at −2.01 V *vs*. Fc^+/Fc in DMF.[11] In contrast to the CVs of the complexes **(5)** and **(6)**, in this report the reduction wave at −1.43 V *vs*. Fc^+/Fc has the same current as the one at −2.01 V *vs*. Fc^+/Fc. The reduction wave of complex **(6)** appears to become more reversible compared to that of the corresponding mononuclear nickel complex [Ni(xbSmSe)].

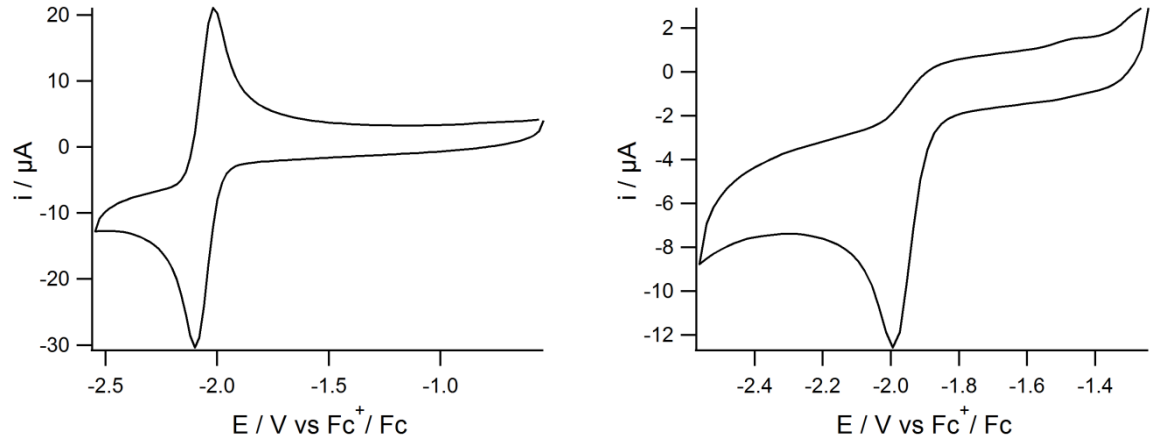

(a) (b)

Figure 2.6: Cyclic voltammograms of (a) compound **(3)** and (b) compound **(4)** (1 mM) in DMF solutions containing $TBAPF_6$ (0.1 M) as the supporting electrolyte and a glassy carbon working electrode at 200 mV s^{-1}.

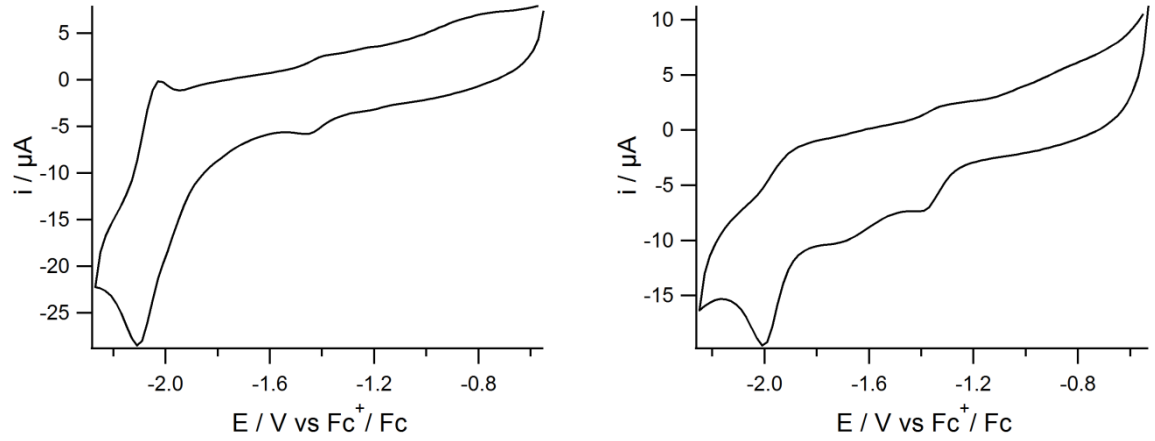

(a) (b)

Figure 2.7: Cyclic voltammograms of (a) compound **(5)** and (b) compound **(6)** (1 mM) in DMF solutions containing $TBAPF_6$ (0.1 M) as the supporting electrolyte and a glassy carbon working electrode at 200 mV s^{-1}.

Table 2.2: Electrochemical data of the Ni and NiFe complexes (vs Fc^+/Fc).[a]

Compound	E_{pa} (V)	E_{pc} (V)
(3)	−2.02	−2.10
(4)		−1.99
(5)	−2.03	−2.10
(6)		−1.99

[a] Experimental conditions: 1 mM solutions of complexes in DMF containing 0.1 M $TBAPF_6$ as the supporting electrolyte. Glassy carbon working electrode, platinum counter electrode, Ag/AgCl reference electrode and scan rate 200 mV s^{-1}. The values have been calculated using Fc/Fc^+ as an internal reference, which was found to have $E_{1/2}$ of 0.54 V vs Ag/AgCl in our conditions.

2.2.5 Electrocatalytic Hydrogen Evolution in the Presence of HOAc

The activity of the new compounds in electrocatalytic proton reduction was studied using cyclic voltammetry with addition of varying amounts of HOAc to DMF solutions of the Ni and NiFe complexes. The reversible reduction observed for complex **(3)** with an E_{pc} at −2.1 V *vs*. Fc^+/Fc becomes irreversible with the addition of HOAc (Figure AII.1). On the other hand, for complex **(4)** the irreversible reduction peak with an E_{pc} at –1.99 V does not change upon addition of HOAc and no catalytic current is observed (Figure AII.2). The quasi-reversible

reduction peak of complex **(5)** with an E_{pc} at −2.1 V *vs*. Fc^+/Fc becomes irreversible with increasing concentrations of HOAc while the E_{pc} shifts to more negative potentials indicating electrocatalytic activity (Figure 2.8a). Again, for complex **(6)** no catalytic wave is observed upon the addition of different equivalents of acid.

To quantify the rate of the hydrogen evolution reaction the foot-of-the-wave (FOW) analysis was applied.[23,24] The FOW analysis was developed by Costentin and Savéant and can be used for the analysis of voltammograms that do not show an S-shaped curve with a fixed plateau current.[23] Using the FOW analysis an estimated k_{obs} of 24 s^{-1} was calculated for complex **(5)** (Figure AII.5).

In order to confirm that indeed dihydrogen gas is formed in the catalytic reaction, a controlled-potential coulometry (CPC) experiment was carried out on a 0.5 mM solution of complex **(5)** in DMF (5 ml) in the presence of 17.5 µl of HOAc (50 equivalents of H^+ per NiFe) at −2.1 V *vs*. Fc^+/Fc. The produced dihydrogen gas was quantified volumetrically by GC analysis. The CPC experiment was run for 50 min, while the solution was stirred continuously. Using complex **(5)** as the electrocatalyst for proton reduction, a total of 64 µl H_2 was produced by 0.5 mM complex in 50 min with 72% faradaic yield. In a control experiment at this potential formation of H_2 is not observed in the absence of the catalyst. In order to compare the activity of the mononuclear [Ni(pbSmSe)] and the dinuclear compound [Ni(pbSmSe)FeCpCO]PF_6 a CPC experiment was also run for complex **(3)**. After 50 min the amount of H_2 produced by compound **(3)** appeared to be very low compared to the NiFe complex **(5)**; the formed H_2 was barely detectable with a concentration falling out of the lower range of the calibration line. A CPC experiment was also carried out using complex **(6)** in DMF solution in the presence of HOAc at −1.9 V *vs*. Fc^+/Fc. In this case dihydrogen evolution was not observed and it can be concluded that this compound is not active as an electrocatalyst for proton reduction with a weak acid such as HOAc. In contrast, the complex [Ni(xbSmS)FeCpCO]BF_4, the thiolate analogue of complex **(6)**, has been reported to be an electrocatalyst for H_2evolution, which achieved 20 turnovers in 4 h in the presence of the stronger acid trifluoroacetic acid.[11]

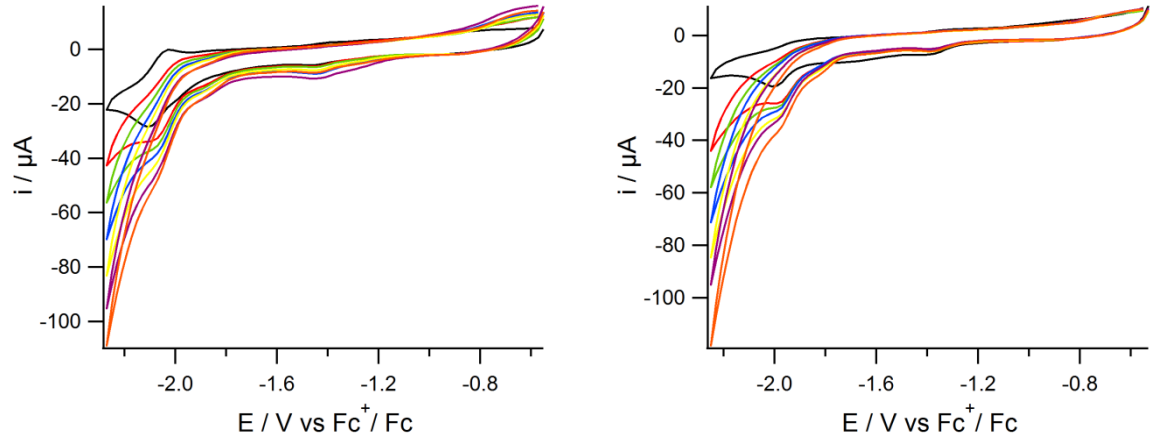

(a) (b)

Figure 2.8: Cyclic voltammograms of (a) compound **(5)** and (b) compound **(6)** (1 mM) in DMF solutions containing $TBAPF_6$ (0.1 M) using a glassy carbon working electrode at 200 mV s^{-1} in the presence of 0 (black), 10 (red), 20 (green), 30 (blue), 40 (yellow), 50 (purple), 60 (orange) mM of acetic acid.

2.3 Discussion

In this work the compounds $[Ni(pbSmSe)FeCpCO]PF_6$ and $[Ni(xbSmSe)FeCpCO]PF_6$ were prepared as mimics of the [NiFeSe] hydrogenase active site. The two compounds showed some different properties by changing the ligand environment of the nickel center. A major structural difference between two NiFe complexes was observed according to the orientation of the {FeCpCO} group relative to the square-planar nickel center. Whereas the {FeCpCO} group and the bridge between the sulfur atoms are on the same side of Ni square plane in complex **(5)**, they are on opposite sides in complex **(6),** which is similar to the analogous thiolate compound $[Ni(xbSmS)FeCpCO]BF_4$.[11] It is not clear what is the cause of this different orientation, but it might just be due to packing effects in the solid state. Secondly, FTIR spectroscopy and mass spectrometry also revealed differences between the two structures. Although based on the crystal structures of the complexes their IR spectra should show only a single CO band, surprisingly compound **(5)** reveals three CO bands and compound **(6)** shows one strong and two weak CO bands. In addition the mass spectra of compound **(5)** shows three major fragments ($[M-PF_6]^+$, $[M-(PF_6)-(CO)]^+$ and $[M-(PF_6)+(CO)]^+$) whereas the compound **(6)** shows two fragments ($[M-PF_6]^+$and $[M-(PF_6)-(CO)]^+$). This might be related to the more rigid nickel(II) center of compound **(5)**, hampering the binding of both selenolate donor atoms of the [Ni(pbSmSe)] moiety to the iron

center and causing the dynamic equilibrium of two compounds containing one or two carbonyl groups bound to the iron center. Finally, only compound **(5)** was found to be active in the electrocatalytic reduction of protons into dihydrogen gas. The disproportionation reaction that seemingly occurs for compound **(5)** but not for **(6)**, potentially generating a 16-electon iron center, might be the cause of the difference in activity. Comparison of the CV results of the mononuclear nickel to those of the nickel-iron complexes show that the nickel center plays an important role in the electrocatalytic reduction of protons. Both [Ni(pbSmSe)] and [Ni(pbSmSe)FeCpCO](PF_6) reveal similar reversible reduction waves whereas both [Ni(xbSmSe)] and [Ni(xbSmSe)FeCpCO]PF_6 show similar irreversible reduction waves at around the same potentials. However, CPC experiments of a solution containing either [Ni(pbSmSe)] and HOAc show that the amount of H_2 produced by the mononuclear nickel is barely detectable and very low compared to the related NiFe complex. We therefore conclude that the interplay of the two metal centers in the [NiFe] complexes seems to be essential for the electrocatalytic activity. Coordination of iron center with the electron-withdrawing groups to the nickel center might help to lower the reduction potential of the nickel center facilitating the reduction of protons.

2.4 Conclusion

Two novel NiFe complexes are reported as mimics of the [NiFeSe] hydrogenase active site. Both [Ni(pbSmSe)FeCpCO]PF_6 and [Ni(xbSmSe)FeCpCO]PF_6 complexes have structural similarities with active site of [NiFeSe] hydrogenase. The compounds contain nickel and iron centers coordinated with two selenolate and two thioether donors. The bond distances between the nickel centers and the selenolate donors are 2.29 Å for complexes **(5)** and **(6)**, whereas the Ni-Se distance in the active site of [NiFeSe] hydrogenase has been reported to be 2.46 Å.[5] The major drawback of the selenium complexes compared to the reported sulfur analogues is their higher air sensitivity. The compound [Ni(pbSmSe)FeCpCO]PF_6 catalyzes the electrocatalytic reduction of protons in the presence of acetic acid, as shown by CV and CPC experiments, whereas [Ni(xbSmSe)FeCpCO]PF_6 does not. The reason for this difference in activity may lie in the disproportionation reaction that seemingly occurs for compound **(5)** but not for **(6)**, generating an active 16-electron species for **(5)**. To the best of our knowledge compound **(5)** is thus the first functional model of the [NiFeSe] hydrogenase active site. Although this NiFe compound is just a very modest catalyst, this work is an initial step for the development of more efficient mimics of the [NiFeSe] hydrogenase

active site.

2.5 Experimental

2.5.1 Materials

All experiments were performed using standard Schlenk techniques or in a glovebox under an argon atmosphere unless otherwise noted. Chemicals were purchased from Acros or Aldrich and were used without further purification. Organic solvents were deoxygenated by the freeze-pump-thaw method and were dried over molecular sieves prior to use. The NMR solvent CD_2Cl_2 for the metal complexes was deoxygenated by the freeze-pump-thaw method and was stored over molecular sieves in a glovebox. The compounds 1,9-dichloro-3,7-dithia-2,2,8,8-tetramethylnonane,[21] bis(3-chloro-2,2-methyl-1-thiapropyl)-o-xylene,[22] [Ni(xbSmSe)][7] were synthesized according to published methods. [$FeCp(CO)_2I$] was purchased from Aldrich. The synthesis of the [NiFe] complexes is based on a method described in literature.[20]

2.5.2 Physical Measurements

NMR spectra were recorded on a 300 MHz Bruker DPX 300 spectrometer and chemical shifts were referenced against the solvent peaks. Mass spectra were obtained with a Finnigan TSQ quantum instrument using ESI. HRMS was recorded on a Thermo Scientific LTQ Orbitrap XL high resolution FT-MS system. Elemental analyses were performed by the Microanalytical Laboratory Kolbe in Germany. IR spectra were recorded on a Perkin-Elmer UATR Two FT-IR spectrometer. Electrochemical measurements were performed at room temperature under argon using an Autolab PGstat10 potentiostat controlled by GPES4 software. A three-electrode cell system was used with a glassy carbon working electrode, a platinum counter electrode and an Ag/AgCl reference electrode. All electrochemistry measurements were done in DMF solution with tetrabutylammonium hexafluoridophosphate as the supporting electrolyte. All potentials are referenced to the internal reference system Fc^+/Fc, which under these conditions was found at 0.54 V *vs*. Ag/AgCl in DMF. Electrocatalysis experiments were carried out by adding different concentrations of acetic acid to the DMF solution of complexes. Controlled-potential coulometry (CPC) experiments were done with the same three-electrode cell system and electrodes. CPC experiments were recorded with an Autolab PGstat10 potentiostat controlled by GPES4 software. Gas chromatographic analysis was performed on a Shimadzu gas chromatograph GC-2010 at 35 °C fitted with a Supelco Carboxen 1010 molecular sieve column. Helium was used as the carrier

gas, and compounds were detected using a thermal conductivity detector operated at 80 mA. The total volume of H_2 produced during the reaction was calculated using a calibration line, which was obtained using the external reference method by injection of known amounts of H_2 into the GC using a Hamilton gas-tight syringe (see Figure AI.3). A solution of complexes **(5)** or **(6)** in DMF (5 ml, 0.5 mM) was placed into a three-electrode cell and prior to each measurement the system was deaerated by bubbling with helium for 10 min. The system was closed, and the headspace was pumped through the solution for 1 min. Afterward, the headspace pumping was temporarily stopped to allow equilibration of the pressure, then the GC measurement was started with a 0.5 mL sample of the headspace injection. The GC valve and the pump (KNF NMS 010 L micro diaphragm pump) were enclosed in a helium-purged housing to prevent air from leaking into the system.

2.5.3 Single Crystal X-ray Crystallography

All reflection intensities were measured at 110(2) K using a SuperNova diffractometer (equipped with Atlas detector) with Mo *K*α radiation (λ = 0.71073 Å) for **(3)** and Cu *K*α radiation (*λ* = 1.54178 Å) for **(5)** and **(6)** under the program CrysAlisPro (Version 1.171.36.32 Agilent Technologies, 2013). The same program was used to refine the cell dimensions and for data reduction. The structures were solved with the program SHELXS-2014/7 and were refined on F^2 with SHELXL-2014/7.[25] Numerical absorption correction based on gaussian integration or Analytical numeric absorption correction over a multifaceted crystal model was applied using CrysAlisPro. The temperature of the data collection was controlled using the system Cryojet (manufactured by Oxford Instruments). The H atoms were placed at calculated positions using the instructions AFIX 23, AFIX 43 or AFIX 137 with isotropic displacement parameters having values 1.2 or 1.5 *U*eq of the attached C atoms.

Additional notes on the structure determinations:

(3) The structure was refined in the space group $P2_1$. The absolute configuration was established by anomalous-dispersion effects in diffraction measurements on the crystal. The Flack parameter refines to −0.002(5). CCDC 1537790 contains the supplementary crystallographic data for [Ni(pbSmSe)].

(5) The crystal lattice contains some amount of significantly disordered solvent molecules found in 'channels' along the **c** direction. Their contribution has been taken out using the SQUEEZE (Spek, 2009) procedure in the final refinement.[26]

(6) The coordination sphere around the Ni center in the complex as well as the CO coordinated to the iron center are found to be slightly disordered over two orientations; the occupancy factor of the major component of the disorder refines to 0.9585(6). Disorder may occur as both orientations have very similar space-filling requirements. CCDC 1537791 and 1537792 contain the supplementary crystallographic data for [Ni(pbSmSe)Fe(CO)Cp](PF_6) and [Ni(xbSmSe)Fe(CO)Cp](PF_6).

2.5.4 Synthesis of Ligand Precursor (1)

A solution of selenourea (1.2 g, 9.6 mmol) in 10 ml ethanol was added to a solution of 1,9-dichloro-3,7-dithia-2,2,8,8-tetramethylnonane (1,4 g, 4.83 mmol) in 5 ml ethanol. The reaction mixture was refluxed for 30 min. The solution was allowed to cool, and the solid product was isolated by filtration. The product was washed with cold ethanol and diethyl ether, and dried in vacuo yielding a white powder. Yield: 2.2 g (86%). ^{1}H NMR (300 MHz, $(CD_3)_2SO$)= δ (ppm): 9.41 (d, J= 11.3 Hz, 8H, NH), 3.61 (s, 4H, CH_2), 2.66 (t, J= 7.2 Hz, 4H, CH_2), 1.73 (q, J= 7.1 Hz, 2H, CH_2), 1.66 (s, 12H, CH_3). ^{13}C NMR (75 MHz, $(CD_3)_2SO$): δ (ppm)= 167.02 ($C(NH)NH_2$), 46.31 (CH_2-Se), 40.57 (CH_2-S), 29.67 (CH_2-CH_2S), 28.07 (CH_3). ESI-MS (H_2O): 233.1, calcd: 233.01 $[M-2Cl]^{2+}$.

2.5.5 Synthesis of [Ni(pbSmSe)] (3)

A solution of NMe_4OH (558 mg, 3.08 mmol), ligand precursor **(1)** (824 mg, 1.54 mmol) and $Ni(acac)_2$ (396 mg, 1.54 mmol) in 170 ml ethanol was refluxed for 1 h. The solvent was evaporated until approximately 30 ml solvent remained, resulting in a green precipitate. The solid was collected by filtration and washed with ethanol. Yield: 429 mg (64%). ^{1}H NMR (300 MHz, CD_2Cl_2) δ (ppm): 2.64 (t, J= 7.1 Hz, 4H, CH_2-S), 2.41 (s, 4H, CH_2-Se), 2.22 (m, 2H, CH_2-CH_2S), 1.57 (s, 12H, CH_3). ^{13}C NMR (75 MHz, CD_2Cl_2):δ (ppm): 29.19 (CH_2, CH_2-CH_2S), 28.80 (CH_2, CH_2-Se), 26.70 (CH_3), 25.39 (CH_2-CH_2S). HR-MS (CH_2Cl_2): 436.89255, calcd: 436.89196 $[M+H]^+$. Elemental Analysis calcd (%) for $C_{11}H_{22}NiS_2Se_2 \cdot 0.2$ $N(CH_3)_4Cl$: C: 31.02 H: 5.38; found C: 30.73 H: 5.86.

2.5.6 Synthesis of [Ni(pbSmSe)Fe(CO)Cp](PF_6) (5)

A solution of [Ni(pbSmSe)] (400 mg, 0.91 mmol) and [$FeCp(CO)_2I$] (279 mg, 0.91 mmol) in 25 ml dichloromethane was stirred at RT for 2 days. The mixture was filtered to remove an insoluble precipitate and the solvent was evaporated using the Schlenk line. The resulting solid was washed with diethyl ether resulting in a brown precipitate which was dried in vacuo. A

solution of NH_4PF_6 (300 mg, 1.84 mmol) in 10 ml acetonitrile was added to the brown solid and the mixture was stirred for 4 h. The solvent was evaporated until dryness, the remaining solid was dissolved in dichloromethane (5 ml) and the solution was filtered to remove NH_4I. A large amount (~30 ml) of diethyl ether was added into the dichloromethane solution, and the mixture was cooled at −35 °C overnight. The resulting brown precipitate was collected by filtration and dried in vacuo. Yield: 105 mg (20%). ^{1}H NMR (300 MHz, CD_2Cl_2) δ (ppm): 4.75 (s, Cp). ESI-MS (CH_3CN): 584.9, calcd: 584.9 $[M-PF_6]^+$, 612.9, calcd: 612.9 $[M-(PF_6)+(CO)]^+$ and 556.9, calcd: 556.9 $[M-(PF_6)-(CO)]^+$. Elemental Analysis calcd (%) for $C_{17}H_{27}F_6FeNiOPS_2Se_2 \cdot 0.25(C_2H_5)_2O$: C: 28.92 H: 3.98; found C: 29.00 H: 3.93. IR (neat): $\tilde{\nu}$ = 2035 (s) , 1987 and 1918 (CO stretch) cm^{-1}, 830 (PF_6 stretch) cm^{-1}.

2.5.7 Synthesis of [Ni(xbSmSe)Fe(CO)Cp](PF$_6$) (6)

A solution of [Ni(xbSmSe)] (200 mg, 0.40 mmol) and [FeCp(CO)$_2$I] (122 mg, 0.40 mmol) in 15 ml dichloromethane was stirred at RT for 2 days. The mixture was filtered to remove an insoluble precipitate and the solvent was evaporated using the Schlenk line. The residue was washed with diethyl ether, resulting in a brown powder which was dried in vacuo. A solution of NH_4PF_6 (132 mg, 0.81 mmol) in 5 ml acetonitrile was added to the brown solid and the resulting mixture was stirred for 4 h. The solvent was evaporated until dryness, the remaining solid was dissolved in dichloromethane (5 ml) and the solution was filtered to remove NH_4I. A large amount (~30 ml) of diethyl ether was added into the dichloromethane solution, and the mixture was cooled at −35 °C overnight. The resulting brown precipitate was collected by filtration and dried in vacuo. Yield: 18 mg (6%). ^{1}H NMR (300 MHz, CD_2Cl_2) δ (ppm): 7.93 (m, Ar), 7.31 (m, Ar), 4.74 (s, Cp), 1.76 (s, -CH_3), 1.66 (s, -CH_3).ESI-MS (CH_3CN): 619.0, calcd: 618.9 $[M-CO-PF_6]^+$, 647.0, calcd: 646.9 $[M-PF_6]^+$. Elemental Analysis calcd (%) for $C_{22}H_{29}F_6FeNiOPS_2Se_2 \cdot 0.3CH_2Cl_2$: C: 32.56 H: 3.64; found C: 32.33 H 3.77. IR (neat): $\tilde{\nu}$ = 1923 (CO stretch) cm^{-1}, 828 (PF_6 stretch) cm^{-1}.

2.6 Acknowledgements

G. K. Spijksma is gratefully acknowledged for HRMS measurement and H. Al Habobe is gratefully acknowledged for ESI-MS measurements.

2.7 References

1. D. Sellmann, F. Lauderbach and F. W. Heinemann, *Eur. J. Inorg. Chem.* 2005, 371.
2. H. Ogata, W. Lubitz and Y. Higuchi, *Dalton Trans.* 2009, 7577.

3. L. De Gioia, *Bioinorganic Fundamentals and Applications: Metals in Natural Living Systems and Metals in Toxicology and Medicine,* Elsevier, 2013, Vol. 3.
4. A. Volbeda, M.H. Charon, C. Piras, E.C. Hatchikian, M. Frey, J. Fontecilla-Camps, *Nature* 1995, 373, 580.
5. E. Garcin, X. Vernede, E. Hatchikian, A. Volbeda, M. Frey and J. Fontecilla-Camps, *Structure* 1999, **7**, 557.
6. M. C. Marques, C. Tapia, O. Gutierrez-Sanz, A. R. Ramos, K. L. Keller, J. D. Wall, A. L. De Lacey, P. M. Matias, I. A. C. Pereira, *Nat. Chem. Biol.,* 2017, **13**, 2335.
7. C. Wombwell and E. Reisner, *Chem. Eur. J.* 2015, **21**, 8096.
8. D. Steinmann, T. Nauser and W. H. Koppenol, *J. Org. Chem.* 2010, **75**, 6696.
9. C. S. Baltazar, M. C. Marques, C. M. Soares, A. M. DeLacey, I. A. Pereira and P. M. Matias, *Eur. J. Inorg. Chem.* 2011, 948.
10. M. Fontecave and V. Artero, *C. R. Chim.* 2011, **14**, 362.
11. S. Canaguier, M. Field, Y. Oudart, J. Pécaut, M. Fontecave and V. Artero, *Chem. Commun.* 2010, **46**, 5876.
12. S. Canaguier, V. Artero and M. Fontecave, *Dalton Trans* 2008, 315.
13. S. Ogo, K. Ichikawa, T. Kishima, T. Matsumoto, H. Nakai, K. Kusaka and T. Ohhara, *Science* 2013, **339**, 682.
14. B. E. Barton and T. B. Rauchfuss, *J. Am Chem. Soc.* 2010, **132**, 14877.
15. T. Liu, S. Chen, M. J. O'Hagan, M. R. DuBois, R. M. Bullock and D. L. DuBois, *J Am Chem Soc*, 2012, **134**, 6257.
16. Y. Oudart, V. Artero, J. Pécaut, C. Lebrun and M. Fontecave, *Eur. J. Inorg. Chem.,* 2007, 2613.
17. S. Canaguier, L. Vaccaro, V. Artero, R. Ostermann, J. Pecaut, M. J. Field and M. Fontecave, *Chem. Eur. J.*, 2009, 15, 9350.
18. Y. Oudart, V. Artero, L. Norel, C. Train, J. Pécaut and M. Fontecave, *J. Organomet. Chem.,* 2009, **694**, 2866.
19. G. M. Chambers, R. Angamuthu, D. L. Gray and T. B. Rauchfuss, *Organometallics*, 2013, **32**, 6324.
20. W. Zhu, A. C. Marr, Q. Wang, F. Neese, D. J. Spencer, A. J. Blake, P. A. Cooke, C. Wilson and M. Schröder, *Proc. Natl. Acad. Sci. USA* 2005, **102**, 18280.
21. K. Weber, I. Heise, T. Weyhermüller and W. Lubitz, *Eur. J. Inorg. Chem.* 2014, 148.
22. J. A. Verhagen, D. D. Ellis, M. Lutz, A. L. Spek and E. Bouwman, *Dalton Trans.* 2002, 1275.
23. C. Costentin, S. Drouet, M. Robert and J. M. Savéant, *J. Am. Chem. Soc.* 2012, **134**, 11235.
24. N. Elgrishi, B. M. Chambers and M. Fontecave, *Chem. Sci.* 2015**, 6**, 2522.
25. G. M. Sheldrick, *Acta Cryst.* 2015, **C71**, 3.
26. A. L. Spek, *Acta Cryst.* 2009, **D65**, 148.

Chapter 3

Nickel-Ruthenium-Based Complexes as Biomimetic Models of [NiFe] and [NiFeSe] Hydrogenases for Dihydrogen Evolution

Abstract

The two heterodinuclear nickel-ruthenium complexes [Ni(xbSmS)RuCp(PPh$_3$)]PF$_6$ and [Ni(xbSmSe)RuCp(PPh$_3$)]PF$_6$ (H$_2$xbSmS = 1,2-bis(4-mercapto-3,3-dimethyl-2-thiabutyl)benzene, H$_2$xbSmSe = 1,2,-bis(2-thiabutyl-3,3-dimethyl-4-selenol)benzene, Cp = cyclopentadienyl) were synthesized as biomimetic models of [NiFe] and [NiFeSe] hydrogenases. The X-ray structural analyses of the complexes show that the two NiRu complexes are isomorphous; in both NiRu complexes the nickel(II) centers are found in a square-planar environment with two thioether donor atoms and two thiolate/selenolate donors that are bridging to the ruthenium(II) center. The Ru(II) ion is further coordinated to a η^5-cyclopentadienyl group and a triphenylphosphine ligand. These complexes catalyze the hydrogen evolution in the presence of acetic acid in acetonitrile solution at around −2.20 V vs. Fc$^+$/Fc with overpotentials of 810 and 830 mV, thus they can be regarded as functional models of the [NiFe] and [NiFeSe] hydrogenases.

This chapter is submitted for publication: G. Gezer, S. Verbeek, M. A. Siegler, and E. Bouwman.

3.1 Introduction

Hydrogenases are enzymes that have a catalytic role in the oxidation of molecular hydrogen (H_2) and the reduction of protons; this catalytic interconversion plays an important role in the metabolism of a number of algae and bacteria.[1] The hydrogenase enzymes are relevant for future energy applications since dihydrogen is a clean source of energy.[2] Researchers are looking for new and cleaner ways for the production of dihydrogen gas and hydrogenases might be a solution for our energy problem.[3] In nature these enzymes are highly efficient catalysts with turnover frequencies ranging between 1500-9000 per second at 30 °C. Unfortunately, it is incredibly difficult to isolate these enzymes in a pure form, and they are very fragile and air-sensitive.[4, 5] With a biomimetic approach the active site of the enzyme can be mimicked by way of the synthesis and characterization of low-molecular mass compounds.[5] Ample research has been done on [NiFe] hydrogenases to unravel its catalytic activity and mechanism in the oxidation of dihydrogen and reduction of protons.[6] A significant amount of data has been gathered over the years concerning the enzyme redox states and the reaction mechanism for the reversible heterolytic splitting of dihydrogen at the [NiFe] hydrogenase active site.[7] The knowledge thus gathered has led to progress in the design, synthesis and characterization of models of the active site of [NiFe] and [FeFe] hydrogenases; a variety of interesting structural models has been published over the past decades and many of these have been investigated for their electrocatalytic activity.[8-11] Reported complexes include NiS_4 compounds,[6,12] mononuclear Ni/Co/Fe complexes with phosphine ligands,[13] thiolate-bridged [NiFe] carbonyl complexes,[14,15] and a number of [NiRu] heterobimetallic complexes.[9,10,16,17] The choice of substituting iron by ruthenium in mimicking the active site is based on the fact that ruthenium complexes are active catalysts in hydrogenation and hydrogen transfer reactions and generally form more stable compounds. Most importantly Ru(II) ions are able to accept both hard and soft ligands such as hydride and dihydrogen, which makes it suitable for replacing the Fe center in models of the [NiFe] hydrogenases.[18] In some [NiFe] hydrogenase mimics a Cp^- or Cp^{*-} ligand has been used instead of the CO ligands coordinated to the iron center; it was shown that this created lower overpotentials for proton reduction.[7,15,19] So far, mostly models for the active site of [NiFe] hydrogenases have been studied, but recently a number of reports describe the first [NiFe] models for the active site in [NiFeSe] hydrogenase containing an S_2Se_2 coordination environment around the nickel center instead of S_4.[20,21,22] However, so far no heterodimetallic nickel-ruthenium complexes have been reported comprising a NiS_2Se_2 unit as mimics of the

[NiFeSe] hydrogenase active site. In this chapter, we describe the synthesis and characterization of the two nickel-ruthenium complexes [Ni(xbSmS)RuCp(PPh_3)]PF_6 and [Ni (xbSmSe)RuCp(PPh_3)]PF_6 as mimics of the active site of the [NiFe] and [NiFeSe] hydrogenases. The compound [Ni(xbSmS)RuCp(PPh_3)]PF_6 has been previously reported without crystallographic information.[10] Herein, we report the detailed structural and electrochemical analysis of the compounds [Ni(xbSmS)RuCp(PPh_3)]PF_6 and [Ni(xbSmSe)RuCp(PPh_3)]PF_6 and their electrocatalytic properties in proton reduction.

3.2 Results

3.2.1 Synthesis and Characterization

The two heterodinuclear compounds [Ni(xbSmS)RuCp(PPh_3)]PF_6 and [Ni(xbSmSe)RuCp(PPh_3)]PF_6 were synthesized following the procedure shown in Scheme 3.1, by a reaction of the nickel complexes with [RuCp(PPh_3)$_2$Cl]. The mononuclear nickel compounds and [RuCp(PPh_3)$_2$Cl] have been reported earlier and were synthesized according to the published methods.[12,21,23] Reaction of the mononuclear nickel complexes with one equivalent of [RuCp(PPh_3)$_2$Cl] in dichloromethane provided the compounds [Ni(xbSmS)RuCp(PPh_3)]Cl and [Ni(xbSmSe)RuCp(PPh_3)]Cl. The counter ion was exchanged by the addition of NH_4PF_6 to a solution of the chloride compounds in acetonitrile resulting in the compounds [Ni(xbSmS)RuCp(PPh_3)]PF_6 **(1)** and [Ni(xbSmSe)RuCp(PPh_3)]PF_6 **(2)** in 20% and 29% yield, respectively. The [NiRu] complexes were characterized by using ^{1}H, ^{31}P, ^{13}C NMR spectroscopy, mass spectrometry, elemental analysis and single crystal X-ray crystallography. Both [NiRu] complexes give rise to sharp, clear resonances in the ^{1}H NMR, ^{31}P NMR and ^{13}C NMR spectra. In the ^{1}H NMR spectra of both compounds the resonances of the four methyl groups are observed as two singlets and the four methylene groups are observed as four doublets.

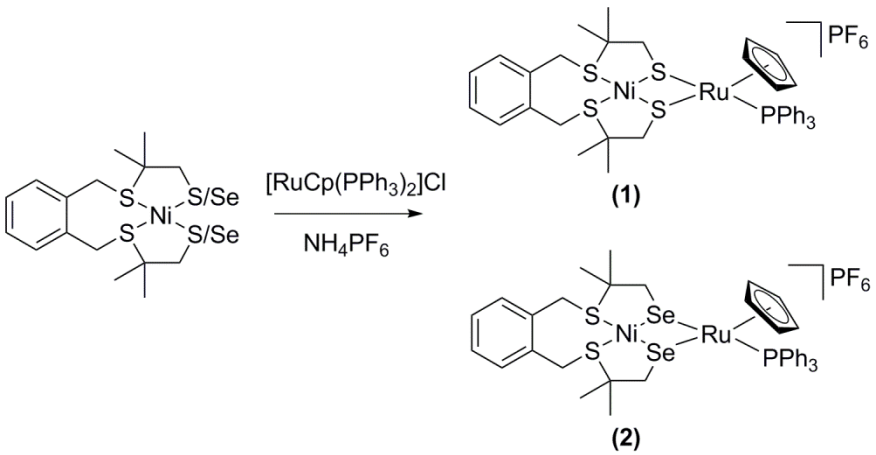

Scheme 3.1: Synthesis scheme of the heterodinuclear NiRu complexes **(1)** and **(2)** from the reaction of [Ni(xbSmS)] and [Ni(xbSmSe)] with $[RuCp(PPh_3)_2]Cl$.

3.2.2 Description of the Structures

Single crystals of the compounds $[Ni(xbSmS)RuCp(PPh_3)]PF_6$ **(1)** and $[Ni(xbSmSe)RuCp(PPh_3)]PF_6$ **(2)** were obtained by vapor diffusion of pentane into acetone solutions of the complexes; crystallographic data are provided in Table AIII.1. Projections of the molecular structures of the heterodinuclear complexes are shown in Figure 3.1; selected bond distances and angles are listed in Table 3.1. The complexes **(1)** and **(2)** both crystallize in the triclinic space group $P\bar{1}$ and are isomorphous. In both structures, the PF_6^- counter ion, the lattice pentane solvent and the triphenylphosphine groups are disordered over two orientations. Both heterodinuclear [NiRu] complexes contain a Ni(II) center in a square-planar environment formed by the two thioethers and two thiolate or selenolate donor atoms from the tetradentate ligand. Both thiolate/selenolate donors are bridging to a Ru(II) center that is coordinated in a pseudo-octahedral 'piano stool' geometry that is completed by the Cp^- and the PPh_3 ligand. This 'piano stool' configuration is most common for cyclopentadienyl complexes with a Ru(II) centre.[9,10,16,17] The Ni-Ru distance (2.8435(4) Å) in complex **(1)** is determined by the sulfur atoms from the thiolate groups which are involved in the bent Ni(μ-$SR)_2$Ru butterfly core and is much shorter compared to previously reported [NiRu] complexes which also contain a Cp^- ligand.[10] For complex **(2)** the Ni-Ru distance (2.9246(5) Å) is slightly longer because of the larger ionic radius of the selenolate donor atom. Apart from the shorter Ni-Ru bonds, the hinge angle of the butterfly core, which is defined by the intersection of the least-square planes defined by NiS_2/$NiSe_2$ and RuS_2/$RuSe_2$, is much sharper (98.80° for **(1)** and 96.57°for **(2)**) than those in previously reported [NiRu] compounds.[9, 10] The metal-

selenolate bond distances in complex **(2)** are approximately 0.1 Å longer than the metal-thiolate bond lengths in complex **(1)**, similar to the differences observed in the reported [NiFe] complexes also containing [Ni(xbSmS)] and [Ni(xbSmSe)].[21] The Ni-thiolate distance in [Ni(xbSmS)RuCp(PPh_3)]PF_6 is 2.19 Å, which is comparable to the distance of 2.21 Å in the [NiFe] hydrogenase active site.[24] The Ni-Se distance in [Ni(xbSmSe)RuCp(PPh_3)]PF_6 is 2.31 Å, significantly shorter than the 2.46 Å found in the [NiFeSe] hydrogenase active site.[25]

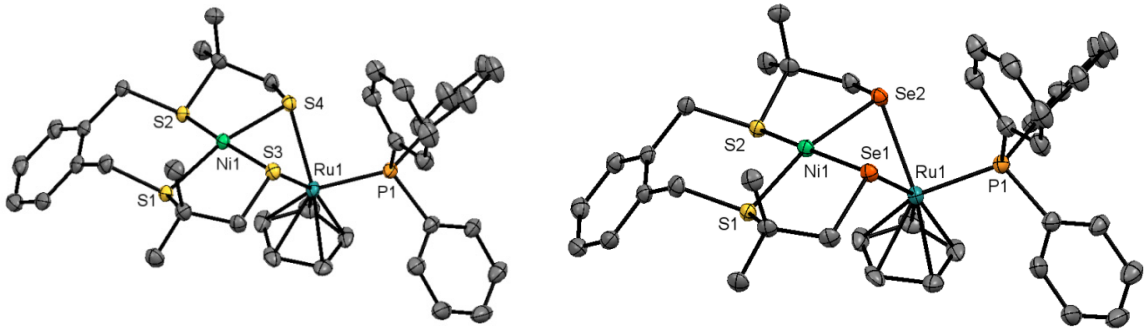

(a) (b)

Figure 3.1: Displacement ellipsoids plots (50% probability level) of (a) [Ni(xbSmS)RuCp(PPh_3)]PF_6 **(1)** and (b) [Ni(xbSmSe)RuCp(PPh_3)]PF_6 **(2)** at 110(2) K. Hydrogen atoms, PF_6^- anion, lattice solvent molecules, and disorder are omitted for clarity.

Table 3.1: Selected bond lengths (Å) and angles (°) for the complexes **(1)** and **(2)**

Distances (Å)	**(1)**	**(2)**	Distances (Å)	**(1)**	**(2)**
Ni1-S1	2.1847(6)	2.1898(8)	Ru1-P1	2.3180(5)	2.3174(7)
Ni1-S2	2.1824(6)	2.1881(8)	Ru1-S4/Se2	2.4256(5)	2.5271(3)
Ni1-S3/Se1	2.1935(6)	2.3107(5)	Ru1-S3/Se1	2.4275(5)	2.5298(3)
Ni1-S4/Se2	2.1876(6)	2.3050(5)	Ni1-Ru1	2.8435(4)	2.9246(5)
Ru1-Cp(centroid)	2.191	2.189			
Angles (°)	**(1)**	**(2)**	Angles (°)	**(1)**	**(2)**
P1-Ru-S4/Se2	92.362(18)	91.999(19)	S2-Ni-S4/Se2	90.21(2)	90.52(2)
P1-Ru-S3/Se1	92.674(19)	92.271(19)	S2-Ni-S1	94.98(2)	94.24(3)
S4/Se2-Ru-S3/Se1	73.502(17)	74.449(10)	Ni-S3/Se1-Ru	75.767(18)	74.188(14)
S4/Se2-Ni-S3/Se1	83.03(2)	83.024(17)	Ni-S4/Se2-Ru	75.909(18)	74.334(14)
S1-Ni-S3/Se1	90.45(2)	90.73(2)			

3.2.3 Electrochemical Analyses

The electrochemical properties of the nickel-ruthenium complexes using cyclic voltammetry were investigated in acetonitrile with 0.1 M tetrabutylammonium hexafluoridophosphate as the supporting electrolyte with a scan rate of 200 mV s^{-1}. A glassy carbon electrode was used as a working electrode and Ag/AgCl was used as a reference electrode, but all the potentials are reported vs. the ferrocene/ferrocinium ($Fc^{0/+}$) couple. The voltammograms of the complexes **(1)** and **(2)** are highly similar; both show one irreversible wave at −1.70 V and −1.65 V *vs*. Fc/Fc^{+} followed by two small waves at −2.01, −2.25 V and −2.18, −2.40 *vs*. Fc/Fc^{+}, respectively (Figure 3.2). The cyclic voltammograms of the mononuclear nickel complexes show one irreversible wave at −1.96 V and −1.93 V *vs*. Fc/Fc^{+} for the compounds [Ni(xbSmS)] and [Ni(xbSmSe)], respectively (Figure AIII.1-2). The cyclic voltammogram of the reference compound **[**$RuCp(PPh_3)(MeCN)_2]PF_6$ shows one irreversible reduction at −2.54 V *vs*. Fc/Fc^{+} (Figure AIII.5).

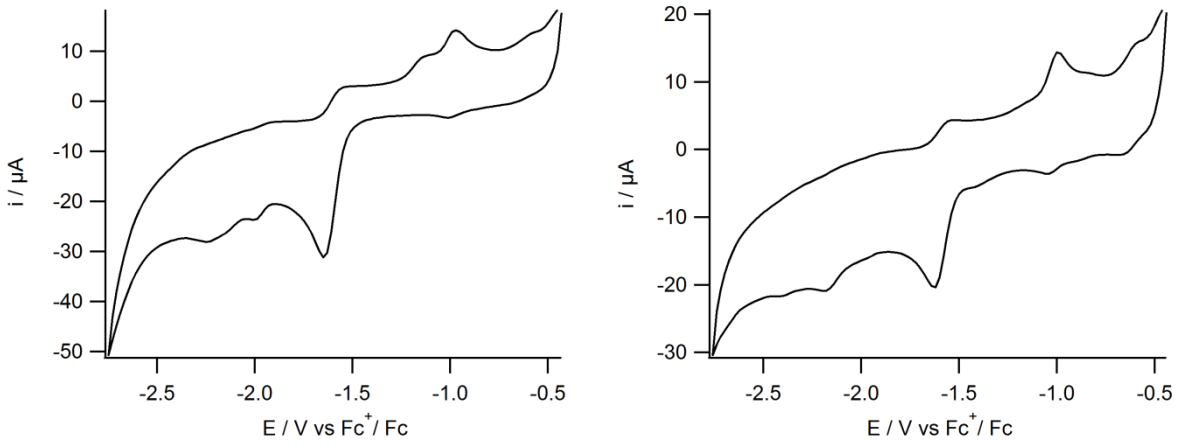

(a) (b)

Figure 3.2: Cyclic voltammograms of **(1)** (a) and **(2)** (b) (1 mM) in an MeCN solution containing $TBAPF_6$ (0.1 M) as the supporting electrolyte and using a glassy carbon electrode at a scan rate of 200 mV s^{-1}.

3.2.4 Electrocatalytic Hydrogen Evolution in the Presence of HOAc

The activity of the compounds in electrocatalytic proton reduction was investigated using cyclic voltammetry with addition of varying amounts of HOAc to MeCN solutions of the NiRu complexes. Both complexes show a catalytic wave at around −2.20 V *vs*. Fc/Fc^{+}, which shifts to more negative potentials with the addition of higher amounts of acid (Figure 3.3).

The overpotential for electrocatalytic proton reduction at an acetic acid concentration of 10 mM of the complexes **(1)** and **(2)** has been calculated using the half-wave potentials, taking homoconjugation of the acid into account.[26] Both complexes display quite similar overpotentials, being 810 mV for complex **(1)** and 830 mV for complex **(2)**. In order to prove that indeed dihydrogen gas is formed in the electrocatalytic reaction, a controlled-potential coulometry (CPC) experiment was carried out on a 1.0 mM solution of complexes **(1)** and **(2)** in acetonitrile (5 ml) in the presence of 7 µl of HOAc (10 equivalents) at −2.35 V *vs*. Fc/Fc^+. The produced dihydrogen gas was quantified volumetrically by GC analysis. The CPC experiments were run for 1 h, while the solution was stirred continuously. Using complex **(1)** as the electrocatalyst for proton reduction, a total of 92 µl H_2 was produced for 1 mM complex in 1 h with 74% faradaic yield. Using complex **(2)** as the electrocatalyst a total of 106 µl H_2 was produced in 1 h with 73% faradaic yield. In the absence of the catalyst formation of H_2 is not observed.

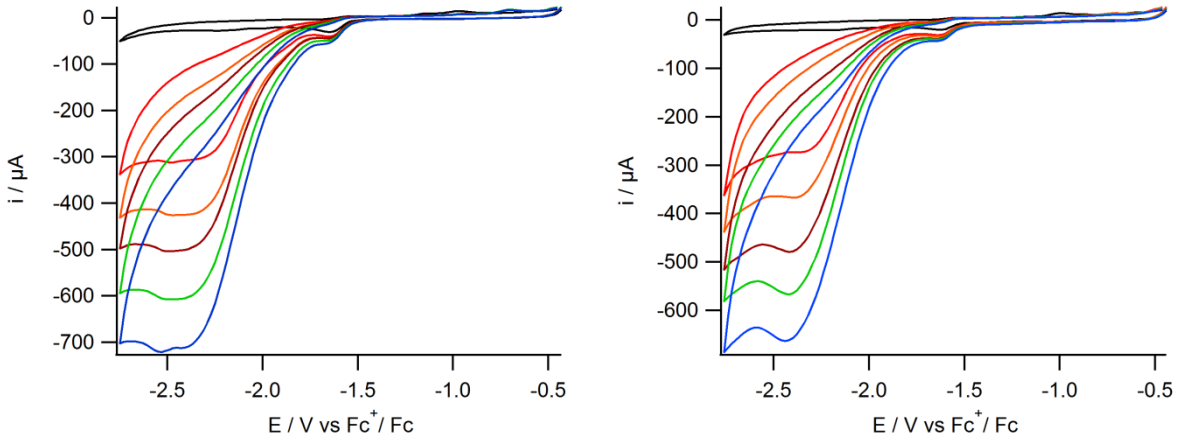

(a) (b)

Figure 3.3: Cyclic voltammograms of **(1)** (a) and **(2)** (b) (1mM) in an MeCN solution of $TBAPF_6$ (0.1 M) using a glassy carbon electrode at a scan rate of 200 mV s^{-1} in the presence of 0 (black), 10 (red), 20 (orange), 30 (brown), 40 (green), 50 (blue) mM of acetic acid.

3.3 Discussion

In this chapter the compounds $[Ni(xbSmS)RuCp(PPh_3)]PF_6$ and $[Ni(xbSmSe)RuCp(PPh_3)]PF_6$ are described as potential mimics of the active site of the [NiFe] and [NiFeSe] hydrogenases. Single crystal X-ray crystallography has shown that the two structures are isomorphous and both have some structural similarities with the active site of the

[NiFe] and [NiFeSe] hydrogenases, but with a Ru ion rather than an Fe center. Although it was anticipated that the compounds would have different electrochemical properties because of the different physical properties of sulfur and selenium, the electrochemical studies of the two compound showed quite similar results: changing the thiolate donor atoms to selenolate does not result in a significant difference of the electrocatalytic properties. Comparison of the cyclic voltammograms of NiRu compounds with those of the mononuclear nickel complexes and the reference compound **[**$RuCp(PPh_3)(MeCN)_2]PF_6$ indicates that the metal centers do not dissociate during catalytic turnover. At 10 equivalents of H^+ the catalytic proton reduction of the mononuclear nickel complex seemingly occurs at lower potentials, but CPC showed the production of lower amounts of H_2 compared to the NiRu compound. The compound $[RuCp(PPh_3)(MeCN)_2]PF_6$ is also active in proton reduction, but only at a much more negative potential, which also indicates that dissociation of the NiRu compound in solution does not occur (see figure AIII.1-2-5). The electrocatalytic properties of a number of different $[Ni(xbSmS)RuCp(L)]^+$ complexes based on the compound [Ni(xbSmS)] have been reported.[10] The complexes $[Ni(xbSmS)RuCp(CO)]PF_6$ and $[Ni(xbSmS)RuCp(dmso)]PF_6$ were shown to have higher catalytic activity than $[Ni(xbSmS)RuCp(PPh_3)]PF_6$ whereas the compound $[Ni(xbSmS)RuCp(PCy_3)]PF_6$ has a lower activity.[10] Unfortunately, because of the different reaction conditions used by us the catalytic activity of our NiRu systems cannot be compared with those reported.[10] Based on these results, however, it is difficult to discriminate the different effects that the ligands and the two metal centers have on the catalytic efficiency of the compound, because of the irreversible reduction waves of both NiRu complexes. The irreversibility of the reduction processes in the NiRu compounds might indicate that the electrocatalysis is due to the formation of a heterogeneous catalyst by the deposition of nickel onto the glassy carbon electrode. However, the electrode was polished in between each single measurement and proton reduction was not observed when using the electrode without polishing in a new solution without added NiRu catalyst. Although these experiments confirm that our complexes retain their structures during the catalytic reaction, the understanding of the active species is still not complete.

3.4 Conclusion

Two NiRu complexes are reported as mimics of the active sites of [NiFe] and [NiFeSe] hydrogenases. Both complexes are structurally highly similar and differ only in the bridging thiolate/selenolate donor atoms. The crystallographic studies show that the compounds in fact

are isomorphous, with the only difference being the longer bond distances in the selenolate analogue. Although cyclic voltammetry and GC analysis of electrocatalytic proton reduction show that both complexes catalyze the hydrogen evolution reaction, the results show that changing the thiolate donor to a selenolate does not make a significant difference in either the activity or the overpotential. Further investigations will be done in order to improve catalytic activity and lower the overpotential for the hydrogen evolution reaction.

3.5 Experimental

3.5.1 Materials

All experiments were performed using standard Schlenk techniques or in a glovebox under an argon or nitrogen atmosphere unless otherwise noted. Chemicals were purchased from Acros or Aldrich and were used without further purification. Organic solvents were deoxygenated by the freeze-pump-thaw method and were dried over molecular sieves prior to use. The NMR solvent CD_2Cl_2 for metal complexes was deoxygenated by the freeze-pump-thaw method and was stored over molecular sieves in a glovebox. The complexes [Ni(xbSmS)],[12] [Ni(xbSmSe)],[21] and $[RuCp(PPh_3)_2Cl]$[23] were synthesized according to published methods.

3.5.2 Physical Measurements

NMR spectra were recorded on a 300 MHz Bruker DPX 300 spectrometer and chemical shifts were referenced against the solvent peak. Mass spectra were obtained with a Finnigan TSQ-quantum instrument using ESI. Elemental analyses were performed by the Microanalytical Laboratory Kolbe in Germany. Electrochemical measurements were performed at room temperature under an argon atmosphere using an Autolab PGstat10 potentiostat controlled by GPES4 software. A three-electrode cell system was used with a glassy carbon working electrode, a platinum counter electrode and an Ag/AgCl reference electrode. All electrochemistry measurements were done in acetonitrile solution with tetrabutylammonium hexafluoridophosphate as the supporting electrolyte; after each run ferrocene was added as an internal reference. All potentials are reported vs the internal reference system Fc/Fc^+, which under these conditions was found at −0.43 V *vs*. Ag/AgCl in MeCN. Electrocatalysis experiments were carried out by adding different concentrations of acetic acid to the MeCN solution of complexes. Controlled-potential coulometry (CPC) experiments were done with the same three-electrode cell system and electrodes. CPC experiments were recorded with an Autolab PGstat10 potentiostat controlled by GPES4 software. Gas chromatographic analysis

was performed on a Shimadzu gas chromatograph GC-2010 at 35 °C fitted with a Supelco Carboxen 1010 molecular sieve column. Helium was used as the carrier gas, and analytes were detected using a thermal conductivity detector operated at 80 mA. The total volume of H_2 produced during the reaction was calculated using a calibration line, which was obtained using the external reference method by injection of known amounts of H_2 into the GC using a Hamilton gas-tight syringe (see Figure AI.3). Complexes **(1)** and **(2)** (1 mmol in 5 ml of acetonitrile) were placed into the three-electrode cell and prior to the each measurement the systems were deaerated by bubbling with helium for 10 min. The system was closed, and the headspace was pumped through the solution for 1 min. Before each GC sampling the headspace pumping was temporarily stopped to allow equilibration of the pressure, then GC measurement was started with a 0.5 mL sample of the headspace injection. The GC valve and the pump (KNF NMS 010 L micro diaphragm pump) were enclosed in a helium-purged housing to prevent air leaking into the system.

3.5.3 Single Crystal X-ray Crystallography

All reflection intensities were measured at 110(2) K using a SuperNova diffractometer (equipped with Atlas detector) with Cu *K*α radiation (λ = 1.54178 Å) under the program CrysAlisPro (Version 1.171.36.32 Agilent Technologies, 2013). The same program was used to refine the cell dimensions and for data reduction. The structures were solved with the program SHELXS-2014/7 (Sheldrick, 2015) and were refined on F^2 with SHELXL-2014/7.[27] Analytical numeric absorption correction using a multifaceted crystal model was applied using CrysAlisPro. The temperature of the data collection was controlled using the system Cryojet (manufactured by Oxford Instruments). The H atoms were placed at calculated positions using the instructions AFIX 23, AFIX 43 or AFIX 137 with isotropic displacement parameters having values 1.2 or 1.5 *U*eq of the attached C atoms. The structures are partly disordered. The three phenyl groups of the triphenylphosphine ligand, the PF_6^- counterion, and the lattice pentane solvent molecule are found to be disordered over two orientations (all occupancy factors can be retrieved from the .cif file). The two structures are isomorphous.

3.5.4 Synthesis of [Ni(xbSmS)RuCp(PPh$_3$)](PF$_6$)

[RuCp(PPh_3)$_2$Cl] (179 mg; 0.246 mmol) and [Ni(xbSmS)] (99 mg; 0.246 mmol) were dissolved in DCM (10 mL) and the mixture was stirred for 5 days. The obtained solution was filtered to remove an insoluble precipitate and evaporated until dryness. To the resulting solid 10 ml ethanol was added, the obtained solution was filtered and evaporated under reduced

pressure. A solution of NH_4PF_6 (81.2 mg; 0.498 mmol) in 10 ml acetonitrile was added to the residual solid and the solution was stirred at room temperature for 4 hours. The solvent was evaporated until dryness, the remaining solid was dissolved in dichloromethane (5 ml) and the solution was filtered to remove NH_4I. To the filtrate an excess of diethyl ether was added and the mixture was placed in the freezer (−35°C) overnight. The precipitate was filtered and dried in vacuo to obtain the pure dark purple product in a yield of 49 mg (20%). Single crystals suitable for X-ray structure determination were obtained from vapor diffusion of pentane into acetone solutions of the complex. ^{1}H NMR [300 MHz, CD_2Cl_2, 298 K] δ 7.45 – 7.35 (m, 19H, Ph-H3-6, $P(C_6H_5)_3$), 4.46 (s, 5H, η^5-C_5H_5), 4.19 (d, J = 12.4 Hz, 2H; Ph–$CH_{eq}H_{ax}$–S–), 3.66 (d, J = 12.4 Hz, 2H; Ph–$CH_{eq}H_{ax}$–S–), 2.14 (d, J = 13.4 Hz, 2H; $C(CH_3)_2$–$CH_{eq}H_{ax}$–S–), 1.98 (d, J = 13.4 Hz, 2H; $C(CH_3)_2$– $CH_{eq}H_{ax}$–S–), 1.70 (s, 6H, Me_{ax}), 1.61 (s, 6H, Me_{eq}); ^{31}P {^{1}H} NMR [121.5 MHz, CD_2Cl_2, 298 K] 48.12 (s, PPh_3), −145.16 (sept, J_{PF}= 710 Hz; PF_6); ^{13}C NMR [75 MHz, CD_2Cl_2, 298 K] 135, 132, 131, 128, 79, 47, 35, 26, 24 ppm. ESI-MS (CH_3OH): 830.8, calcd: 831.0 $[M-PF_6]^+$.

3.5.5 Synthesis of [Ni(xbSmSe)RuCp(PPh$_3$)](PF$_6$)

$[RuCp(PPh_3)_2Cl]$ (179 mg; 0.246 mmol) and [Ni(xbSmSe)] (99 mg; 0.246 mmol) were dissolved in DCM (10 mL) and the mixture was stirred for 5 days. The obtained solution was filtered to remove an insoluble precipitate and evaporated until dryness. To the resulting solid 10 ml ethanol was added, the obtained solution was filtered and evaporated under reduced pressure. A solution of NH_4PF_6 (81.2 mg; 0.498 mmol) in 10 ml acetonitrile was added to the residual solid and the solution was stirred at room temperature for 4 hours. The solvent was evaporated until dryness, the remaining solid was dissolved in dichloromethane (5 ml) and the solution was filtered to remove NH_4I. To the filtrate an excess of diethyl ether was added and the mixture was placed in the freezer (−35°C) overnight. The precipitate was filtered and dried in vacuo to obtain the pure dark purple product in a yield of 130 mg (29%). Single crystals suitable for X-ray structure determination were obtained from vapor diffusion of pentane into acetone solutions of the complex. ^{1}H NMR [300 MHz, CD_2Cl_2, 298 K] δ 7.43 – 7.24 (m, 19H, Ph-H3-6, $P(C_6H_5)_3$), 4.45 (s, 5H, η^5-C_5H_5), 4.23 (d, J = 12.6 Hz, 2H; Ph–$CH_{eq}H_{ax}$–S–), 3.63 (d, J = 12.6 Hz, 2H; Ph–$CH_{eq}H_{ax}$–S–), 2.38 (d, J = 12.0 Hz, 2H; $C(CH_3)_2$–$CH_{eq}H_{ax}$–Se–), 2.13 (d, J = 12.3 Hz, 2H; $C(CH_3)_2$– $CH_{eq}H_{ax}$–Se–), 1.75 (s, 6H, Me_{ax}), 1.61 (s, 6H, Me_{eq}); ^{31}P {^{1}H} NMR [121.5 MHz, CD_2Cl_2, 298 K] 46.97 (s, PPh_3), −144.08 (sept, J_{PF}= 714 Hz; PF_6); ^{13}C NMR [75 MHz, CD_2Cl_2, 298 K] 135, 132, 130, 128, 78, 35, 27, 25 ppm.

ESI-MS (CH_3OH): 926.7, calcd: 926.9 $[M-PF_6]^+$. Elemental Analysis calcd (%) for $C_{39}H_{44}F_6NiP_2RuS_2Se_2 \bullet 0.30\ C_5H_{12}$ (1106.57): C 44.86, H 4.50; found: C 44.80, H 4.83.

3.6 Acknowledgements

Mr. J.J.M. van Brussel and Mr. W. Jesse are gratefully acknowledged for performing the ESI-MS measurements.

3.7 References

1. P. M. Vignais, B. Billoud and J. Meyer, *FEMS Microbiol. Rev*, 2001, **25**, 455.
2. H. Ogata, W. Lubitz and Y. Higuchi, *Dalton Trans*, 2009, 7577.
3. J. C. Fontecilla-Camps, A. Volbeda, C. Cavazza and Y. Nicolet, *Chem. Rev.*, 2007, **107**, 4273.
4. H. R. Pershad, J. L. C. Duff, H. A. Heering, E. C. Duin, S. P. J. Albracht and F. A. Armstrong, *Biochemistry*, 1999, **38**, 8992.
5. V. Artero and M. Fontecave, *Coord. Chem. Rev.*, 2005, **249**, 1518.
6. K. Weber, I. Heise, T. Weyhermüller and W. Lubitz, *Eur. J. Inorg. Chem.*, 2014, **2014**, 148.
7. S. Kaur-Ghumaan and M. Stein, *Dalton Trans*, 2014, **43**, 9392.
8. S. Canaguier, V. Fourmond, C. U. Perotto, J. Fize, J. Pecaut, M. Fontecave, M. J. Field and V. Artero, *Chem. Commun.*, 2013, **49**, 5004.
9. Y. Oudart, V. Artero, J. Pécaut, C. Lebrun and M. Fontecave, *Eur. J. Inorg. Chem.*, 2007, 2613.
10. S. Canaguier, L. Vaccaro, V. Artero, R. Ostermann, J. Pecaut, M. J. Field and M. Fontecave, *Chem. Eur. J.*, 2009, **15**, 9350.
11. T. R. Simmons and V. Artero, *Angew. Chem.*, 2013, **52**, 6143.
12. J. A. W. Verhagen, D. D. Ellis, M. Lutz, A. L. Spek and E. Bouwman, *Dalton Trans*, 2002, 1275.
13. T. Liu, S. Chen, M. J. O'Hagan, M. Rakowski DuBois, R. M. Bullock and D. L. DuBois, *J Am Chem Soc*, 2012, **134**, 6257.
14. W. Zhu, A. C. Marr, Q. Wang, F. Neese, D. J. Spencer, A. J. Blake, P. A. Cooke, C. Wilson and M. Schroder, *Proc. Natl. Acad. Sci. USA*, 2005, **102**, 18280.
15. S. Canaguier, M. Field, Y. Oudart, J. Pecaut, M. Fontecave and V. Artero, *Chem. Commun.*, 2010, **46**, 5876.
16. Y. Oudart, V. Artero, L. Norel, C. Train, J. Pécaut and M. Fontecave, *J. Organomet. Chem.*, 2009, **694**, 2866.
17. G. M. Chambers, R. Angamuthu, D. L. Gray and T. B. Rauchfuss, *Organometallics*, 2013, **32**, 6324.
18. T. R. Simmons, G. Berggren, M. Bacchi, M. Fontecave and V. Artero, *Coord. Chem. Rev.*, 2014, **271**, 127.
19. K. Weber, O. F. Erdem, E. Bill, T. Weyhermuller and W. Lubitz, *Inorg. Chem.*, 2014, **53**, 6329.

20. C. Wombwell and E. Reisner, *Dalton Trans*, 2014, **43**, 4483.
21. C. Wombwell and E. Reisner, *Chem. Eur. J.*, 2015, **21**, 8096.
22. G. Gezer, D. Durán Jiménez, M. A. Siegler and E. Bouwman, *Dalton Trans*, 2017, **46**, 7506.
23. J. L. Clark and S. B. Duckett, *Dalton Trans*, 2014, **43**, 1162.
24. M. V. Rampersad, S. P. Jeffery, M. L. Golden, J. Lee, J. H. Reibenspies, D. J. Darensbourg and M. Y. Darensbourg, *J. Am. Chem. Soc.*, 2005, **127**, 17323.
25. Y. Higuchi, H. Ogata, K. Miki, N. Yasuoka, T. Yagi, *Structure* 1999, **7**, 549.
26. V. Fourmond, P. A. Jacques, M. Fontecave and V. Artero, *Inorg. Chem.*, 2010, **49**, 10338.
27. G. M. Sheldrick, *Acta Cryst.* 2015, **C71**, 3.

Chapter 4

Dealkylation through C–S and Ni–S bond cleavage relevant to the mechanism of methyl-coenzyme M reductase (MCR)

Abstract

With the tetradentate ligands H_2ebSmS (3,6-dithia-2,2,7,7-tetramethyloctane-1,8-dithiol), H_2ebSmSe (3,6-dithia-2,2,7,7-tetramethyloctane-1,8-diselenol) and H_2pbSmSe (3,7-dithia-2,2,8,8-tetramethylnonane-1,9-diselenol) two nickel complexes were obtained. The compound [Ni(pbSmSe)] has the expected square-planar geometry, but in [Ni_2(ebSmS)$_2$] the restricted coordination angle of the ethylene bridge results in an unusual dinuclear compound in which the nickel ions are in square-pyramidal geometries. The intended four-coordinate, square-planar nickel compounds of these ligands appear to be reactive and readily decompose with loss of one of the alkylthiolate or alkylselenolate arms, resulting in dinuclear complexes of new tridentate ligands. Thus, the novel dinuclear 5-coordinate nickel(II) dithioether-dithiolato complex [Ni_2(ebSmS)$_2$], possessing an unusual coplanar structure and Ni···H anagostic interactions, decomposes in the presence of light through C–S and Ni–S bond cleavage to yield another dinuclear nickel(II) complex of a new asymmetric tridentate thioether-dithiolate ligand. Similar behaviour is observed for the mononuclear nickel(II) dithioether-diselenolato complex [Ni(pbSmSe)], which in the presence of light yields a dinuclear nickel(II) complex of a new asymmetric tridentate thioether-thiolate-selenolate ligand. The compound [Ni(ebSmSe)] is the most reactive as it could not be isolated; instead only the 'decomposed' compound was obtained.

This chapter is to be submitted for publication: G. Gezer, R. Angamuthu, W. Roorda, M. A. Siegler, M. Lutz, A. L. Spek and E. Bouwman.

'Parts of this chapter have been reported in R. Angamuthu PhD Thesis, *Structural and Functional Models for [NiFe] Hydrogenase*, Leiden University, Leiden, 2009.'

4.1 Introduction

Metal thiolates, especially nickel thiolates, are enjoying much attention among bioinorganic and organometallic chemists; they are important in the context of structural and/or functional models for enzymes such as hydrogenases (H_2ase),[1] superoxide dismutases (SOD),[2,3] carbon monoxide dehydrogenase/acetylcoenzyme A synthase (CODH/ACS)[4,5] and methyl coenzyme M reductase (MCR).[6,7,8] Moreover, the research efforts of the biomimetic community have been directed to the selenium-containing proteins; recently a number of biomimetic compounds as models for the active site in the enzymes containing a selenocysteine in their active site have been reported, in which thiolate donor atoms have been substituted by selenolates.[9,10] MCR is a key enzyme in biological methane formation by methanogenic archaea. Coenzyme F430 in MCR, a Ni-tetrahydrocorphinoid (Figure 4.1), catalyzes the reaction of methyl-coenzyme M (CH_3-SCoM; methylthioethyl sulfonate) with coenzyme B (HS-CoB; 7-mercaptoheptanoyl-threonine phosphate) to form methane and the disulfide Co-S-S-CoB.[6,7] In the past years two widely accepted mechanistic pathways have been proposed for this reaction from the results of a number of experimental and theoretical studies on F430.[6] The key question to be resolved was whether the catalysis involves a nucleophilic attack of the Ni(I) centre of F430 on the methyl group of CH_3-SCoM (in the presence of H^+) to form a Ni(III)-CH_3 intermediate (and HS–CoM), or that the Ni(I) centre attacks the thioether sulfur of CH_3-SCoM to form a Ni(II)-SCoM intermediate (and a $CH_3^{\bullet}$ radical).[7,11-13] Recently, new investigations have been done in order to understand reaction mechanism of methyl-coenzyme M and Ni(II)-thiolate was identified as an intermediate.[14]

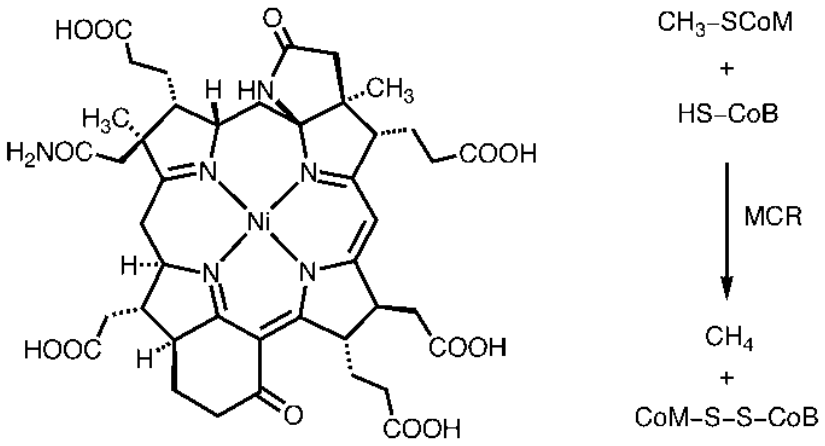

Figure 4.1: Structure of coenzyme F430 (left) and the reaction catalysed by MCR (right).

On the other hand, *S*-dealkylation is an industrially important process as it plays a role in desulfurization techniques or in alkyl transfer reactions toward new organosulfur compounds. In contrast to the ubiquitous *S*-dealkylation of terminal alkyl groups of organosulfur ligands involving C–S bond cleavage,[15-18] dealkylation involving both C–S and Ni–S bond cleavage is rather less common, and is reported only to occur in strongly reducing conditions.[19-20] The focus of our research includes the study of the synthesis and reactivity of nickel thiolate and selenolate compounds in relation with the structures and functions of nickel-containing enzymes. Reported herein are the synthesis of the thiouronium precursor to a new chelating tetradentate S_4-donor dithioether-dithiolate ligand and the corresponding selenouronium precursor of the tetradentate S_2Se_2-donor dithioether-diselenolate ligand and their nickel complexes. It is shown that upon irradiation of the nickel complexes new dinuclear nickel compounds are formed of asymmetric tridentate dianionic ligands.

4.2 Results

4.2.1 Synthesis and Characterization

The thiouronium and selenouronium salts of the ligands, convenient and easy to handle precursors for the dithiolate and diselenolate ligands H_2ebSmS and H_2ebSmSe, were synthesized in three reaction steps starting from 1,2-ethanedithiol, and were obtained as white powders in high purities and in 76% and 85% yield, respectively (Scheme 4.1). The reaction of $Ni(acac)_2$ (Hacac = acetylacetone) with one equivalent of the dithiouronium dichloride precursor of the ligand H_2ebSmS in toluene, in the presence of two equivalents of tetramethylammonium hydroxide resulted in an immediate color change of the initial pale green solution to deep brown (Scheme 4.2). The new nickel complex $[Ni_2(ebSmS)_2]$ **(1)** was isolated as a reddish-brown powder in 63% yield and characterized by single crystal X-ray crystallography, mass spectrometry and elemental analysis. The compound **(1)** gives broad signals in ^{1}H NMR spectra. Single crystals of **(1)** suitable for X-ray structure determination were obtained within hours from a dichloromethane solution. Unexpectedly, allowing a solution of **(1)** in acetonitrile to stand for 2 weeks resulted in crystals of the dinuclear compound $[Ni_2(emSmS)_2]$ **(2)** (H_2emSmS = 2,2-dimethyl-3-thiapentane-1,5-dithiol), as evidenced by X-ray structure determination. The nickel complex **(3)** was isolated as a dark green powder from the reaction of $Ni(acac)_2$ with one equivalent of the diselenouronium dichloride precursor of the ligand H_2pbSmSe in ethanol in the presence of two equivalents of tetramethylammonium hydroxide; the characterization and crystal structure of **(3)** has been

reported.[21] Single crystals of **(3)** were obtained by vapor diffusion of pentane into dichloromethane solutions of the complexes in dark. Again, unexpectedly crystals of the 'decomposed' compound $[Ni_2(pmSmSe)_2]$ **(4)** (H_2pmSmSe = 2,2-dimethyl-3-thiahexane-1-selenol-6-thiol) were obtained by vapor diffusion of pentane into dichloromethane solution of **(3)** in 2-3 weeks as evidenced by X-ray structure determination. The reaction of $Ni(acac)_2$ with one equivalent of the diselenouronium dichloride precursor of the ligand H_2ebSmSe in ethanol in the presence of two equivalents of tetramethylammonium hydroxide did not result in the formation of the expected compound [Ni(ebSmSe)] **(5)** or its dinuclear analog similar to **(1)**. Instead the nickel complex $[Ni_2(ebSmSe)_2]$ **(6)** (H_2emSmSe = 2,2-dimethyl-3-thiapentane-1-selenol-5-thiol) was isolated as a brown powder in 52% yield, as shown by single crystal X-ray crystallography, mass spectrometry and elemental analysis. Single crystals of **(6)** were obtained by vapor diffusion of pentane into a dichloromethane solution of the complex.

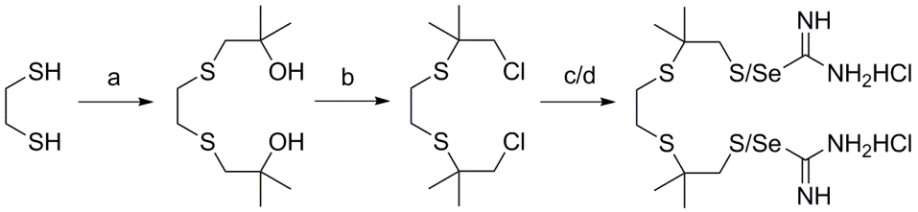

Scheme 4.1: Synthesis of the thiouronium and selenouronium salt precursors for the ligands H_2ebSmS and H_2ebSmSe. (a) $ClCH_2C(CH_3)_2OH$, NaOH, ethanol, Δ, (b) $SOCl_2$, $CHCl_3$, RT, (c) $S=C(NH_2)_2$, ethanol, Δ, (d) $Se=C(NH_2)_2$ ethanol, Δ.

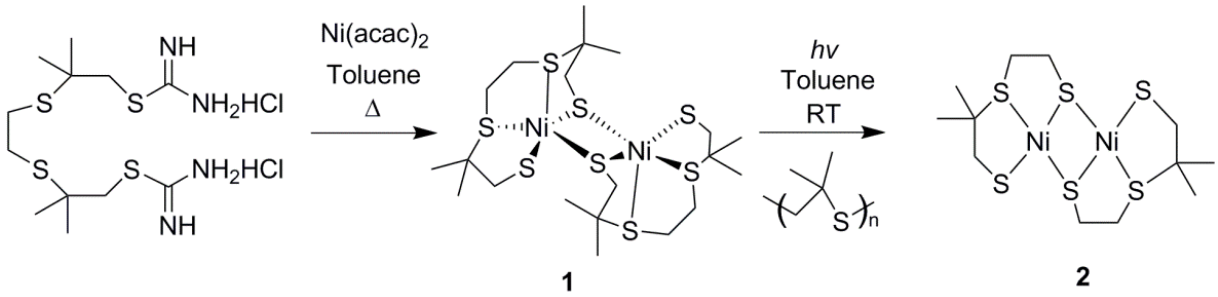

Scheme 4.2: Schematic drawing of $[Ni_2(ebSmS)_2]$ **(1)** and the formation of $[Ni_2(emSmS)_2]$ **(2)** and oligo-isobutylene sulfide upon irradiation.

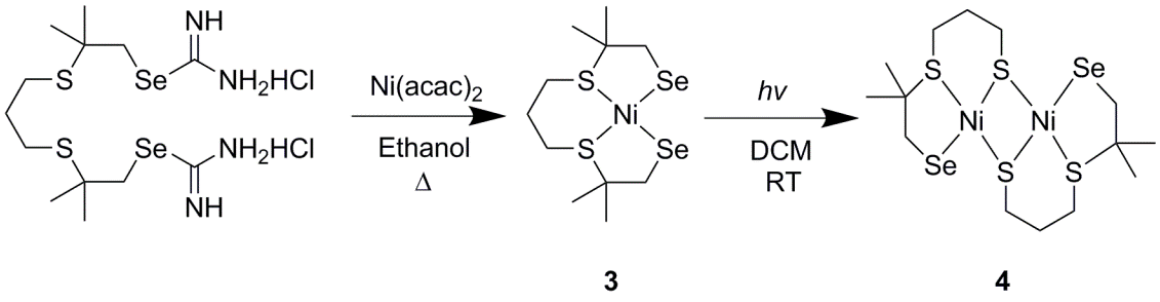

Scheme 4.3: Schematic drawing of [Ni(pbSmSe)] **(3)** and the formation of $[Ni_2(pmSmSe)_2]$ **(4)** upon irradiation.

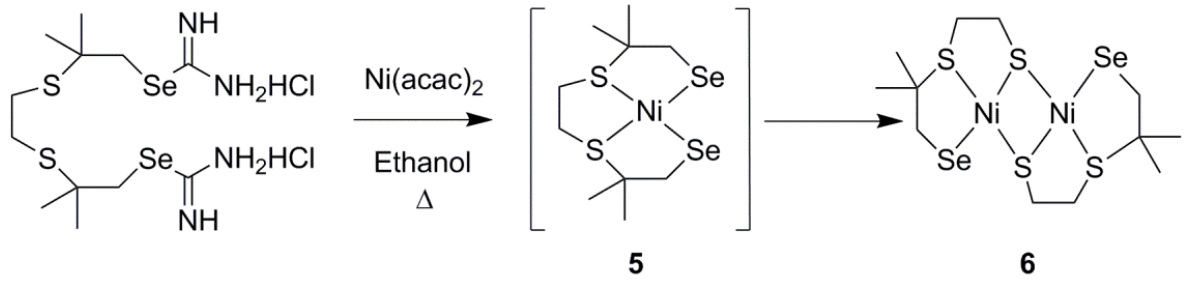

Scheme 4.4: Schematic drawing of synthesis of $[Ni_2(emSmSe)_2]$ **(6)**, assumedly via the reactive intermediate [Ni(ebSmSe)] **(5)**.

4.2.2 Description of the Structures

A projection of the molecular structure of the complex **(1)** is shown in Figure 4.2a; selected bond distances and angles are listed in Table 4.1. The asymmetric unit of **(1)** contains one molecule of the dinuclear complex and one molecule of dichloromethane. Two thiolate sulfur donors from the same ligand coordinate to a nickel centre in *trans* positions of each NiS_4 basal plane. One of these thiolate sulfur atoms is bound in a terminal position, whereas the other thiolate is bridging to the adjacent nickel centre. One of the thioether sulfur donors of one ligand and the bridging thiolate sulfur from the other ligand occupy the remaining two *trans* positions in the basal plane; the remaining thioether of the ligand binds in the apical position of the Ni(II) centre. One of the ligands in **(1)** is disordered over two conformations: the major component is related by an approximate two fold axis to the other ligand, the minor component is related by an approximate inversion centre. As a result, one rather short Ni–S thioether distance (Ni1A–S19B, 2.139(4) Å) is observed in the minor component. The τ value, used to describe five-coordinate compounds, for complex **(1)** was calculated to be 0.13 and 0.15 for the two Ni centers, indicating that the geometry of the nickel ion is slightly distorted square pyramidal.

Projections of the molecular structures of the complexes **(2)**, **(4)** and **(6)** are shown in Figure 4.2b and 4.3; selected bond distances and angles are listed in Table 4.1 and 4.2. The compounds **(2)**, **(4)** and **(6)** are highly similar dinuclear nickel complexes comprising different asymmetric tridentate ligands that are derived from the parent tetradentate ligands by loss of one isobutylenethiol/selenol arm. The asymmetric unit of **(2)** contains one dinuclear nickel complex of the tridentate thioether-dithiolate ligand ($emSmS^{2-}$) and the asymmetric units of **(4)** and **(6)** contain the dinuclear nickel(II) compounds with the tridentate thioether-thiolate-selenolate ligands ($pmSmSe^{2-}$ and $emSmSe^{2-}$). The compounds **(2)** and **(6)** have quite similar butterfly cores with hinge angles of 77.70º and 76.76º, respectively. However changing the ethylene bridge to propylene in compound **(4)** results in a smaller hinge angle of 64.99º. The $Ni–S_{thiolate}$ and $Ni–Se_{selenolate}$ distances are slightly longer than the $Ni–S_{thioether}$ distances for complex **(2)**, **(4)** and **(6)**. This observation is in contrast to previous reports,[4,22-25] but is not unprecedented especially for complex **(4)** and **(6)** due to the larger ionic radius of selenium.[26-28] In contrast to the common butterfly or folded structures as in **(2)**, **(4)**, **(6)** and other dinuclear or oligonuclear nickel thiolate complexes,[25,29] the molecular structure of complex **(1)** exhibits an unusual coplanar structure of the two basal planes of the nickel coordination geometries. The dihedral angle between the two basal NiS_4 planes in complex **(1)** is only 2.99(7)º. This structure may be due to the $Ni\cdots H_{Me}$ anagostic interactions (2.66 Å and 2.74 Å) with Ni···H–C angles of 132.76º and 132.87º, which may be strong enough to not allow the NiS_4 planes to fold (Fig. 4.2a).[30] In literature the anagostic interaction is described by M···H–C distances of ~2.3-2.9 Å and M···H–C angles of ~110-170º.[31] Complex **(1)** has the shortest $Ni\cdots H_{Me}$ distances compared to other structures (Table 4.3).

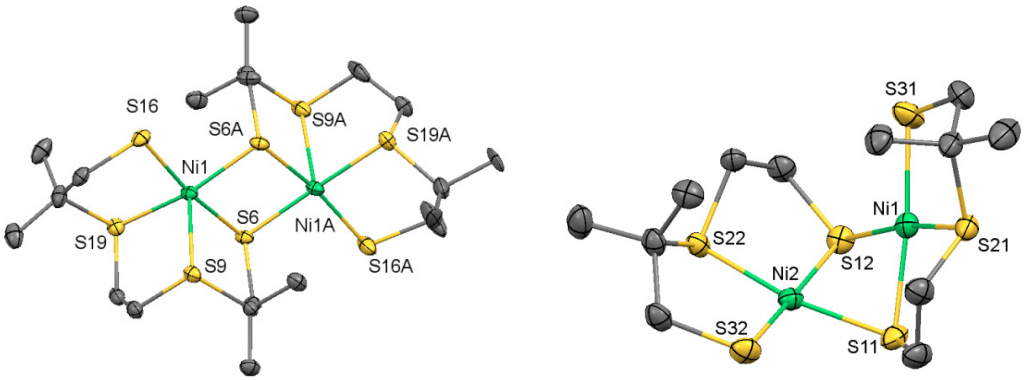

(a) (b)

Figure 4.2: Displacement ellipsoid plot (50% probability level) of $[Ni_2(ebSmS)_2]$ **(1)** (a) at 110(2) K and $[Ni_2(emSmS)_2]$ **(2)** (b) at 150(2) K. Lattice dichloromethane molecules, partial disorder and hydrogen atoms are omitted for clarity.

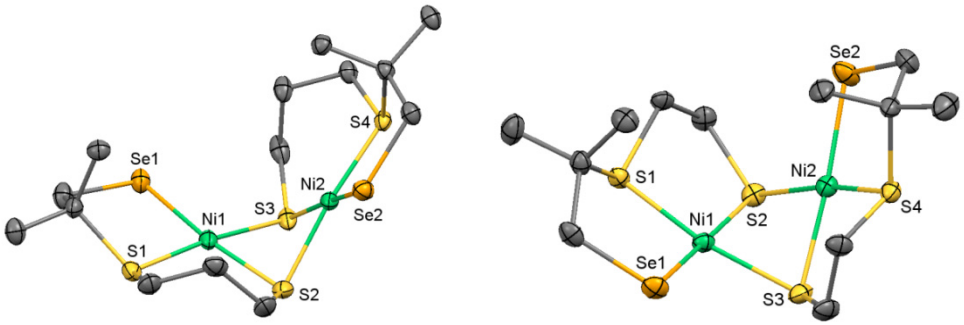

(a) (b)

Figure 4.3: Displacement ellipsoid plots (50% probability level) of $[Ni_2(pmSmSe)_2]$ **(4)** (a) and $[Ni_2(emSmSe)_2]$ **(6)** (b) at 100(2) K. Hydrogen atoms are omitted for clarity.

Table 4.1: Selected bond lengths (Å) and angles (°) for the complexes **(1)** and **(2)**.

Distances (Å)	**(1)**	Distances(Å)	**(2)**
Ni1-S6	2.2345(11)	Ni1-S31	2.1604(6)
Ni1-S9	2.6010(11)	Ni2-S32	2.1559(5)
Ni1-S16	2.1928(11)	Ni1-S21	2.1387(5)
Ni1-S19	2.2359(12)	Ni2-S12	2.2057(5)
Ni1-S6A	2.2096(12)	Ni1-S11	2.2107(6)
Ni1A-S6	2.2139(12)	Ni2-S22	2.1347(5)
Ni1A-S6A	2.2285(12)	Ni1-S12	2.1783(5)
Ni1A-S9A	2.7038(12)	Ni2-S11	2.1818(6)
Ni1A-S16A	2.1966(13)		
Ni1A-S19A	2.246(3)		
Angles (°)	**(1)**	Angles (°)	**(2)**
S6-Ni1-S9	87.41(4)	S11-Ni1-S12	81.53(2)
S6-Ni1-S16	170.97(5)	S12-Ni1-S21	170.35(2)
S6-Ni1-S19	94.84(4)	S11-Ni2-S12	81.57(2)
S6-Ni1-S6A	83.70(4)	S12-Ni2-S22	89.25(2)
Ni1-S6-Ni1A	96.12(4)	Ni1-S11-Ni2	75.99(2)
Ni1-S6A-Ni1A	96.42(4)	Ni1-S12-Ni2	76.17(2)
S16-Ni1-S19	89.76(4)	S11-Ni1-S21	89.18(2)
S16-Ni1-S6A	89.66(5)	S12-Ni1-S31	97.55(2)
S9-Ni1-S6A	108.47(4)	S11-Ni2-S22	169.37(2)
S19-Ni1-S6A	163.26(5)	S12-Ni2-S32	175.06(2)
S9-Ni1-S16	100.53(4)	S11-Ni1-S31	173.30(2)
S9-Ni1-S19	88.07(4)	S21-Ni1-S31	91.37(2)

Table 4.2: Selected bond lengths (Å) and angles (°) for the complexes **(4)** and **(6)**.

Distances (Å)	**(4)**	**(6)**	Distances (Å)	**(4)**	**(6)**
Ni1-Se1	2.2929(12)	2.2756(6)	Ni1-S2	2.1932(19)	2.2079(9)
Ni2-Se2	2.2921(12)	2.2788(6)	Ni2-S4	2.1544(18)	2.1444(9)
Ni1-S1	2.1586(19)	2.1396(9)	Ni1-S3	2.1968(18)	2.1855(10)
Ni2-S3	2.2005(18)	2.2161(10)	Ni2-S2	2.1989(18)	2.1810(9)
Angles (°)	**(4)**	**(6)**	Angles (°)	**(4)**	**(6)**
S2-Ni1-S3	78.49(7)	81.94(3)	S3-Ni1-Se1	94.24(5)	97.30(3)
S3-Ni1-S1	173.44(7)	169.77(4)	S2-Ni2-S4	172.27(7)	170.46(4)
S2-Ni2-S3	78.29(7)	81.94(3)	S3-Ni2-Se2	172.38(7)	175.06(4)
S3-Ni2-S4	98.39(6)	84.16(4)	S2-Ni1-Se1	172.42(7)	176.79(4)
Ni1-S2-Ni2	80.45(5)	75.97(3)	S1-Ni1-Se1	88.69(6)	91.02(3)
Ni1-S3-Ni2	80.33(5)	75.71(3)	S2-Ni2-Se2	94.79(6)	97.30(3)
S2-Ni1-S1	98.76(7)	89.34(3)	S4-Ni2-Se2	88.86(6)	91.28(3)

Table 4.3: Shortest Ni-H_{Me} distances in complexes **(1)**, **(2), (3), (4)** and **(6).**[a]

Distances (Å)	**(1)**	**(2)**	**(3)**	**(4)**	**(6)**
Ni-H_{Me}	2.66	3.09	3.26	3.11	3.18
Ni-H_{Me}	2.74	3.16	3.35	3.12	3.11

[a] data for **(3)** taken from ref 21.

4.2.3 Reactivity Studies

Compound **(2)** was unexpectedly formed from a solution of **(1)** left for crystallization over two weeks' time. In order to investigate the mechanism of formation of **(2)** from **(1)**, a toluene solution of **(1)** was irradiated using a mercury arc lamp; samples were collected at regular time intervals and were analyzed using ESI-MS spectrometry. Interestingly, the formation of **(2)** is clearly identified from the ESI-MS spectra, showing the gradual disappearance of molecular ion peaks at *m/z* 326.72 for $[Ni(ebSmS)+H]^+$ **(1)** with simultaneous growth of the peak corresponding to **(2)** at *m/z* 238.86 for $[Ni(emSmS)+H]^+$ (Fig. AIV.1). When using a mercury lamp the decomposition reaction needs about 12 hours to reach completion with near quantitative formation of **(2)**. In an endeavour to determine the fate of the isobutylenethiolate side arms lost in this reaction, the reaction mixture after irradiation was gently distilled at a temperature of 85 ºC. A few drops of a low-boiling product were obtained; ESI-MS spectrometry and NMR spectroscopy (Fig. AIV.2-5) confirmed the identity of (oligo) isobutylene sulfide as the main by-product. The remaining mixture was passed through a neutral alumina column and pure **(2)** was thus obtained in 87% yield. Similarly, the formation of compound **(4)** also occurred from a solution of **(3)** in dichloromethane, left for crystallization over 2-3 weeks' time. To investigate the formation of **(4)** from **(3)** a dichloromethane solution of **(3)** was irradiated using a xenon lamp; samples were collected at regular time intervals and were analyzed using HRMS spectrometry, again showing the gradual disappearance of molecular ion peaks of **(3)** with simultaneous growth of the peak corresponding to **(4)** (Fig. AIV.6). Compound **(3)** needs only two hours of irradiation with the xenon lamp to give complete conversion to compound **(4)**. The formation of compound **(4)** was also monitored with UV-VIS spectroscopy. The dark green compound **(3)** shows a small absorption band at 410 nm with an absorption coefficient ε of 480 $M^{-1}cm^{-1}$. Upon irradiation over 2 h the absorption shifts to 430 nm resulting in a new band with an absorption coefficient of 2300 $M^{-1}cm^{-1}$ ascribed to the formation of the brown-coloured compound **(4)** (Fig.4.4). The nickel compound of the tetradentate ligand $ebSmSe^{2-}$ could not be isolated; instead

complex **(6)** was formed directly from the reaction mixture. When kept in the dark the compounds **(1)** and **(3)** are found to be rather stable and yield [NiFe] complexes of interest as hydrogenase model systems upon reaction with iron carbonyl complexes (see Chapter 2).[21,32]

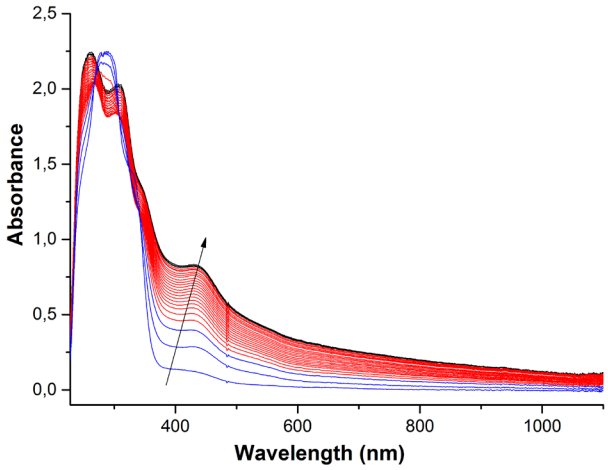

Figure 4.4: Evolution of the UV-VIS spectra of complex **(3)** (1 mM) in dichloromethane upon irradiation with a xenon lamp over 2 h. Spectra were recorded with a transmission dipprobe set at a path length of 2 mm.

4.3 Discussion

In this work we have encountered the unique reactivity of $[Ni_2(ebSmS)_2]$ **(1)** and [Ni(pbSmSe)] **(3)** in the formation of the dinuclear low-spin nickel complexes $[Ni_2(emSmS)_2]$ **(2)** and $[Ni_2(pmSmSe)_2]$ **(4)** comprising new asymmetric tridentate ligands. However, the nickel complex [Ni(ebSmSe)] **(5)** could not be isolated and only its decomposition product $[Ni_2(ebSmSe)_2]$ **(6)** was obtained. The reactivity of the compounds **(1)**, **(3)** and the elusive compound **(5)** is clearly different, which may be related to the difference in ionic radii of the sulfur and selenium donor atoms and the flexibility of the carbon bridge between the two thioether donor atoms in the tetradentate ligands. Both the compounds **(2)** and **(6)** are 'decomposed' structures of the ethylene-bridged ligands $ebSmS^{2-}$ comprising thiolate donor atoms and $ebSmSe^{2-}$ having selenolate donor atoms. Whereas the unusual dinuclear structure of compound **(1)** containing 5-coordinate nickel ions indicates that the ethylene-bridged ligand is too strained to accommodate the expected square-planar geometry of the nickel(II) ion, the compound [Ni(ebSmSe)] **(5)** with the selenolate donor atoms could not be isolated, indicating that the larger radius of the selenolate group induces even more strain in the tetradentate ligand. The propylene bridge in the compounds [Ni(pbSmSe)] **(3)** and the related thiolate-containing compound [Ni(pbSmS)][25] clearly is large enough to accommodate the

square-planar geometry of the nickel ion. However, whereas compound **(3)** with the larger selenolate donor atoms is relatively unstable and decomposes to give **(4)**, the related 'decomposition' product so far has not been reported for the thiolate analogue [Ni(pbSmS)].[25,33]

4.4 Conclusion

In summary, three new nickel(II) complexes were obtained comprising new asymmetric tridentate thioether-dithiolate or thioether-thiolate-selenolate ligands. The nickel thiolate compound **(1)** presented here shows a novel coplanar dinuclear structure with 5-coordinate nickel centers involved in Ni···H anagostic interactions. Upon irradiation of this compound clean conversion to the 'decomposed' compound **(2)** with the concomitant release of oligo-isobutylene sulfide is observed, which must occur through light-induced C–S and Ni–S bond cleavage. The broad signals observed in ^{1}H NMR spectra of **(1)**, the short Ni–S distances observed in the X-ray crystal structure in combination with the unusual disorder are indicative of the presence of partial Ni(I)-S$^{\bullet}$ character. Further exploration of this light-induced reaction with a combination of spectroscopic techniques and the study of the reactivity of **(1)** and **(3)** with other substrates or small molecules are in progress and may shed light onto the reaction pathway and pave the way toward new organosulfur derivatives.

4.5 Experimental

4.5.1 Materials

All experiments were performed using standard Schlenk techniques or in a glovebox under an argon or nitrogen atmosphere unless otherwise noted. Chemicals were purchased from Acros or Aldrich and were used without further purification. Organic solvents were deoxygenated by the freeze-pump-thaw method and were dried over molecular sieves prior to use. The NMR solvent CD_2Cl_2 for the metal complexes was deoxygenated by the freeze-pump-thaw method and was stored over molecular sieves in a glovebox. Complex **(3)** was synthesized according to a published procedure.[21]

4.5.2 Physical Measurements

NMR spectra were recorded on a 300 MHz Bruker DPX 300 spectrometer and chemical shifts were referenced against the solvent peaks. Mass spectra were obtained with a Finnigan TSQ quantum instrument using ESI. HRMS was recorded on a Thermo Scientific LTQ Orbitrap XL high resolution FT-MS system. Elemental analyses were performed by the

Microanalytical Laboratory Kolbe in Germany. Irradiations were carried out at room temperature using a Hanau TQ81 high-pressure mercury arc lamp for complex **(1)** and a Lot Xenon lamp for complex **(3)** with continuous stirring. UV-vis spectra were collected using a transmission dipprobe with 2 mm path length on an Avantes Avaspec-2048 spectrometer with Avalight-DH-S-BAL light source.

4.5.3 Single Crystal X-ray Crystallography

X-ray intensities for **(1)** and **(2)** were measured on a Nonius KappaCCD diffractometer with rotating anode (graphite monochromator, $\lambda = 0.71073$ Å). Intensity integration was performed with EvalCCD[34] (for **(1)**) or HKL2000[35] (for **(2)**). Absorption correction was based on multiple measured reflections. The structures were solved with SHELXS-97[36] using Direct Methods and refined against F^2 of all reflections using SHELXL-2016/6.[37] Non-hydrogen atoms were refined freely with anisotropic displacement parameters. Hydrogen atoms were introduced in calculated positions and refined with a riding model. Geometry calculations and checking for higher symmetry was performed with the PLATON program.[38] The reflection intensities for **(4)** and **(6)** were measured at 110(2) K using a SuperNova diffractometer (equipped with Atlas detector) with Cu *K*α radiation ($\lambda = 1.54178$ Å) under the program CrysAlisPro (Version 1.171.36.32 Agilent Technologies, 2013). The same program was used to refine the cell dimensions and for data reduction. The structure was solved with the program SHELXS-2014/7 and was refined on F^2 with SHELXL-2014/7.[37] Analytical numeric absorption correction using a multifaceted crystal model was applied using CrysAlisPro. The temperature of the data collection was controlled using the system Cryojet (manufactured by Oxford Instruments). The H atoms were placed at calculated positions (unless otherwise specified) using the instructions AFIX 23 or AFIX 137 with isotropic displacement parameters having values 1.2 or 1.5 *U*eq of the attached C atoms. Both structures are ordered.

4.5.4 Synthesis of 4,7-dithia-2,9-dimethyldecane-2,9-diol: To a solution of 1,2-ethanedithiol (5.65 g, 60 mmol) in 70 ml ethanol was added 1-chloro-2-methyl-2-propanol (13.03 g, 120 mmol) and NaOH (4.81 g, 120 mmol) in 45 ml water. After refluxing for two hours, the formed NaCl was removed by filtration. After evaporating the ethanol under reduced pressure, water was added and the product was extracted with chloroform. The combined chloroform layers were dried with $MgSO_4$ and evaporated to get 10.68 g of a colorless oil (98%). ^{1}H NMR: δ_H [300.13 MHz, $CDCl_3$, 298 K] 2.78 (m, 2H, –O*H*), 2.70 (s, 4H, –S–C*H*$_2$–C(CH$_3$)$_2$OH), 2.57 (s, 4H, –S–C*H*$_2$–C*H*$_2$–S–) 1.62 (s, 12H, –C(C*H*$_3$)$_2$OH). ^{13}C

NMR: δ_C [75.47 MHz, $CDCl_3$, 298 K] 70.3 (–*C*$(CH_3)_2$OH), 46.4 (–S–*C*H_2–C$(CH_3)_2$OH), 34.1 (–S–*C*H_2–*C*H_2–S–), 28.3 (–(*C*$H_3)_2$OH).

4.5.5 Synthesis of 1,8-dichloro-3,6-dithia-2,2,7,7-tetramethyloctane: To a solution of 4,7-dithia-2,9-dimethyldecane-2,9-diol **(**10.68 g, 58.72 mmol) in 20 ml $CHCl_3$ was added drop-wise a solution of $SOCl_2$ (17.85 g, 150 mmol) in $CHCl_3$. The color of the solution initially turned in yellow and orange at the final stage of the addition of $SOCl_2$. After an hour stirring the chloroform and excess $SOCl_2$ were evaporated under reduced pressure to yield 12.33 g of a yellow oil (quantitative yield). ^{1}H NMR: δ_H [300.13 MHz, $CDCl_3$, 298 K] 2.93 (s, 4H, –C*H*$_2$–Cl), 2.81 (s, 4H, –S–C*H*$_2$–C*H*$_2$–S–), 1.62 (s, 12H, –C*H*$_3$). ^{13}C NMR: δ_C [75.47 MHz, $CDCl_3$, 298 K] 70.0 (–*C*H$_2$–Cl), 48.01 (–S–CH$_2$–CH$_2$–*C*$(CH_3)_2$Cl), 34.3 (–S–*C*H$_2$–*C*H$_2$–S), 31.3 (–*C*H$_3$).

4.5.6 Synthesis of 1,8-dithiouronium-3,6-dithia-2,2,7,7-tetramethyloctane dichloride: Thiourea (7.99 g, 105 mmol) and 1,8-dichloro-3,6-dithia-2,2,7,7-tetramethyloctane (12.11 g, 55.24 mmol) were dissolved in ethanol (85 ml) and refluxed for one hour. After 30 min an off-white precipitate was formed. The solution was allowed to cool, the solid product was collected by filtration, washed with cold ethanol and diethyl ether, and dried under vacuum to get 17.64 g of the pure compound (76%). ^{1}H NMR: δ_H [300.13 MHz, DMSO-d_6, 298 K] 9.33 (d, 8H, –SC$^+$(N*H*$_2)_2$Cl$^-$) 3.56 (s, 4H, –C*H*$_2$–SC$^+$$(NH_2)_2Cl^-$), 2.71 (s, 4H, –S–C*H*$_2$–C*H*$_2$–S–), 1.31 (s, 12H, –C*H*$_3$). ^{13}C NMR: δ_C [75.47 MHz, DMSO-d_6, 298 K] 170.3 (–CH$_2$–S*C*$^+$$(NH_2)_2Cl^-$), 45.5 (–*C*H$_2$–SC$^+$$(NH_2)_2Cl^-$), 42.5 (–S–*C*$(CH_3)_2$–) 28.0 (–S–*C*H$_2$–*C*H$_2$–S–), 27.5 (–*C*H$_3$). MS (ESI): (*m/z*) calculated for $C_{12}H_{27}S_4N_4$ $[M-2Cl-H]^+$ requires (monoisotopic mass) 355.11, found 354.74.

4.5.7 Synthesis of 1,8-diselenouronium-3,6-dithia-2,2,7,7-tetramethyloctane dichloride: A solution of selenourea (594 mg, 4.83 mmol) in 5 ml ethanol was added to a solution of 1,8-dichloro-3,6-dithia-2,2,7,7-tetramethyloctane (665 mg, 2.42 mmol) in 5 ml ethanol; the reaction mixture was refluxed for 30 min. The solution was allowed to cool, and the solid product was collected by filtration. The product was washed with cold ethanol and diethyl ether, and dried in vacuo yielding 1.07 g of pure compound (85%). ^{1}H NMR: δ_H [300.13 MHz, DMSO-d_6, 298 K] 9.39 (d, 8H, –SeC$^+$(N*H*$_2)_2$Cl$^-$) 3.62 (s, 4H, –C*H*$_2$–SeC$^+$$(NH_2)_2Cl^-$), 2.77 (s, 4H, –S–C*H*$_2$–C*H*$_2$–S–), 1.37 (s, 12H, –C*H*$_3$). ^{13}C NMR: δ_C [75.47 MHz, DMSO-d_6, 298 K] 166.92 (–CH$_2$–Se*C*$^+$$(NH_2)_2Cl^-$), 45.69 (–*C*H$_2$–SeC$^+$$(NH_2)_2Cl^-$), 40.55 (–S–*C*$(CH_3)_2$–) 28.13

(–S–CH_2–CH_2–S–), 28 (–CH_3). MS (ESI): (*m/z*) calculated for $[M–2Cl]^{2+}$ requires (monoisotopic mass) 225.21, found 224.4.

4.5.8 Synthesis of $[Ni_2(ebSmS)_2]$ (1): To a two-necked flask charged with a solution of $Ni(acac)_2$ (0.768g, 3 mmol) in 60 ml dry toluene was added the ligand as the dithiouronium dichloride precursor of the ligand H_2ebSmS (1.284 g, 3 mmol). After 10 minutes stirring at 50 °C, NMe_4OH (2.73 ml, 6 mmol) was added to the mint-green solution, resulting in a colour change to dark brown. The reaction mixture was refluxed for three hours. After evaporating the solvent, CH_2Cl_2 was added and the insoluble by-products were removed by filtration. The filtrate was passed through alumina and the first dark-red band was collected and evaporated to yield 0.14 g of pure $[Ni_2(ebSmS)_2]$ **(1)** (15%). Performing the reaction and the following work-up procedure in darkness drastically improved the yield to 63%. Elemental Analysis (%): Calculated for $C_{20}H_{40}S_8Ni_2{\cdot}0.4CH_2Cl_2$: C 35.59, H 5.97, S 37.26; found C 35.57, H 5.98, S 37.19. MS (ESI): (*m/z*) calculated for $C_{10}H_{21}S_4Ni$ $[M/2+H]^+$ requires (monoisotopic mass) 326.99, found 326.72.

4.5.9 Formation of $[Ni_2(emSmS)_2]$ (2): Compound **(1)** (0.98 g, 3 mmol) was dissolved in 50 ml toluene and the solution was irradiated using a Hanau TQ81 high-pressure mercury arc lamp. Completion of the reaction was monitored by recording ESI-MS spectra of the samples collected in regular intervals. The reaction needed 12 hrs for completion; the formed isobutylene sulfide was collected from the reaction mixture by gentle distillation. Oligo-isobutylene sulfide started to distill over when the temperature was around 85 ºC; the collection flask was kept at 0 ºC using an ice bath. The remaining mixture was passed through a neutral alumina column and pure **(2)** was thus obtained in 87% yield. Elemental Analysis (%): Calculated for $C_{12}H_{24}S_6Ni_2$: C 30.15, H 5.06, S 40.24; found C 30.27, H 5.18, S 40.29. MS (ESI): (*m/z*) calculated for $C_6H_{13}S_3Ni$ $[M/2+H]^+$ requires (monoisotopic mass) 238.95, found 238.86.

4.5.10 Formation of $[Ni_2(pmSmSe)_2]$ (4): Compound **(3)** was dissolved in dichloromethane and the solution was irradiated using a LOT xenon lamp. Completion of the reaction was monitored by recording HRMS spectra of the samples collected in regular intervals. The reaction needed 2 hrs of irradiation to reach completion. Crystals of **(4)** were obtained by vapor diffusion of pentane into the DCM solution of **(3)** in daylight. HR-MS (CH_2Cl_2): (*m/z*) calculated for $C_{14}H_{28}Ni_2S_4Se_2$ $[M+H]^+$ requires (monoisotopic mass) 599.8095, found

599.8111. Elemental Analysis (%): Calculated for $C_{14}H_{28}Ni_2S_4Se_2$: C 28.03, H 4.70; found C 28.08, H 4.71.

4.5.11 [Ni(ebSmSe)] (5): A solution of NMe_4OH (164 mg, 0.906 mmol) and ligand precursor (1,8-diselenouronium-3,6-dithia-2,2,7,7-tetramethyloctane dichloride) (236 mg, 0.453 mmol) were dissolved in 30 ml ethanol and mixed with $Ni(acac)_2$ (116 mg, 0.453 mmol) in 30 ml toluene. This immediately resulted in a colour change to dark reddish-brown. Unfortunately, a pure compound could not be isolated.

4.5.12 [Ni_2(emSmSe)$_2$] (6): A solution of NMe_4OH (164 mg, 0.906 mmol), the dithiouronium dichloride precursor of the ligand H_2ebSmSe (236 mg, 0.453 mmol) and $Ni(acac)_2$ (116 mg, 0.453 mmol) were refluxed in 60 ml ethanol for 1 h. The solvent was evaporated until approximately 10 ml solvent remained, resulting in a brown precipitate. The solid was collected by filtration and washed with ethanol. Yield: 133.7 mg (52%) MS (ESI): (*m/z*) calculated for $C_{12}H_{24}S_4Se_2Ni_2$ $[M+H]^+$ requires 572.79, (monoisotopic mass) found 572.78. Elemental Analysis (%): Calculated for $C_{12}H_{28}Ni_2S_4Se_2$: C 25.20, H 4.23; found C 25.26, H 4.21.

4.6 Acknowledgements

G. K. Spijksma is gratefully acknowledged for HRMS measurement and J.J.M. van Brussel is gratefully acknowledged for ESI-MS measurements.

4.7 References

1. C. Tard and C. J. Pickett, *Chem. Rev.*, 2009, **109**, 2245.
2. V. Mathrubootham, J. Thomas, R. Staples, J. McCraken, J. Shearer and E. L. Hegg, *Inorg. Chem.*, 2010, **49**, 5393.
3. J. Shearer, K. P. Neupane and P. E. Callan, *Inorg. Chem.*, 2009, **48**, 10560.
4. R. Angamuthu, L. L. Gelauff, M. A. Siegler, A. L. Spek and E. Bouwman, *Chem. Commun.*, 2009, 2700.
5. K. N. Green, S. M. Brothers, B. Lee, M. Y. Darensbourg and D. A. Rockcliffe, *Inorg. Chem.*, 2009, **48**, 2780.
6. U. Ermler, *Dalton Trans.*, 2005, 3451.
7. U. Ermler, W. Grabarse, S. Shima, M. Goubeaud and R. K. Thauer, *Science*, 1997, **278**, 1457.
8. T. Wongnate and S. W. Ragsdale, *J. Biol. Chem.,*2015, **290**, 932.
9. S. Castellano, A. V. Lobanov, C. Chapple, S. V. Novoselov, M. Albrecht, D. Hua, A. Lescure, T. Lengauer, A. Krol, V. N. Gladyshev and R. Guigo, *Proc. Natl. Acad. Sci. USA.*, 2005, **102**, 16188.
10. J. A. Gámez, M. Yáñez, *Chem. Commun.*, 2011, **47**, 3939.

11. V. Pelmenschikov and P. E. M. Siegbahn, *J. Biol. Inorg. Chem.*, 2003, **8**, 653.
12. V. Pelmenschikov, M. R. A. Blomberg, P. E. M. Siegbahn and R. H. Crabtree, *J. Am. Chem. Soc.*, 2002, **124**, 4039.
13. E. C. Duin and M. L. McKee, *J. Phys. Chem. B*, 2008, **112**, 2466.
14. T. Wongnate, D. Sliwa, B. Ginovska, D. Smith, M. W. Wolf, N. Lehnert, S. Raugei and S. W. Ragsdale, *Science*, 2016, **352**, 6288.
15. A. Beganskiene, L. R. Pignotti, V. Baltramiejunaite, R. L. Luck and E. Urnezius, *Inorg. Chim. Acta*, 2008, **361**, 1349.
16. M. D. Curtis and S. H. Druker, *J. Am. Chem. Soc.*, 1997, **119**, 1027.
17. J. S. Kim, J. H. Reibenspies and M. Y. Darensbourg, *J. Am. Chem. Soc.*, 1996, **118**, 4115.
18. J. S. Kim, J. H. Reibenspies and M. Y. Darensbourg, *Inorg. Chim. Acta*, 1996, **250**, 283.
19. M. Y. Cha, S. C. Shoner and J. A. Kovacs, *Inorg. Chem.*, 1993, **32**, 1860.
20. D. Sellmann and W. Reisser, *J. Organomet. Chem.*, 1985, **294**, 333.
21. G. Gezer, D. Duran Jiménez, M. A. Siegler and E. Bouwman, *Dalton Trans.*, 2017, **46**,7506.
22. J. A. W. Verhagen, M. Lutz, A. L. Spek and E. Bouwman, *Eur. J. Inorg. Chem.*, 2003, 3968.
23. J. A. W. Verhagen, D. D. Ellis, M. Lutz, A. L. Spek and E. Bouwman, *Dalton Trans.*, 2002, 1275.
24. R. Angamuthu, H. Kooijman, M. Lutz, A. L. Spek and E. Bouwman, *Dalton Trans.*, 2007, 4641.
25. K. Weber, I. Heise, T. Weyhermüller and W. Lubitz, *Eur. J. Inorg. Chem.* 2014, 148.
26. D. Sellmann, D. Haussinger and F. W. Heinemann, *Eur. J. Inorg. Chem.*, 1999, 1715.
27. R. Cao, M. C. Hong, F. L. Jiang, X. L. Xie and H. Q. Liu, *Dalton Trans.*, 1994, 3459.
28. C. Wombwell and E. Reisner, *Chem. Eur. J.* 2015, **21**, 8096.
29. C. Zhang, S. Takada, M. Kölzer, T. Matsumoto and K. Tatsumi, *Angew. Chem.-Int. Edit.*, 2006, **45**, 3768.
30. M. Brookhart, M. L. H. Green and G. Parkin, *Proc. Natl. Acad. Sci. U. S. A.*, 2007, **104**, 6908.
31. M. K. Yadav, G. Rajput, L. B. Prasad, M. G. B. Drew and N. Singh, *New J. Chem.,*2015, **39**, 5493.
32. R. Angamuthu, PhD Thesis, *Structural and Functional Models for [NiFe] Hydrogenase*, Leiden University, Leiden, 2009.
33. K. Weber, O. F. Erdem, E. Bill, T. Weyhermüller and W. Lubitz, *Inorg. Chem.,* 2014, **53**, 6329.
34. A. J. M. Duisenberg, L. M. J. Kroon-Batenburg, A. M. M. Schreurs, *J. Appl. Cryst.*, 2003, **36**, 220.
35. Z. Otwinowski, W. Minor, *Methods in Enzymology, (C.W. Carter, Jr. & R.M. Sweet, Eds) Academic Press,* 1997, ***276***, 307.
36. G. M. Sheldrick, *Acta Cryst.*, 2008, ***A64***, 112.
37. G. M. Sheldrick, *Acta Cryst.,* 2015, **C71**, 3.
38. A. L. Spek, *J. Appl. Cryst.*, 2003, ***36***, 7.

Chapter 5

Synthesis and Characterization of Trinuclear [NiRu] Complexes for Electrocatalytic Proton Reduction

Abstract

Two new trinuclear compounds [{Ni(xbSmS)}$_2$Ru(phen)$_2$](PF$_6$)$_2$ and [{Ni(xbSmSe)}$_2$Ru(phen)$_2$](PF$_6$)$_2$ were synthesized by the reaction of [Ni(xbSmS)] and [Ni(xbSmSe)] with cis-[Ru(phen)$_2$(Cl)$_2$] (H$_2$xbSmS = 1,2-bis(4-mercapto-3,3-dimethyl-2-thiabutyl)benzene; H$_2$xbSmSe = 1,2,-bis(2-thiabutyl-3,3-dimethyl-4-selenol)benzene; phen = phenanthroline). The two [Ni$_2$Ru] complexes were characterized by ESI-MS, NMR, elemental analysis, single crystal X-ray crystallography and electrochemical techniques. X-ray structure determinations showed that the trinuclear complex cations in ***(1)*** *and* ***(2)*** *contain two square-planar nickel centers bound in cis positions to the octahedral ruthenium ion via a bridging thiolate or selenolate donor atom. Electrocatalytic proton reduction occurs for both complexes in acetonitrile with addition of varying amounts of acetic acid at a potential of −2.1 V vs. Fc$^+$/Fc with faradaic yields of around 65%.*

This chapter is submitted for publication: G. Gezer, D. Durán Jiménez, M. A. Siegler, and E. Bouwman.

5.1 Introduction

Molecular hydrogen (H_2) is a perfect candidate as energy carrier to be used as an alternative to fossil fuels. The hydrogen economy relies on the vision of replacing fossil fuels by dihydrogen as a low-carbon energy source.[1] A way of producing dihydrogen gas is via the (electrocatalytic) hydrogen evolution reaction (HER), in which protons are combined with electrons to yield molecular hydrogen as shown in equation 1.[2]

$$2H^+ + 2e^- \rightleftarrows H_2 \qquad [1]$$

In 1930 Stephenson and Stickland reported an enzyme found in certain microorganisms capable of molecular hydrogen activation for which they proposed the name hydrogenase.[3] It was discovered that in microorganisms containing this hydrogenase dihydrogen can be produced or used as a source of electrons in a global H_2 cycle. The hydrogenase family is divided in three classes based on the identity of the metal ions in the active site, the [NiFe], [FeFe] and [Fe] hydrogenases, which catalyze proton reduction or dihydrogen oxidation at very high rates.[4] Many structural and functional models for the active site in [FeFe] hydrogenase have been reported, but especially functional models of the [NiFe] hydrogenases are less mature.[5] In order to produce efficient functional models of the active site of [NiFe] hydrogenases organometallic [NiFe] and even [NiRu] coordination compounds have been prepared.[4] The choice for ruthenium to replace iron in mimicking the active site is based on the fact that ruthenium complexes are active as (homogeneous) catalysts in hydrogenation and hydrogen transfer reactions and generally form more stable coordination compounds. Most significant is the fact that Ru(II) ions are able to accept both hard and soft ligands such as hydride and dihydrogen, which makes it suitable for replacing the Fe center in models of the [NiFe] hydrogenases.[4] In the past decade several heterodinuclear [NiRu] complexes have been reported as structural and functional models of [NiFe] hydrogenases.[6-8,10] A subclass of [NiFe] hydrogenases comprises the [NiFeSe] hydrogenases, in which one of the non-bridging cysteines (Cys) in the active site of the enzyme is replaced by selenocysteine (Sec).[11] Until now only few studies have been directed to mimic the active site of [NiFeSe] hydrogenase using a selenolate ligand coordinated to the nickel center.[12,13]

The aim of this research is the synthesis and characterization of novel electrocatalyst for the reduction of protons to dihydrogen gas. Previously it has been shown that catalysts based on heterodinuclear [NiRu] compounds are very promising electrocatalysts for the HER.[9] The

introduction of large and bulky ligands for steric protection of the ruthenium center in the [NiRu]-based catalysts has been reported to result in increased stability during the catalytic cycle.[9] In this chapter our study is described of two new trinuclear [NiRu] complexes derived from a reaction of the compounds [Ni(xbSmS)][14] and [Ni(xbSmSe)][15] with *cis*-$[Ru(phen)_2(Cl)_2]$ (H_2xbSmS = 1,2-bis(4-mercapto-3,3-dimethyl-2-thiabutyl)benzene; H_2xbSmSe = 1,2,-bis(2-thiabutyl-3,3-dimethyl-4-selenol)benzene; phen = phenanthroline).[16] Both NiS_4 and NiS_2Se_2 complexes are used in order to investigate the effect of changing the sulfur donor atom to selenium, as inspired by the active sites in [NiFe] and [NiFeSe] hydrogenases.

5.2 Results

5.2.1 Synthesis and Characterization

The mononuclear nickel and ruthenium precursor complexes were synthesized following reported procedures.[14,15,16] The novel trinuclear complexes $[\{Ni(xbSmS)\}_2Ru(phen)_2](PF_6)_2$ **(1)** and $[\{Ni(xbSmSe)\}_2Ru(phen)_2](PF_6)_2$ **(2)** were synthesized by refluxing an ethanolic solution of the compound [Ni(xbSmS)] or [Ni(xbSmSe)] with the compound *cis*-$[Ru(phen)_2(Cl)_2]$ and were obtained as dark reddish-brown solids in 43% and 46% yield, respectively (Scheme 5.1). The chloride anions were exchanged with PF_6^- anions using NH_4PF_6. It was our intention to make dinuclear NiRu complexes with two bridging thiolates starting from a 1:1 ratio of the nickel and ruthenium complexes. However, the NMR spectra of the obtained complexes were not in agreement with the expected dinuclear compounds. The crystal structures of the obtained complexes surprisingly showed that trinuclear $[Ni_2Ru]$ complexes were obtained instead. The synthesis of the compounds was then optimized using a 2:1 ratio of the precursor nickel and ruthenium complexes. Both $[Ni_2Ru]$ complexes were characterized by ^{1}H NMR spectroscopy, mass spectrometry, elemental analysis and single crystal X-ray crystallography. Although acetone solutions of both complexes give rise to sharp resonances in the ^{1}H NMR spectra, it is difficult to assign all peaks in the aromatic region. The ESI-MS spectra of the complexes exhibit the parent molecular ion peaks at *m/z* = 633.7 and 727.2 for **(1)** and **(2)** respectively, for the trinuclear dicationic compound $[M-2(PF_6)]^{2+}$.

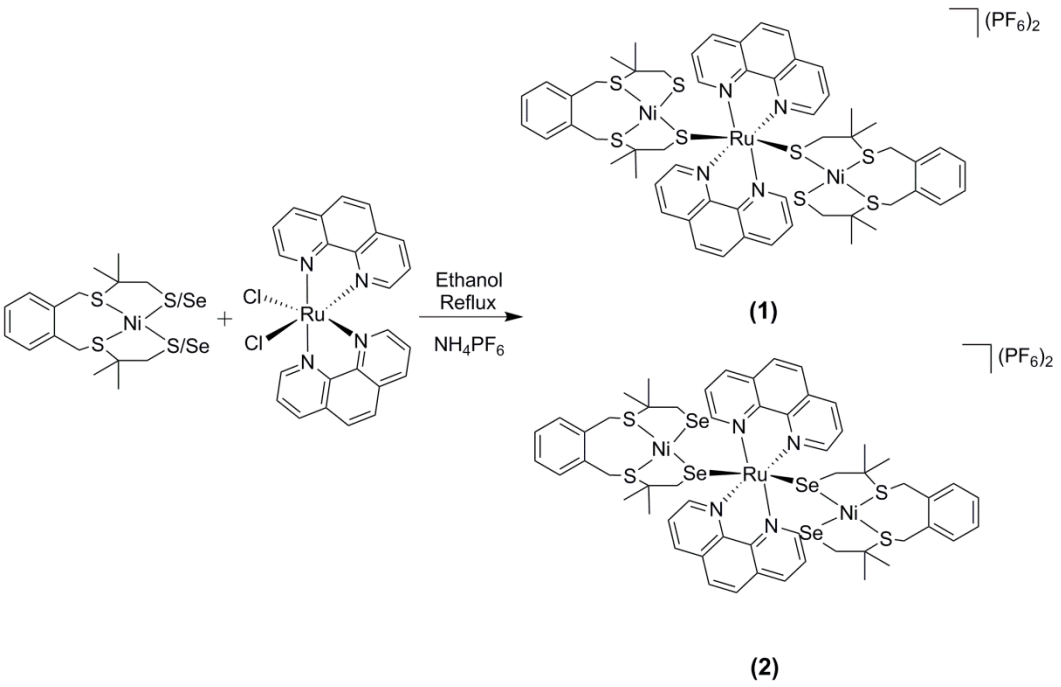

Scheme 5.1: Synthesis scheme of the complexes $[\{Ni(xbSmS)\}_2Ru(phen)_2](PF_6)_2$ **(1)** and $[\{Ni(xbSmSe)\}_2Ru(phen)_2](PF_6)_2$ **(2)**

5.2.2 Description of the Structures

Single crystals of the compounds $[\{Ni(xbSmS)\}_2Ru(phen)_2](PF_6)_2$ **(1)** and $[\{Ni(xbSmSe)\}_2Ru(phen)_2](PF_6)_2$ **(2)** were obtained by vapor diffusion of 2-propanol into acetone solutions of the complexes. Projections of the structures of **(1)** and **(2)** are given in Figure 5.1; selected interatomic distances and angles are provided in Table 5.1. For complex **(1)**, one of the two Ni complexes and one phenanthroline ligand coordinated to Ru are disordered over two orientations. The crystal structure further contains lattice acetone solvent molecules that together with the PF_6^- ions are disordered over two orientations. The crystal lattice of complex **(2)** also contains some amounts of lattice acetone solvent molecules and two PF_6^- ions disordered over two or three orientations. The trinuclear complex cations in **(1)** and **(2)** contain two square-planar nickel centers bound in *cis* positions to the octahedral ruthenium ion via a bridging thiolate or selenolate donor atom with S-Ru-S and Se-Ru-Se angles of 90.80(15)° and 88.969(13)°, respectively. The square-planar coordination environment of the Ni(II) centers comprises two thioether and two thiolate/selenolate donor atoms in mutual cis positions and is slightly distorted with dihedral angles of 12.17° and 16.9°, defined by the planes $S_{thioether}$-Ni-$S_{thioether}$ and $S_{thiolate}$-Ni-$S_{thiolate}$ for complex **(1),** and 9.74° and 12.14° defined by the planes S-Ni-S and Se-Ni-Se for complex **(2)**. The Ru(II)

centers are octahedral, *cis*-coordinated to two thiolate/selenolate ligands. The ruthenium center is also bound to two 1,10-phenanthroline ligands making the metal compound chiral, but due to the centrosymmetric space group both enantiomers are present in the crystal lattice. The Ni-$S_{thiolate}$ and Ni-$S_{thioether}$ distances in complex **(1)** are quite similar, but obviously the Ni-$Se_{selenolate}$ distances in complex **(2)** are longer than the Ni-$S_{thioether}$ distances due to the larger radius of the selenium donor atom. The Ni-Ru distances are 3.72-3.77 Å in complex **(1)** and significantly longer at 3.92-3.98 Å in complex **(2)**.

Table 5.1: Selected bond lengths (Å) and angles (°) for the complexes **(1)** and **(2)**

Distances (Å)	**(1)**	Distances (Å)	**(2)**
Ni1-S11	2.2172(8)	Ni1-Se2	2.3295(5)
Ni1-S21	2.1913(8)	Ni1-S2	2.1970(9)
Ni1-S31	2.1677(8)	Ni1-S1	2.1728(9)
Ni1-S41	2.1669(9)	Ni1-Se1	2.2920(5)
Ni3-S12	2.229(6)	Ni2-Se3	2.3308(5)
Ni3-S22	2.196(6)	Ni2-S3	2.1890(9)
Ni3-S32	2.176(7)	Ni2-S4	2.1821(8)
Ni3-S42	2.172(7)	Ni2-Se4	2.2852(5)
Ru1-S11	2.3898(6)	Ru1-Se2	2.4997(4)
Ru1-S12	2.319(7)	Ru1-Se3	2.5124(4)
Ru1-N11	2.077(2)	Ru1-N4	2.065(3)
Ru1-N12	2.094(5)	Ru1-N2	2.075(3)
Angles (°)	**(1)**	Angles (°)	**(2)**
S11-Ni1-S41	84.84(3)	Se2-Ni1-Se1	82.506(17)
S11-Ni1-S21	85.83(3)	Se2-Ni1-S2	86.15(3)
S31-Ni1-S41	88.90(3)	S1-Ni1-Se1	88.65(3)
S21-Ni1-S31	102.98(3)	S2-Ni1-S1	103.50(3)
S11-Ni1-S41	84.84(3)	Se2-Ni1-Se1	82.506(17)
S11-Ni1-S21	85.83(3)	Se2-Ni1-S2	86.15(3)
S31-Ni1-S41	88.90(3)	S1-Ni1-Se1	88.65(3)
S21-Ni1-S31	102.98(3)	S2-Ni1-S1	103.50(3)
N11-Ru1-N21	79.59(11)	N4-Ru1-N3	79.58(11)
N12-Ru1-N22	77.2(3)	N2-Ru1-N1	79.46(10)
N12-Ru1-S11	167.9(2)	N2-Ru1-Se2	172.71(8)
N11-Ru1-S12	175.14(17)	N4-Ru1-Se3	173.27(8)
S11-Ru1-S12	90.80(15)	Se2-Ru1-Se3	88.969(13)

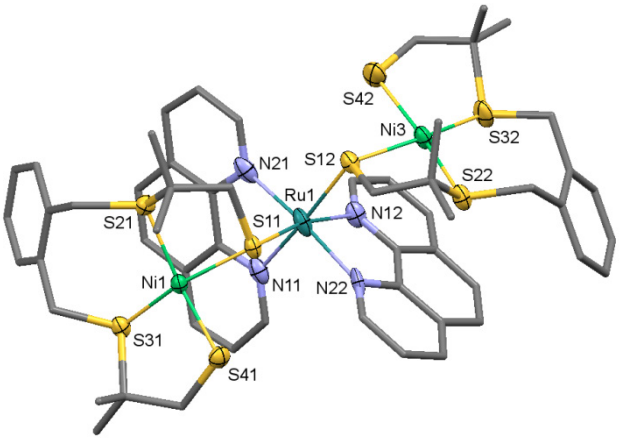

(a)

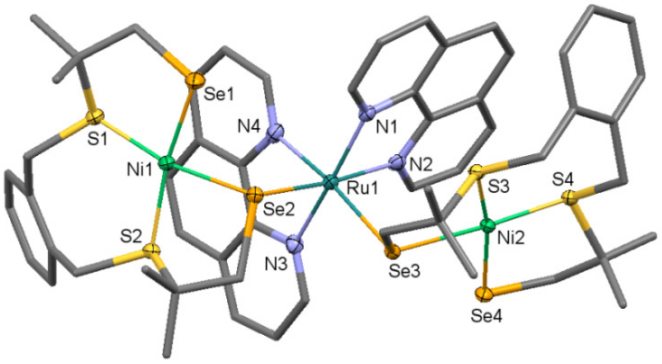

(b)

Figure 5.1: The molecular structures of (a) $[\{Ni(xbSmS)\}_2Ru(phen)_2](PF_6)_2$ and (b) $[\{Ni(xbSmSe)\}_2Ru(phen)_2](PF_6)_2$ at 110(2) K. Displacement ellipsoids (50% probability level) are shown for the atoms belonging to the first coordination spheres around the Ni and Ru metal centers. Hydrogen atoms, PF_6^- anions, lattice solvent molecules, and disorder are omitted for clarity.

5.2.3 Electrochemical Analyses

The cyclic voltammograms of the $[Ni_2Ru]$ complexes were recorded in acetonitrile solution with 0.1 M tetrabutylammonium hexafluoridophosphate as the supporting electrolyte with a scan rate of 200 mV s^{-1}. A glassy carbon electrode was used as a working electrode and Ag/AgCl was used as a reference electrode. All potentials are reported vs. the ferrocene/ferrocinium ($Fc^{0/+}$) couple ($E_{½}$ = 0.43 V vs Ag/AgCl). For both compounds **(1)** and **(2)** three irreversible reduction waves were observed with E_{pc} at −1.69, −2.05, and −2.19 V *vs*.

Fc^+/Fc for **(1)** and at −1.68, −2.04, −2.26 V *vs*. Fc^+/Fc for **(2)** (Figure 5.2a). The cyclic voltammograms of the mononuclear nickel complexes show one irreversible wave with E_{pc} at −1.96 V and −1.93 V *vs*. Fc/Fc^+ for the compounds [Ni(xbSmS)] and [Ni(xbSmSe)], respectively (Figure 5.2b). The cyclic voltammogram of *cis*-$[Ru(phen)_2(Cl)_2]$ only shows a very small reduction event, indicating that the Ru(I) oxidation state is not really accessible (Figure 5.2b). The first reduction wave for the compounds **(1)** and **(2)**, of which the peak current - compared to the second and third reduction processes - seems to indicate a two-electron process, might be assigned to the reduction of Ni^{II} to Ni^{I}. The apparent shift in the reduction potential of the nickel centers might be explained by the coordination of the dicationic ruthenium complex, the overall positive charge of the trinuclear compound making the Ni center more readily reduced.

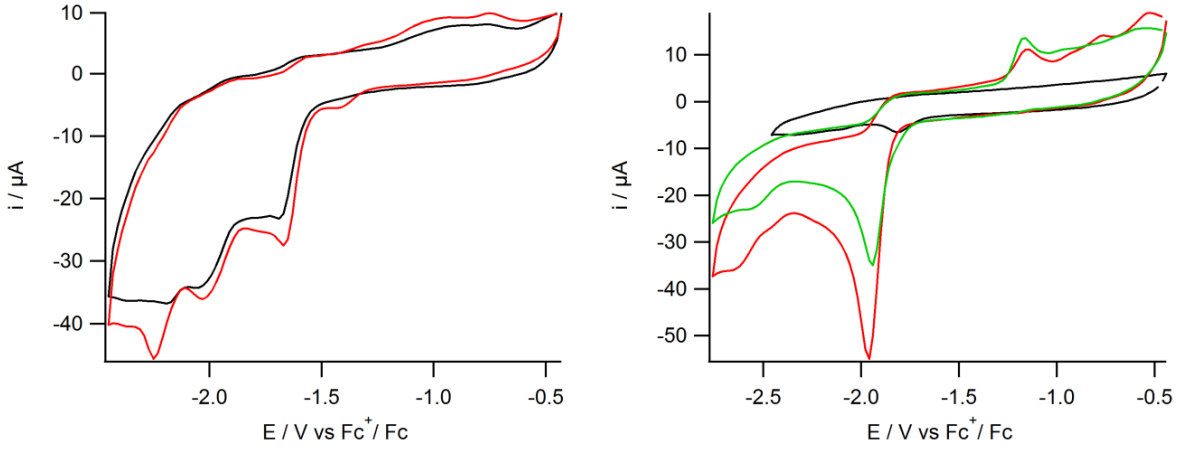

(a) (b)

Figure 5.2: Cyclic voltammograms of 1 mM solutions of (a) compound **(1)** (black) and compound **(2)** (red)**,** (b) *cis*-$[Ru(phen)_2(Cl)_2]$(black), [Ni(xbSmS)](red), [Ni(xbSmSe)](green) in acetonitrile containing $TBAPF_6$ (0.1 M) as the supporting electrolyte and a glassy carbon working electrode at 200 mV s^{-1}.

5.2.4 Electrocatalytic Hydrogen Evolution in the Presence of HOAc

The activity of the new $[Ni_2Ru]$ compounds in electrocatalytic proton reduction was studied using cyclic voltammetry by the addition of varying amounts of HOAc to acetonitrile solutions. Both complexes show electrocatalytic activity with a peak potential around −2.1 V *vs*. Fc^+/Fc, as is clear from the increasing catalytic current that appears with the addition of higher amounts of acid (Figure 5.3). The potential at which proton reduction occurs, becomes

slightly more negative at higher concentrations of acid. The overpotential for electrocatalytic proton reduction at an acetic acid concentration of 10 mM of the complexes **(1)** and **(2)** has been calculated using the half-wave potentials of the catalytic peaks, taking homoconjugation of the acid into account.[17] Both complexes display quite similar overpotentials, being 640 mV for complex **(1)** and 650 mV for complex **(2)**. In order to confirm that indeed dihydrogen gas is formed in the catalytic reaction, controlled-potential coulometry (CPC) experiments were carried out using 0.5 mM solutions of complexes **(1)** and **(2)** in acetonitrile (5 ml) in the presence of 10.5 µl of HOAc (30 equivalents of H^+ per Ni_2Ru compound) at −2.1 V *vs*. Fc^+/Fc. The quantification of produced dihydrogen gas was done volumetrically by GC analysis. The CPC experiment was run for 1 h, while the solution was stirred continuously. Using complex **(1)** as the electrocatalyst for proton reduction, a total of 49 µl (2 µmol) H_2 was produced per 0.5 mM complex in 1 h with 64% faradaic yield, whereas for complex **(2)** a total of 56 µl (2.3 µmol) H_2 was produced per 0.5 mM complex in 1 h with 63% faradaic yield. In a control experiment in the absence of the catalyst formation of H_2 is not observed at this potential.

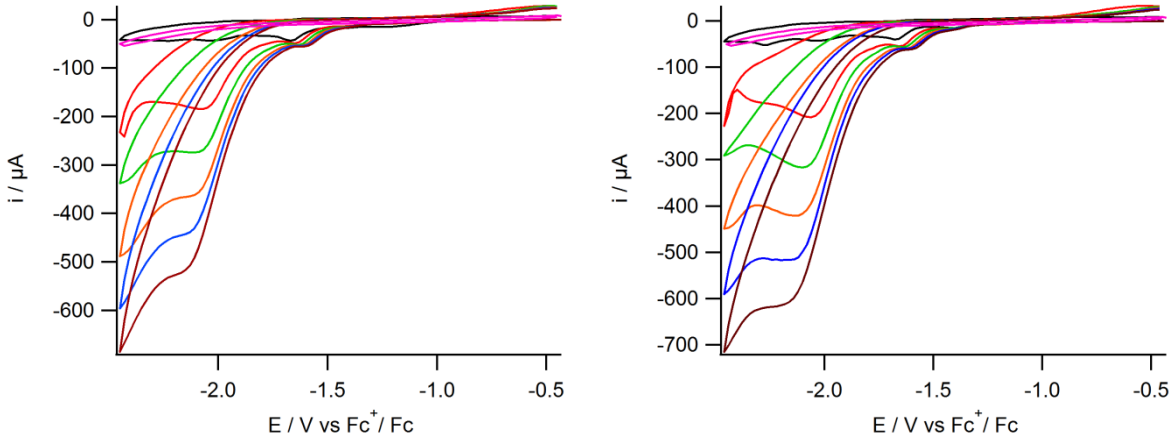

(a) (b)

Figure 5.3: Cyclic voltammograms of 1 mM solutions of (a) compound **(1)** and (b) compound **(2)** in acetonitrile containing $TBAPF_6$ (0.1 M) using a glassy carbon working electrode at 200 mV s^{-1} in the presence of 0 (black), 10 (red), 20 (green), 30 (orange), 40 (blue), 50 (brown) mM of acetic acid and blank with 50 mM of acetic acid (pink).

5.3 Discussion

In this work the compounds [{Ni(xbSmS)}$_2$Ru(phen)$_2$](PF$_6$)$_2$ **(1)** and [{Ni(xbSmSe)}$_2$Ru(phen)$_2$](PF$_6$)$_2$ **(2)** were prepared as functional mimics of the [NiFe] and [NiFeSe] hydrogenases active site. X-ray crystallography showed that the trinuclear complex cations in **(1)** and **(2)** contain two square-planar nickel centers bound in *cis* positions to the octahedral ruthenium ion via a bridging thiolate or selenolate donor atom. The electrochemical properties of the two [Ni$_2$Ru] complexes are highly similar. The substitution of the thiolate donor by a selenolate donor atom does not have a significant effect neither on the structure, nor on the electrocatalytic activity. This finding is similar to the results for the dinuclear [NiRu] compounds reported in Chapter 3. Comparison of the electrocatalytic activity of the two dicationic trinuclear complexes with that of the monocationic dinuclear [NiRu] complexes described in Chapter 3 shows that the trinuclear [Ni$_2$Ru] complexes operate at lower overpotentials, but are less efficient. The irreversibility of the reduction processes give rise to the question whether the structures are stable during catalysis. The cyclic voltammograms of the parent mononuclear nickel and ruthenium complexes are different from those of the trinuclear [Ni$_2$Ru] complexes, indicating that dissociation of the trinuclear [NiRu] compounds in solution does not occur. However, the cyclic voltammograms of both [Ni$_2$Ru] compounds show changes after the first scan (Figure AV.1-2), which might be due to partial decomposition. However, more studies should be done to gain insight concerning the electrocatalytic mechanism and active species in proton reduction.

5.4 Conclusion

Two new trinuclear compounds [{Ni(xbSmS)}$_2$Ru(phen)$_2$](PF$_6$)$_2$ and [{Ni(xbSmSe)}$_2$Ru(phen)$_2$](PF$_6$)$_2$ were synthesized with nickel complexes of tetradentate dithiolate or diselenolate ligands acting as monodentate ligands to cis-octahedral ruthenium(II) ions. Both complexes are air stable and in the presence of acetic acid catalyze the hydrogen evolution reaction as shown by CV and CPC experiments. Changing the thiolate donor atom to selenolate does not make a significant difference in the electrocatalytic activity of the resulting compounds.

5.5 Experimental

5.5.1 General

All experiments were performed using standard Schlenk techniques under a nitrogen atmosphere unless otherwise noted. Chemicals were purchased from Acros or Aldrich and were used without further purification. Organic solvents were deoxygenated by the freeze-pump-thaw method and were dried over molecular sieves prior to use. NMR spectra were recorded on a 300 MHz Bruker DPX 300 spectrometer and chemical shifts were referenced against the solvent peak. Mass spectra were obtained with a Finnigan TSQ-quantum instrument using ESI. Elemental analyses were performed by the Microanalytical Laboratory Kolbe in Germany. Electrochemical measurements were performed at room temperature under argon using an Autolab PGstat10 potentiostat controlled by GPES4 software. A three-electrode cell system was used with a glassy carbon working electrode, a platinum counter electrode and an Ag/AgCl reference electrode. All electrochemistry measurements were done in acetonitrile solution with tetrabutylammonium hexafluoridophosphate as the supporting electrolyte; after each run ferrocene was added as an internal reference. All potentials are referenced to half-wave potential of the redox couple of Fc^+/Fc, which under these conditions was found at 0.43 V *vs*. Ag/AgCl in acetonitrile, with a ΔE of 99 mV. Controlled-potential coulometry (CPC) experiments were done with the same three-electrode cell system and electrodes. CPC experiments were recorded with an Autolab PGstat10 potentiostat controlled by GPES4 software. Gas chromatographic analysis was performed on a Shimadzu gas chromatograph GC-2010 at 35 °C fitted with a Supelco Carboxen 1010 molecular sieve column. Helium was used as the carrier gas, and analytes were detected using a thermal conductivity detector operated at 80 mA. The total volume of H_2 produced during the reaction was calculated using a calibration line, which was obtained using the external reference method by injection of known amounts of H_2 into the GC using a Hamilton gas-tight syringe. A solution of complexes **(1)** or **(2)** in acetonitrile (5 ml, 0.5 mM) was placed into a three-electrode cell and prior to each measurement the system was deaerated by bubbling with helium gas for 10 min. The system was closed, and the headspace was pumped through the solution for 1 min. Before each GC sampling the headspace pumping was temporarily stopped to allow equilibration of the pressure and then GC measurement was started with a 0.5 mL sample of the headspace injection. The GC valve and the pump (KNF NMS 010 L micro diaphragm pump) were enclosed in a helium-purged housing to prevent air leaking into the system.

5.5.2 Single Crystal X-ray Crystallography

All reflection intensities were measured at 110(2) K using a SuperNova diffractometer (equipped with Atlas detector) with Cu *K*α radiation (λ = 1.54178 Å) for complex **(1)** and Mo *K*α radiation (λ = 0.71073 Å) for complex **(2)** under the program CrysAlisPro (Version 1.171.36.32 Agilent Technologies, 2013). The same program was used to refine the cell dimensions and for data reduction. The structure was solved with the program SHELXS-2014/7 and was refined on F^2 with SHELXL-2014/7.[18] Analytical numeric absorption correction using a multifaceted crystal model was applied using CrysAlisPro. The temperature of the data collection was controlled using the system Cryojet (manufactured by Oxford Instruments). The H atoms were placed at calculated positions using the instructions AFIX 23, AFIX 43 or AFIX 137 with isotropic displacement parameters having values 1.2 or 1.5 *U*eq of the attached C atoms. Both structures are partly disordered.

Additional notes on the structure determination:

(1) One of the two Ni complexes and one phenanthroline ligand coordinated to Ru are disordered over two orientations. The occupancy factors of the major components of the disorder refine to 0.543(12) and 0.550(6), respectively. The two PF_6^- counterions are found to be disordered over two orientations. The occupancy factors of the major components of the disorder refine to 0.683(4) and 0.695(4). The asymmetric unit contains 1.437 lattice acetone molecules. All solvent molecules are disordered over two orientations, but one of the two crystallographically independent solvent molecules is found at a special position.

(2) The two PF_6^- counterions are disordered over two or three orientations. All occupancy factors can be retrieved from the crystallographic information file. The crystal lattice contains some amount of lattice acetone solvent molecules. In the asymmetric unit, there is one ordered acetone molecule (with occupancy factor refining to 0.887(5)) and another acetone molecule disordered over an inversion center (and thus its occupancy factor was constrained to 0.5).

5.5.3 Synthesis of $[\{Ni(xbSmS)\}_2Ru(phen)_2](PF_6)_2$

Cis-$[Ru(phen)_2(Cl)_2]$ (0.119 g, 0.223 mmol) was dissolved in 8 ml ethanol and the solution was refluxed for 2 h. This solution was transferred, with a cannula, to a Schlenk flask containing [Ni(xbSmS)] (0.180 g, 0.446 mmol) and the resulting reaction mixture was refluxed for 24 h. After the reaction NH_4PF_6 (0.081 g, 0.496 mmol) was added to the hot ethanolic reaction mixture and the solution was stirred for 30 min, resulting in a dark reddish-

brown solid. The solid was collected by filtration in a yield of 0.155 g (0.097 mmol, 43%). ^{1}H NMR (300 MHz, $(CD_3)_2CO$) δ (ppm): 10.29 (d, Py-H), 8.71-7.17 (aromatic region), 4.12 (d, CH_2-S21/31), 4.03 (d, CH_2-S22/32), 2.33 (d, C-CH_2-S11/41), 1.64 (d, C-CH_2-S12/42), 1.47 (t, CH_3). ESI-MS (MeCN): 633.7, calcd: 633.03, $[M\text{-}2(PF_6)]^{2+}$. Elemental Analysis calcd (%) for $C_{56}H_{64}F_{12}N_4Ni_2P_2RuS_8$: C: 43.17, H: 4.14, N: 3.60; found C: 43.48, H: 4.28, N: 3.48.

5.5.4 Synthesis of $[\{Ni(xbSmSe)\}_2Ru(phen)_2](PF_6)_2$

Cis-$[Ru(phen)_2(Cl)_2]$ (0.119 g, 0.223 mmol) was dissolved in 8 ml ethanol and the solution was refluxed for 2 h. This solution was transferred, with a cannula, to a Schlenk flask containing [Ni(xbSmSe)] (0.222 g, 0.446 mmol) and the resulting reaction mixture was refluxed for 24 h. Then NH_4PF_6 (0.081 g, 0.496 mmol) was added while the reaction mixture was still hot and the solution was stirred for 30 min. After filtration a dark reddish-brown solid was obtained in a yield of 0.180 g (0.103 mmol, 46%). ^{1}H NMR (300 MHz, $(CD_3)_2CO$) δ (ppm): 10.22 (d, Py-H), 8.66-7.22 (aromatic region), 4.18 (d, CH_2-S1/2), 4.07 (d, CH_2-S3/4), 2.53 (d, C-CH_2-Se1/2), 1.65 (d, C-CH_2-Se3/4), 1.50 (t, CH_3). ESI-MS (MeCN): 727.2, calcd: 727.2 $[M\text{-}2(PF_6)]^{2+}$. Elemental Analysis calcd (%) for $C_{56}H_{64}F_{12}N_4Ni_2P_2RuS_4Se_4 \cdot 0.3C_3H_6O$: C: 38.86, H: 3.79, N: 3.16; found C: 39.12, H: 3.9,0 N: 3.08.

5.6 Acknowledgement

Mr. J.J.M. van Brussel and Mr. W. Jesse are gratefully acknowledged for performing the ESI-MS measurements.

5.7 References

1. C. Tard, C. Pickett, *J. Chem. Rev.*, 2009, **109**, 2245.
2. M. T. Koper and E. Bouwman, *Angew. Chem. Int. Ed.*, 2010, **49**, 3723.
3. M. Stephenson, L. H. Stickland, *Biochem J.*, 1931, **25(1)**, 205.
4. T. R. Simmons, G. Berggren, M. Bacchi, M. Fontecave and V. Artero, *Coord. Chem. Rev.*, 2014, **271**, 127.
5. G. M. Chambers, M. T. Huynh, Y. Li, S. Hammes-Schiffer, T. B. Rauchfuss, E. Reijerse and W. Lubitz, *Inorg. Chem.*, 2016, **55**, 419.
6. S. Canaguier, M. Fontecave and V. Artero, *Eur. J. Inorg. Chem.*, 2011, 1094.
7. S. Canaguier, L. Vaccaro, V. Artero, R. Ostermann, J. Pecaut, M. J. Field and M. Fontecave, *Chem. Eur. J.*, 2009, **15**, 9350.
8. Y. Oudart, V. Artero, L. Norel, C. Train, J. Pécaut and M. Fontecave, *J. Organomet. Chem.,* 2009, **694**, 2866.
9. Y. Oudart, V. Artero, J. Pécaut, C. Lebrun and M. Fontecave, *Eur. J. Inorg. Chem.*,

2007, 2613.
10. G. M. Chambers, R. Angamuthu, D. L. Gray and T. B. Rauchfuss, *Organometallics*, 2013, **32**, 6324
11. E. Garcin, X. Vernede, E. Hatchikian, A. Volbeda, M. Frey and J. Fontecilla-Camps, *Structure* 1999, **7**, 557.
12. C. Wombwell and E. Reisner, *Chem. Eur. J.* 2015, **21**, 8096.
13. G. Gezer, D. Durán Jiménez, M. A. Siegler and E. Bouwman, *Dalton Trans.*, 2017, **46**,7506.
14. J. A. Verhagen, D. D. Ellis, M. Lutz, A. L. Spek and E. Bouwman, *Dalton Trans.,* 2002, 1275.
15. C. Wombwell and E. Reisner, *Chem. Eur. J.* 2015, **21**, 8096.
16. J. E. Collins, J. J. S. Lamba, J. Christopher Love, J. E. McAlvin, N. Christina, B. P. Peters, W. Xufeng and C. L. Fraser, *Inorg. Chem*, 1999, **38**, 2020.
17. V. Fourmond, P. A. Jacques, M. Fontecave and V. Artero, *Inorg. Chem.*, 2010, **49**, 10338.
18. G. M. Sheldrick, *Acta Cryst*, 2015, **C71**, 3.

Chapter 6

Summary, Conclusions and Outlook

6.1 Summary

6.1.1 Introduction

The growing demand of energy indicates that global energy resources in the form of fossil fuels will not be sufficient in the future. In order to solve potential future energy problems development of a sustainable hydrogen economy is highly desirable. Researchers are looking for new and cleaner ways for the production of dihydrogen gas. The structure and function of hydrogenases have raised the attention of synthetic chemists in the past decades, since new catalysts for proton reduction may be developed by using biomimetic, functional models of hydrogenases. Three types of hydrogenases are known, being the [FeFe], [Fe] and [NiFe] hydrogenases.[1] A significant amount of data has been gathered over the years concerning the enzyme redox states and the reaction mechanism for the reversible heterolytic splitting of dihydrogen at the [NiFe] hydrogenase active site.[6] The [NiFeSe] hydrogenases form a subclass of the [NiFe] hydrogenases, in which one of the cysteines (Cys) in the active site of the enzyme is replaced by selenocysteine (Sec).[2] In the past decades a large number of structural and functional models for the active site in [NiFe] hydrogenase have been reported with overpotentials for proton reduction as low as 50 mV.[3-5] This thesis deals with the synthesis and characterization of new structural and functional models of the nickel-containing enzymes [NiFe] and [NiFeSe] hydrogenases.

6.1.2 Electrocatalytic Proton Reduction by a Model for [NiFeSe] Hydrogenases

The [NiFeSe] hydrogenase forms a subclass of the [NiFe] hydrogenases, in which one of the non-bridging cysteines (Cys) in the active site of the enzyme is replaced by selenocysteine (Sec); compared to their cysteine homologues the [NiFeSe] hydrogenases have higher catalytic activity in the hydrogen evolution reaction.[2,7-8] In Chapter 2, the synthesis and characterization is described of the two novel heterodinuclear compounds [Ni(pbSmSe)FeCpCO]PF_6 and [Ni(xbSmSe)FeCpCO]PF_6 as mimics of the [NiFeSe] hydrogenase active site. X-ray structure determinations showed that in both NiFe complexes the nickel(II) center is in a square-planar S_2Se_2 environment; the two selenolate donors are bridging to the iron(II) center that is further coordinated to an η^5-cyclopentadienyl group and a carbon monoxide ligand. The compounds show some structural similarities with the active site of [NiFeSe] hydrogenase. Electrochemical studies showed that only the complex [Ni(pbSmSe)FeCpCO]PF_6 is an electrocatalyst for the

production of H_2 in DMF in the presence of acetic acid at −2.1 V vs. Fc^+/Fc; a foot-of-the-wave (FOW) analysis of the catalytic currents yielded an estimation of k_{obs} of 24 s^{-1}.

6.1.3 Nickel-Ruthenium Based Complexes as Biomimetic Models of [NiFe] and [NiFeSe] Hydrogenases for Dihydrogen Evolution

Many ruthenium complexes are active catalysts in hydrogenation and hydrogen transfer reactions and generally ruthenium forms more stable coordination compounds than iron. Most importantly Ru(II) ions are able to accept both hard and soft ligands such as hydride and dihydrogen, which makes it suitable for replacing the Fe center in models of the [NiFe] hydrogenase.[9] In Chapter 3, the synthesis and characterization of the two nickel-ruthenium complexes $[Ni(xbSmS)RuCp(PPh_3)]PF_6$ and $[Ni(xbSmSe)RuCp(PPh_3)]PF_6$ are reported as mimics of the active site of the [NiFe] and [NiFeSe] hydrogenases. The X-ray structural analyses of the complexes show that the two NiRu complexes are isomorphous; in both NiRu complexes the nickel(II) centers are in a square-planar environment with two thioether donor atoms, and two thiolate or selenolate donors that are bridging to the ruthenium(II) center. The Ru(II) ion is further coordinated to an η^5-cyclopentadienyl group and a triphenylphosphane ligand. These complexes catalyze the dihydrogen evolution reaction in the presence of acetic acid in acetonitrile solutions at around −2.20 V vs. Fc^+/Fc with overpotentials of 810 and 830 mV. Thus they can be regarded as functional models of the [NiFe] and [NiFeSe] hydrogenases, albeit with relatively high overpotentials and rather low activity.

6.1.4 Dealkylation Through C–S and Ni–S Bond Cleavage Relevant to the Mechanism of Methyl-coenzyme M Reductase (MCR)

Nickel thiolate compounds are enjoying much attention among bioinorganic and organometallic chemists, as they are important in the context of structural and/or functional models for enzymes. Recently a number of biomimetic compounds have been reported as models for the active site in the enzymes containing a selenocysteine in their active site, in which thiolate donor atoms have been substituted by selenolates.[10,11] In Chapter 4, the syntheses are reported of the thiouronium precursor to a new chelating tetradentate dithioether-dithiolate ligand (H_2ebSmS) and the corresponding selenouronium precursor of the tetradentate dithioether-diselenolate ligand (H_2ebSmSe) as well as their nickel complexes. The complexes $[Ni_2(ebSmS)_2]$ and [Ni(pbSmSe)] were obtained, but were found to be light

sensitive and to result in partially 'decomposed' compounds upon irradiation. In all of the 'decomposed' compounds one of the alkylthiolate or alkylselenolate arms of the ligand is lost from the tetradentate ligand, resulting in dinuclear nickel(II) compounds of new asymmetric tridentate ligands. The compound [Ni(ebSmSe)] was found to be the most reactive for which only the 'decomposed' compound was obtained. The results are potentially relevant to the mechanism of action of methyl-coenzyme M reductase.

6.1.5 Synthesis and Characterization of Trinuclear [NiRu] Complexes for Electrocatalytic Proton Reduction

[NiFe] and [NiRu] complexes have been reported as structural and functional models of [NiFe] hydrogenases.[9,12,13] In Chapter 5, the synthesis and characterization are described of two new trinuclear [Ni_2Ru] complexes comprising either NiS_4 or NiS_2Se_2 complexes in order to investigate the effect of changing the sulfur donor atom to selenium on their electrocatalytic properties. The X-ray structure determinations showed that the trinuclear complex cations in [{Ni(xbSmS)}$_2$Ru(phen)$_2$](PF$_6$)$_2$ and [{Ni(xbSmSe)}$_2$Ru(phen)$_2$](PF$_6$)$_2$ contain two square-planar nickel centers bound in cis positions to the octahedral ruthenium ion via a bridging thiolate or selenolate donor atom. Electrocatalytic proton reduction occurs for both complexes in acetonitrile with addition of varying amounts of acetic acid at a potential of −2.1 V vs. Fc^+/Fc with faradaic yields of around 65%. Unexpectedly, the effect of replacing the thiolate with selenolate donor atoms appeared to be negligible.

6.2 Conclusions and Outlook

The aim of the research described in this thesis was to synthesize Ni, NiFe and NiRu complexes as mimics of [NiFe] and [NiFeSe] hydrogenases and to investigate their electrocatalytic properties for dihydrogen production. Different ligands containing thioether and thiolate or selenolate donor atoms were prepared, the synthesis and characterization of nickel complexes with these ligands were carried out and several nickel-iron and nickel-ruthenium complexes were obtained and characterized with a combination of spectroscopic techniques.

As the [NiFeSe] hydrogenases generally show higher catalytic activities than the [NiFe] hydrogenases, in the research described in this thesis the effect was studied of changing thiolate to selenolate donor atoms on the electrochemical properties and electrocatalytic activity of the molecular catalysts. Unfortunately and rather unexpectedly no significant

differences were observed, neither in the observed redox potentials and overpotential for proton reduction, nor in the electrocatalytic activity. In Chapter 2, it was shown that changing the ligand environment of the nickel center does have an influence on catalytic activity. Comparison of two related [NiFe] complexes having the same ligands bound to the iron center showed that an increased flexibility of the ligand bound to the nickel center helps to increase the catalytic activity for proton reduction. Furthermore, the interplay of two metal centers in the [NiFe] compounds seems to be beneficial for obtaining higher catalytic activity, as the separate mononuclear [Ni] and [Fe] complexes constituting the heterodinuclear [NiFe] compounds showed lower catalytic activity.

Heterodinuclear [NiRu] (Chapter 3) and heterotrinuclear [Ni_2Ru] compounds (Chapter 5) were synthesized to investigate their catalytic activity for proton reduction. Especially the [Ni_2Ru] complexes described in Chapter 5 were found to be quite stable compared to the [NiFe] complexes. Although the compound [Ni(xbSmSe)FeCpCO]PF_6 does not show catalytic activity (Chapter 2), the compound [Ni(xbSmSe)RuCp(PPh_3)]PF_6 does have catalytic activity for proton reduction (Chapter 4) which shows again the importance of second metal center and its ligand environment.

During the course of our studies to heterodinuclear model systems for hydrogenases we encountered unusual reactivity of a number of the intermediate [Ni] compounds, resulting in dealkylation of the ligands (Chapter 4). The reactivity of the compounds was found to depend on the strain of the carbon chain in the tetradentate ligand as well as the presence of either thiolate or selenolate donor groups. This reactivity not only may be of importance for the study of models for methyl-coenzyme M reductase, but also for industrial applications such as hydrodesulfurization reactions. Further exploration of this light-induced reaction with a combination of spectroscopic techniques and computational studies may shed light on the reaction pathway and pave the way toward new catalysts for desulfurisation of organosulfur derivatives.

In general, the aim of synthesizing structural mimics of the [NiFe] and [NiFeSe] hydrogenases has been successful, but unfortunately the catalytic activities of the obtained compounds are not outstanding. Although it was shown that both metal centers have influence on catalytic activity, it is assumed that the nickel center is the active site for proton reduction. In order to improve catalytic efficiency modifications are necessary for both Ni and Fe centers. A more electron-withdrawing ligand at the nickel center would help in lowering the reduction potential of the nickel ion, but on the other hand would not be beneficial for

obtaining a nickel-hydride intermediate. Further investigations thus could be directed to the design of new models in which the ligands of the iron center are substituted with electron-withdrawing groups, which may aid in lowering the reduction potential of the heterodinuclear compound without hampering formation of the nickel-hydride intermediate. Furthermore, additional proton acceptors built into the ligands for either the nickel or the iron center most likely will result in higher catalytic efficiencies.

6.3 References

1. H. Ogata, W. Lubitz and Y. Higuchi, *Dalton Trans.* 2009, 7577.
2. C. Wombwell and E. Reisner, *Chem. Eur. J.* 2015, **21**, 8096.
3. M. Fontecave and V. Artero, *C. R. Chim.* 2011, **14**, 362.
4. S. Canaguier, M. Field, Y. Oudart, J. Pécaut, M. Fontecave and V. Artero, *Chem. Commun.* 2010, **46**, 5876.
5. S. Canaguier, V. Artero and M. Fontecave, *Dalton Trans*., 2008, 315.
6. S. Kaur-Ghumaan and M. Stein, *Dalton Trans*, 2014, **43**, 9392.
7. L. De Gioia, *Bioinorganic Fundamentals and Applications: Metals in Natural Living Systems and Metals in Toxicology and Medicine,* Elsevier, 2013, Vol. 3.
8. E. Garcin, X. Vernede, E. Hatchikian, A. Volbeda, M. Frey and J. Fontecilla-Camps, *Structure* 1999, **7**, 557.
9. T. R. Simmons, G. Berggren, M. Bacchi, M. Fontecave and V. Artero, *Coord. Chem. Rev.*, 2014, **271**, 127.
10. S. Castellano, A. V. Lobanov, C. Chapple, S. V. Novoselov, M. Albrecht, D. Hua, A. Lescure, T. Lengauer, A. Krol, V. N. Gladyshev and R. Guigo, *Proc. Natl. Acad. Sci. USA*., 2005, **102**, 16188.
11. V. Pelmenschikov and P. E. M. Siegbahn, *J. Biol. Inorg. Chem.*, 2003, **8**, 653.
12. Y. Oudart, V. Artero, L. Norel, C. Train, J. Pécaut and M. Fontecave, *J. Organomet. Chem.,* 2009, **694**, 2866.
13. G. M. Chambers, R. Angamuthu, D. L. Gray and T. B. Rauchfuss, *Organometallics*, 2013, **32**, 6324.

Appendix I

Details of GC and CV Measurements for H_2 Evolution

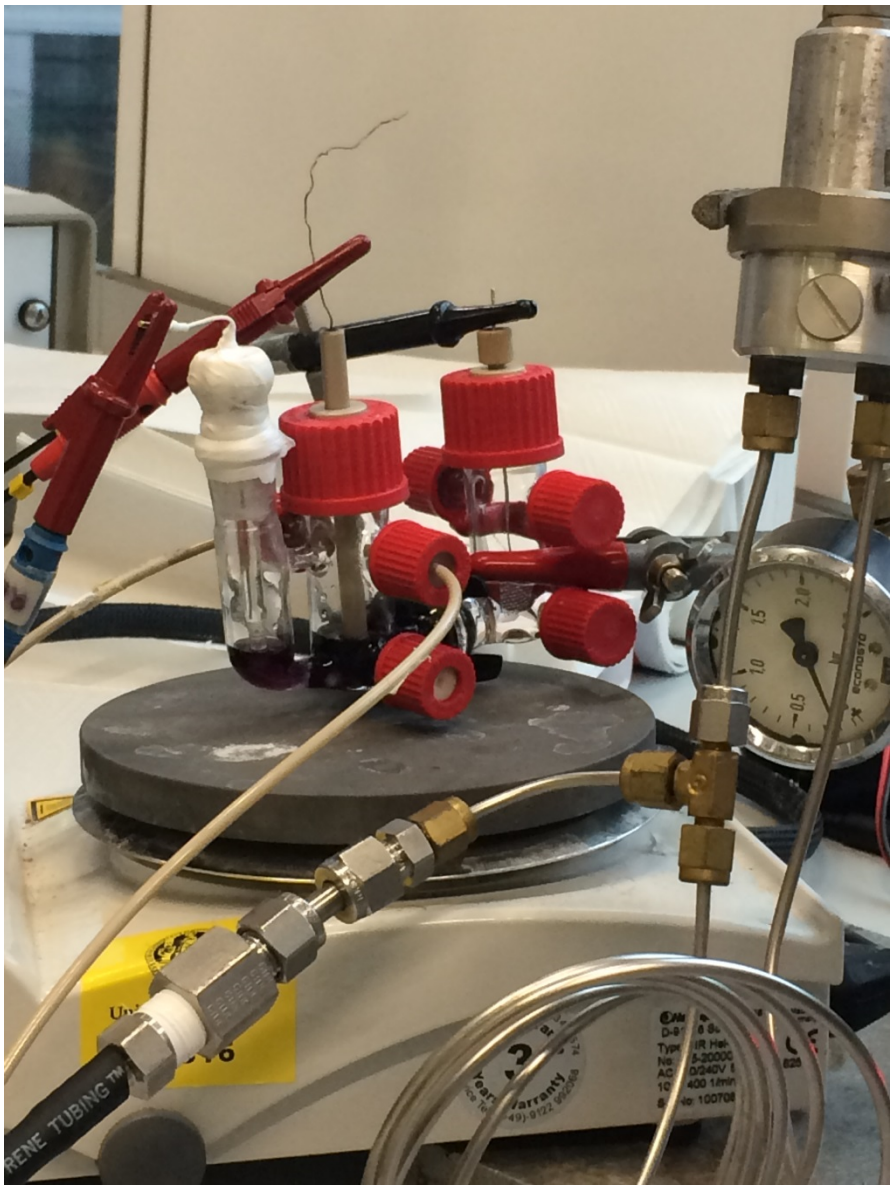

Figure AI.1: Photograph of the controlled-potential coulometry (CPC) experiment setup.

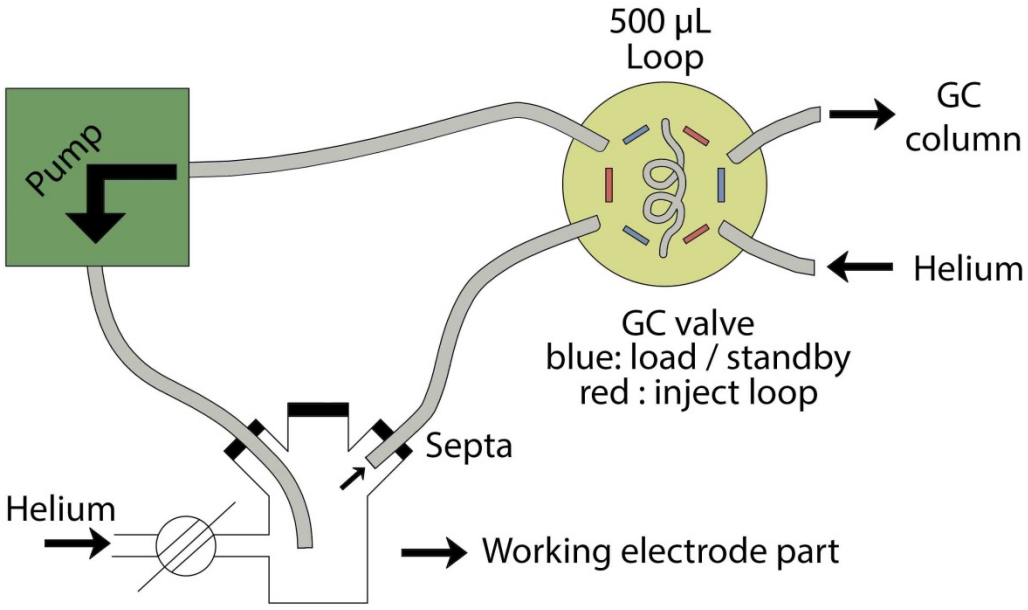

Figure AI.2: Schematic drawing of hydrogen evolution setup.

Hydrogen evolution experiments were done with the three-electrode cell system and electrodes (Figure AI.1). Schematic drawing of the connection from working electrode compartment to the GC setup is shown in Figure AI.2. The reactor is magnetically stirred during the electrolysis. Prior to each measurement the system was deaerated by bubbling with helium for 10 min, while having the pump running. The GC valve and the pump (KNF NMS 010 L micro diaphragm pump) were enclosed in a helium-purged housing to prevent air from leaking into the system. Samples are taken by switching the GC valve from load position (blue) to the inject position (red) while pump is switched off.

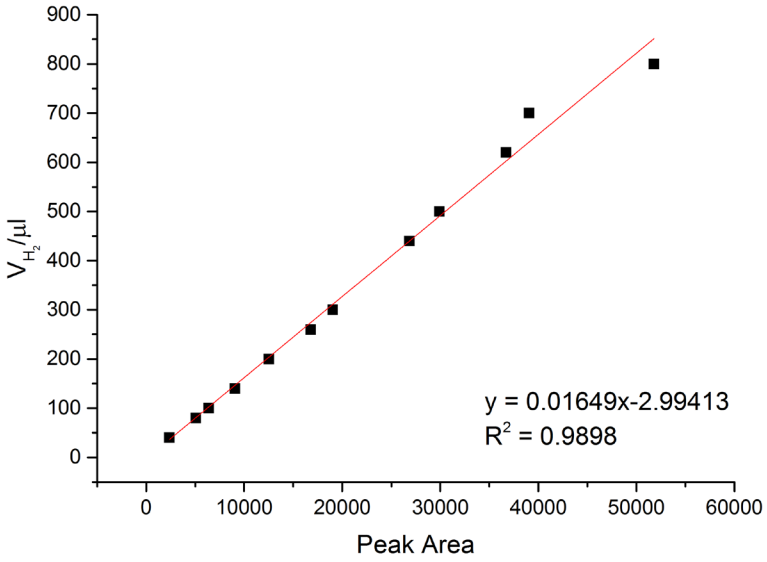

Figure AI.3: Calibration line used for CPC experiments. The observed peak areas of the GC are plotted against the volume of H_2 in the sample with an R^2 value of 0.9898.

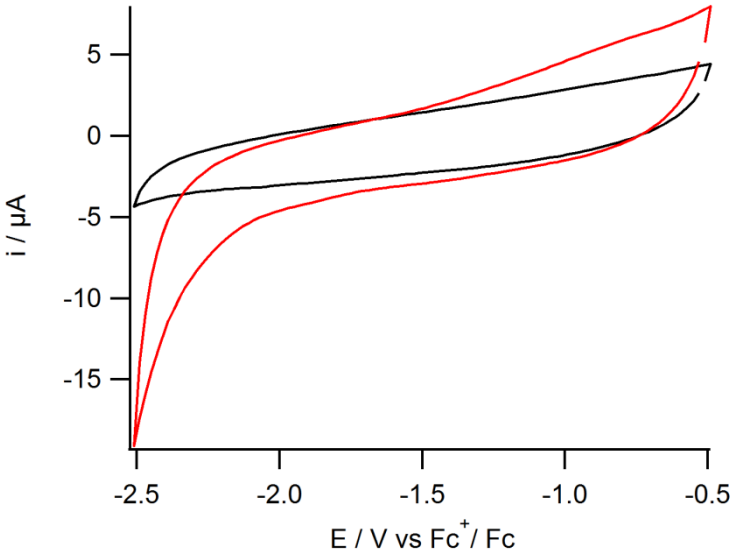

Figure AI.4: Cyclic voltammogram of $TBAPF_6$ (0.1 M) in DMF solution with a glassy carbon working electrode at 200 mV s^{-1} in the presence of 0 (black), 60 (red) mM of acetic acid.

Appendix II

Supplementary Information on Chapter 2

Table AII.1: Crystal and structure refinement data for complexes **(3)**, **(5)** and **(6)**

Data were collected at 110 K using a SuperNova, Dual, Cu at zero, Atlas. H-atom parameters were constrained.

	(3)	**(5)**	**(6)**
Crystal data			
Chemical formula	$C_{11}H_{22}NiS_2Se_2$	$C_{17}H_{27}FeNiOS_2Se_2 \cdot F_6P$	$C_{22}H_{29}FeNiOS_2Se_2 \cdot F_6P \cdot CH_2Cl_2$
M_r	435.03	728.95	875.95
Crystal system, space group	Monoclinic, $P2_1$	Trigonal, R-3:H	Monoclinic, $P2_1/c$
a, b, c (Å)	7.2301 (2), 10.3586 (2), 10.5707 (3)	31.5009 (7), 31.5009 (7), 14.4145 (4)	10.32665 (13), 22.8030 (2), 13.72057 (17)
α, β, γ (°)	90, 103.465 (3), 90	90, 90, 120	90, 105.9916 (13), 90
V (Å^3)	769.92 (4)	12387.3 (6)	3105.87 (6)
Z	2	18	4
Radiation type	Mo $K\alpha$	Cu $K\alpha$	Cu $K\alpha$
μ (mm^{-1})	6.23	10.52	11.00
Crystal size (mm)	0.26 × 0.19 × 0.03	0.18 × 0.05 × 0.04	0.36 × 0.08 × 0.04

	(3)	(5)	(6)
Data collection			
T_{min}, T_{max}	0.316, 0.839	0.414, 0.788	0.161, 0.716
No. of measured, independent and observed [$I > 2\sigma(I)$] reflections	11826, 3544, 3416	16503, 5401, 4525	20451, 6094, 5655
R_{int}	0.030	0.032	0.033
$(\sin \theta/\lambda)_{max}$ (Å^{-1})	0.649	0.616	0.616
Refinement			
$R[F^2 > 2\sigma(F^2)]$, $wR(F^2)$, S	0.022, 0.050, 1.04	0.039, 0.084, 1.06	0.030, 0.077, 1.03
No. of reflections	3544	5401	6094
No. of parameters	149	284	405
No. of restraints	1	0	181
	$w = 1/[\sigma^2(F_o^2) + (0.0249P)^2 + 0.0526P]$ where $P = (F_o^2 + 2F_c^2)/3$	$w = 1/[\sigma^2(F_o^2) + (0.0255P)^2 + 67.0697P]$ where $P = (F_o^2 + 2F_c^2)/3$	$w = 1/[\sigma^2(F_o^2) + (0.0416P)^2 + 2.5519P]$ where $P = (F_o^2 + 2F_c^2)/3$
$\Delta\rho_{max}$, $\Delta\rho_{min}$ (e Å^{-3})	0.47, -0.33	0.47, -0.92	0.90, -0.89

Computer programs: *CrysAlis PRO*, Agilent Technologies, Version 1.171.36.32 (release 02-08-2013 CrysAlis171 .NET) (compiled Aug 2 2013, 16:46:58), *SHELXS2014*/7 (Sheldrick, 2015), *SHELXS2014*/7 (Sheldrick, 2014), *SHELXL2014*/7 (Sheldrick, 2015), *SHELXL2014*/7 (Sheldrick, 2014), *SHELXTL* v6.10 (Sheldrick, 2008).[1]

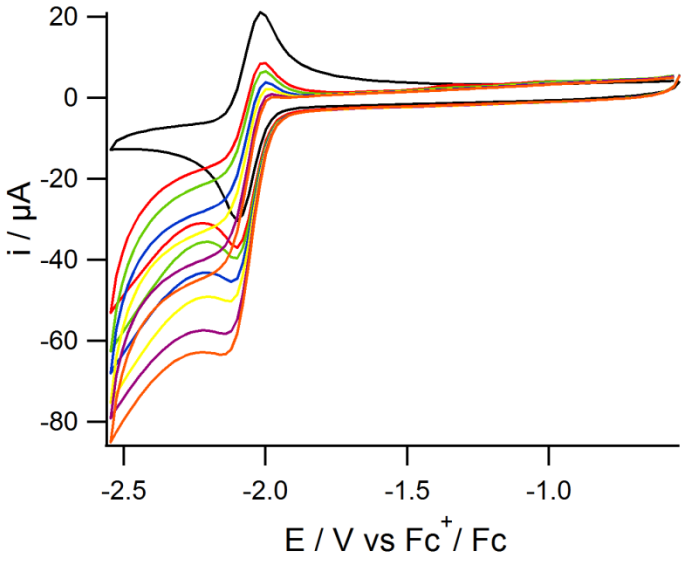

Figure AII.1: Cyclic voltammogram of [Ni(pbSmSe)] **(3)** (1mM) in a DMF solution of $TBAPF_6$ (0.1 M) using a glassy carbon electrode at 200 mV s^{-1} with 0 (black), 10 (red), 20 (green), 30 (blue), 40 (yellow), 50 (purple), 60 (orange) mM of acetic acid.

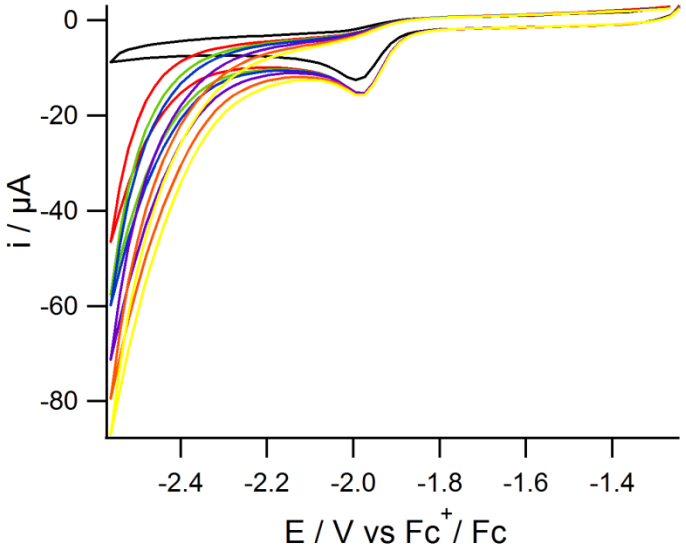

Figure AII.2: Cyclic voltammogram of [Ni(xbSmSe)] **(4)** (1 mM) in a DMF solution of $TBAPF_6$ (0.1 M) using a glassy carbon electrode at 200 mV s^{-1} with 0 (black), 10 (red), 20 (green), 30 (blue), 40 (yellow), 50 (purple), 60 (orange) mM of acetic acid.

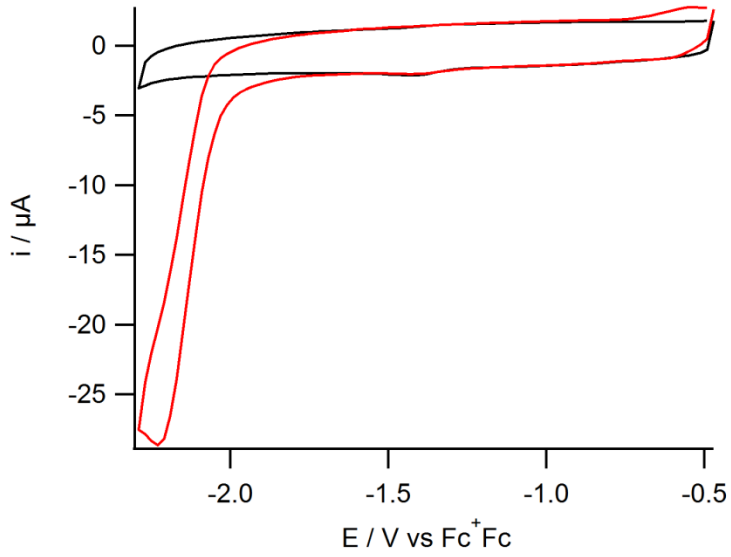

Figure AII.3: Cyclic voltammogram of [Ni(pbSmSe)] **(3)** (1 mM) in a DCM solution of $TBAPF_6$ (0.1 M) using a glassy carbon electrode at 200 mV s^{-1} (blank (black), [Ni(pbSmSe)] (red)).

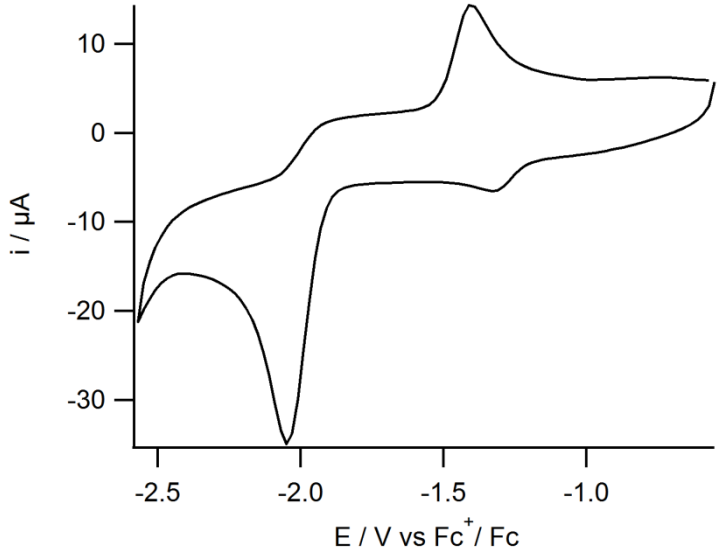

Figure AII.4: Cyclic voltammogram of $[FeCp(CO)_2I]$ (1 mM) in a DMF solution of $TBAPF_6$ (0.1 M) using a glassy carbon electrode at 200 mV s^{-1}.

Foot-of-the Wave Analysis

CV results were analyzed by using *FOWA* which helps to quantify the rates of HER. The observable rate constant (k_{obs}) can be obtained by plotting i/i_p^0 *vs* 1/1+exp[(F/RT)(E-E^0)] which gives a linear function at a certain scan rate. [2,3] For the complex **(5),** which has diffusion controlled reversible reaction, the current peaks (i and i_p^0) can be calculated according to equation (1) and (2): [2,3]

$$i_p^0 = 0.4463\mathrm{FSC_p}^0\sqrt{\frac{F\nu D}{RT}} \qquad (1)$$

$$i = \frac{2\mathrm{FS}C_p^0\sqrt{\frac{F\nu D}{RT}}}{1+\exp[\frac{F}{RT}(E-E^0)}} \qquad (2)$$

where i_p^0 =90.17 μA , F is the Faraday's constant, S the surface of electrode, C_p^0 the concentration of the complex in solution, D the diffusion coefficient, E^0 the half-wave potential of the redox couple triggering catalysis, R the gas constant and T the temperature. Combining equation (1) and (2) gives us equation (3) which shows us plotting i/i_p^0 *vs* 1/1+exp[(F/RT)(E-E^0)] gives access of the observed rate constant (k_{obs}).

$$\frac{i}{i_p^0} = \frac{\frac{2}{04463}\sqrt{\frac{RT(k_{obs})}{F\nu}}}{1+\exp[\frac{F}{RT}(E-E^0)]} \qquad (3)$$

i (μA)	i / i_p^0	1/1+exp[F/RT(E–E^0)]
20.25	0.225	022x10^{-4}
21.93	0.243	1.964x10^{-3}
24.38	0.270	4.269x10^{-3}
27.95	0.310	9.256x10^{-3}
32.74	0.363	0.01995
38.23	0.424	0.04247
43.53	0.483	0.0881
48.01	0.532	0.174

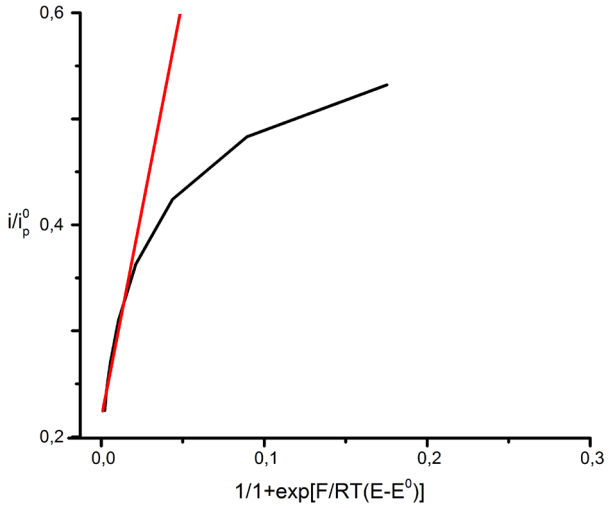

Figure AII.5: Plot of i/i_p^0 vs. 1/1+exp[F/RT(E−E^0)] using FOWA of the complex **(5)** for H_2 evolution at 200 mV s^{-1} and a concentration of HOAc of 60 mM. The experimental data (black) can be fitted linearly near the foot of the catalytic wave and the slope (red) gives the access to the observed rate constant k_{obs}= k × C_A^0 according to equation (4).[2] Equation (5)[2] gives us access to *k* which is 402 $M^{-1}s^{-1}$ and k_{obs} is 24 s^{-1}.

$$slope = \frac{2}{0.4463}\sqrt{(k_{obs})\frac{RT}{Fv}} \qquad (4)$$

$$k = \frac{slope^2 (0.4463)^2 Fv}{4RTC_A^0} \qquad (5)$$

H_2 evolution calculations are based on a calibration line obtained by the external reference method by injection of known amounts of H_2 into the system (Figure.AI2). During the CPC experiment hydrogen is only produced from the local concentration of catalyst at the electrode surface. For this measurement, a glassy carbon electrode with 3 mm diameter was used. After 50 min the area of the H_2 peak is 4054 for the complex **(5)** and according to the equation from calibration line (Fig.AI.3):

y = (0.01649x4054)−2.99413 = 64 µl H_2

$(64x10^{-6})÷(24.465) = 2.62x10^{-6}$ mol H_2

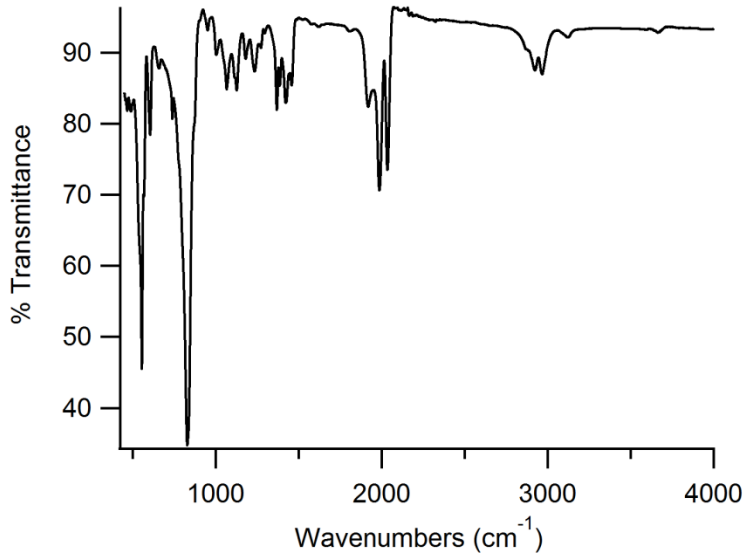

Figure AII.6: FTIR spectrum of the complex **(5)**.

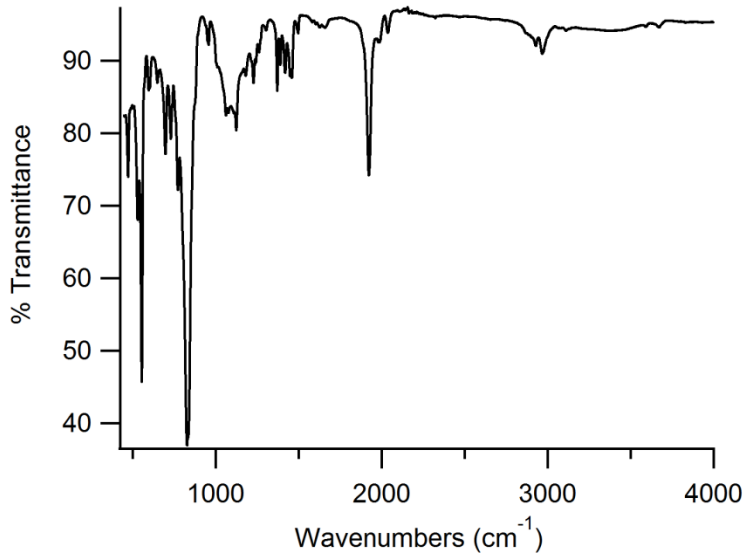

Figure AII.7: FTIR spectrum of the complex **(6)**.

References

1. G. M. Sheldrick, *Acta Cryst.,* 2015, **C71**, 3.
2. C. Costentin, S. Drouet, M. Robert and J. M. Savéant, *J. Am. Chem. Soc.* 2012, **134**, 11235.
3. N. Elgrishi, B. M. Chambers and M. Fontecave, *Chem. Sci.* 2015**, 6**, 2522.

Appendix III

Supplementary Information on Chapter 3

Table AIII.1: Crystal and structure refinement data for complexes **(1)** and **(2)**

Experiments were carried out at 110 K using a SuperNova, Dual, Cu at zero, Atlas. H-atom parameters were constrained.

	(1)	**(2)**
Crystal data		
Chemical formula	$2(C_{39}H_{44}NiPRuS_4)\cdot 2(F_6P)\cdot C_5H_{12}$	$2(C_{39}H_{44}NiPRuS_2Se_2)\cdot 2(F_6P)\cdot C_5H_{12}$
M_r	2025.54	2213.14
Crystal system, space group	Triclinic, *P*−1	Triclinic, *P*−1
a, *b*, *c* (Å)	10.4124 (3), 13.6997 (3), 16.9554 (5)	10.4311 (2), 13.7933 (3), 17.0273 (3)
α, β, γ (°)	71.664 (2), 86.558 (2), 69.587 (2)	71.685 (2), 86.5782 (17), 69.258 (2)
V (Å^3)	2148.30 (11)	2171.35 (8)
Z	1	1
Radiation type	Cu *K*α	Cu *K*α
μ (mm^{-1})	6.39	7.34
Crystal size (mm)	0.23 × 0.17 × 0.02	0.17 × 0.13 × 0.03

	(1)	(2)
Data collection		
Absorption correction	Analytical *CrysAlis PRO*, Agilent Technologies, Version 1.171.36.32 (release 02-08-2013 CrysAlis171 .NET) (compiled Aug 2 2013,16:46:58) Analytical numeric absorption correction using a multifaceted crystal model based on expressions derived by R.C. Clark & J.S. Reid. (Clark, R. C. & Reid, J. S. (1995). Acta Cryst. A51, 887-897)[1]	Analytical *CrysAlis PRO*, Agilent Technologies, Version 1.171.36.32 (release 02-08-2013 CrysAlis171 .NET) (compiled Aug 2 2013,16:46:58) Analytical numeric absorption correction using a multifaceted crystal model based on expressions derived by R.C. Clark & J.S. Reid. (Clark, R. C. & Reid, J. S. (1995). Acta Cryst. A51, 887-897)[1]
T_{min}, T_{max}	0.436, 0.866	0.408, 0.833
No. of measured, independent and observed [$I > 2\sigma(I)$] reflections	27501, 8405, 7525	27022, 8480, 7577
R_{int}	0.039	0.033
$(\sin \theta/\lambda)_{max}$ (Å^{-1})	0.617	0.616
$R[F^2 > 2\sigma(F^2)]$, $wR(F^2)$, S	0.028, 0.073, 1.03	0.029, 0.074, 1.06
No. of reflections	8405	8480
No. of parameters	731	719
No. of restraints	875	851
Δ_{max}, $\Delta\rangle_{min}$ (e Å^{-3})	0.57, -0.57	0.64, -0.61

Computer programs: *CrysAlis PRO*, Agilent Technologies, Version 1.171.36.32 (release 02-08-2013 CrysAlis171 .NET) (compiled Aug 2 2013, 16:46:58), *SHELXS2014*/7 (Sheldrick, 2015), *SHELXL2014*/7 (Sheldrick, 2015), *SHELXTL* v6.10 (Sheldrick, 2008).[2]

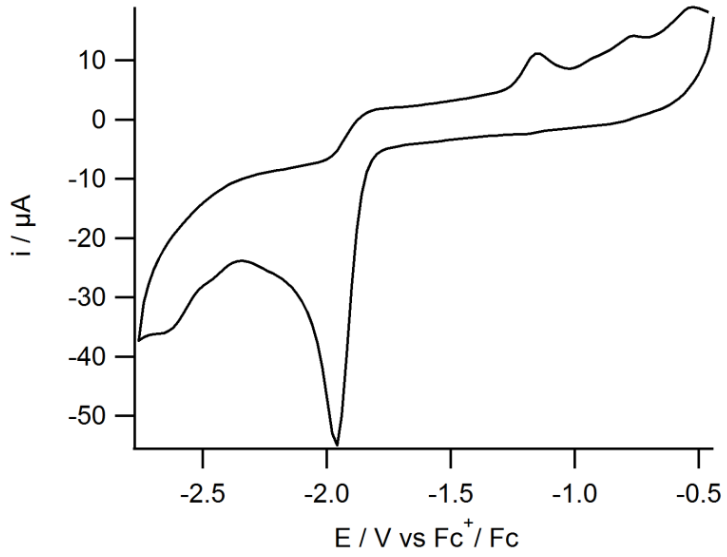

Figure AIII.1: Cyclic voltammogram of [Ni(xbSmS)] (1 mM) in an MeCN solution containing $TBAPF_6$ (0.1 M) as the supporting electrolyte and using a glassy carbon electrode at 200 mV s^{-1}.

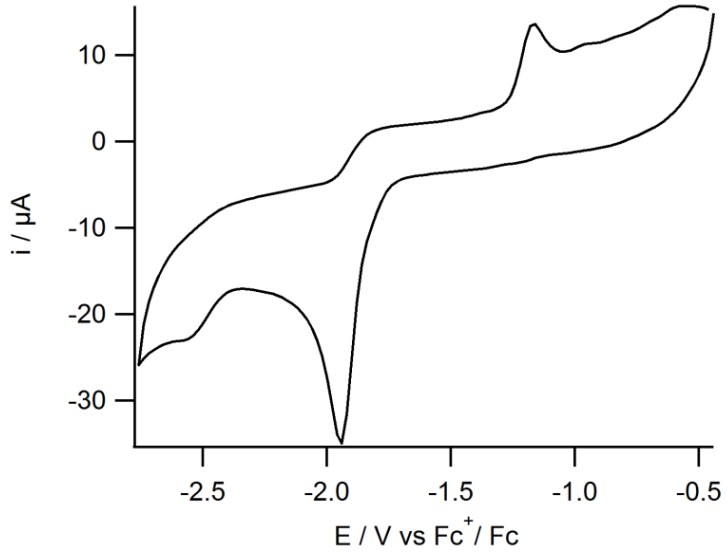

Figure AIII.2: Cyclic voltammogram of [Ni(xbSmSe)] (1 mM) in an MeCN solution containing $TBAPF_6$ (0.1 M) as the supporting electrolyte and using a glassy carbon electrode at 200 mV s^{-1}.

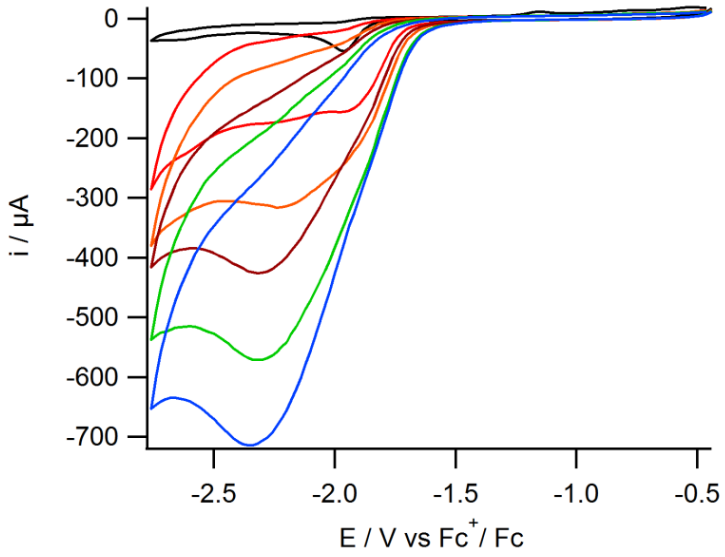

Figure AIII.3: Cyclic voltammogram of [Ni(xbSmS)] (1 mM) in an MeCN solution containing $TBAPF_6$ (0.1 M) as the supporting electrolyte and using a glassy carbon electrode at 200 mV s^{-1} in the presence of 0 (black), 10 (red), 20 (orange), 30 (brown), 40 (green), 50 (blue) mM of acetic acid.

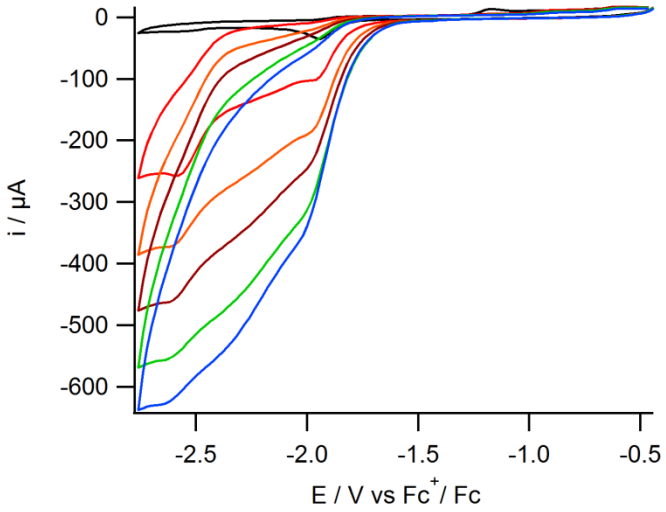

Figure AIII.4: Cyclic voltammogram of [Ni(xbSmSe)] (1 mM) in an MeCN solution containing $TBAPF_6$ (0.1 M) as the supporting electrolyte and using a glassy carbon electrode at 200 mV s^{-1} in the presence of 0 (black), 10 (red), 20 (orange), 30 (brown), 40 (green), 50 (blue) mM of acetic acid.

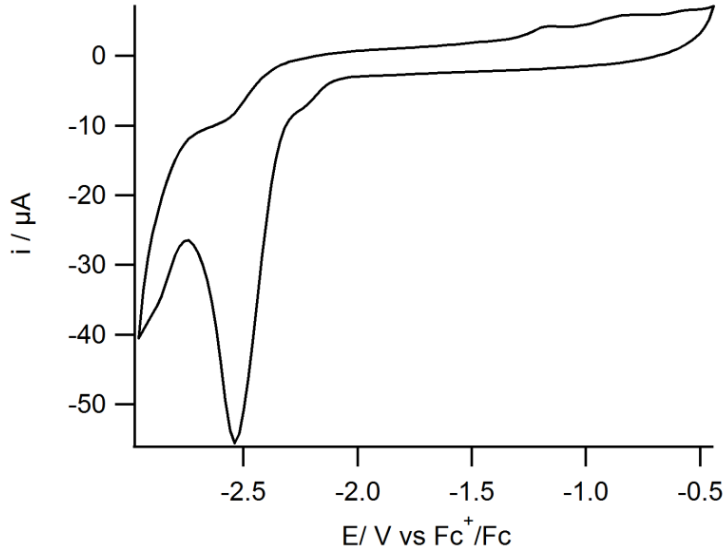

Figure AIII.5: Cyclic voltammogram of **[**$RuCp(PPh_3)(MeCN)_2]PF_6$ (1 mM) in an MeCN solution containing $TBAPF_6$ (0.1 M) as the supporting electrolyte and using a glassy carbon electrode at 200 mV s^{-1}.

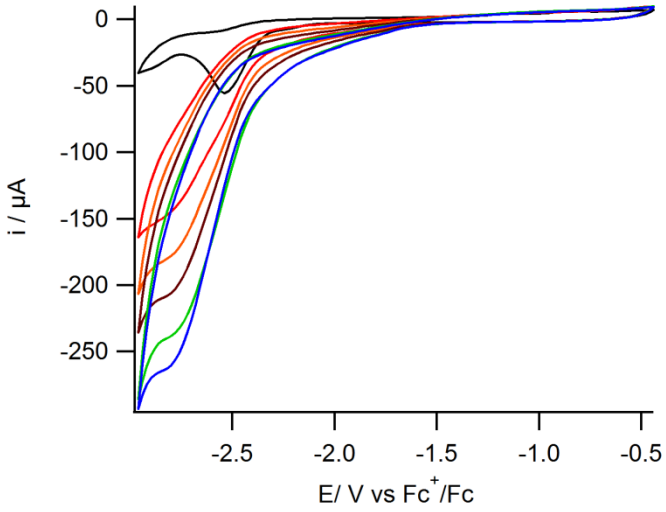

Figure AIII.6: Cyclic voltammogram of **[**$RuCp(PPh_3)(MeCN)_2]PF_6$ (1 mM) in an MeCN solution containing $TBAPF_6$ (0.1 M) as the supporting electrolyte and using a glassy carbon electrode at 200 mV s^{-1} in the presence of 0 (black), 10 (red), 20 (orange), 30 (brown), 40 (green), 50 (blue) mM of acetic acid.

References

1. R.C. Clark and J.S. Reid, *Acta Cryst.*, 1995, **A51**, 887.
2. G. M. Sheldrick, *Acta Cryst.,* 2015, **C71**, 3.

Appendix IV

Supplementary Information on Chapter 4

Table AIV.1: Crystal and structure refinement data for complexes **(1)**, **(2)**, **(4)** and **(6)**

Data were collected at 110 K for **(1)**, **(4)** and **(6)**, at 150 K for **(2)**

	(1)	**(2)**	**(4)**	**(6)**
Chemical formula	$C_{20}H_{40}Ni_2S_8$ CH_2Cl_2	$C_{12}H_{24}Ni_2S_6$	$C_{14}H_{28}Ni_2S_4Se_2$	$C_{12}H_{24}Ni_2S_4Se_2$
M_r	739.35	478.09	599.94	571.89
Crystal system, space group	Orthorhombic, *Pna2₁*	Orthorhombic, *Pbca*	Orthorhombic, *Pna*2₁	Orthorhombic, *Pbca*
a, *b*, *c* (Å)	10.5534(3), 23.6789(8), 12.4717(3)	12.9460(1), 22.3503(2), 12.9344(1)	12.08190 (17), 14.03764 (18), 12.21318 (17)	12.8544 (2), 13.3702 (3), 22.4216 (5)
V (Å^3)	3116.58(16)	3742.53(5)	2071.37 (5)	3853.51 (14)
Z	4	8	4	8
μ (mm^{-1})	1.93	2.67	9.98	10.69
Data collection				
R_{int}	0.042	0.046	0.018	0.038
$(\sin\theta/\lambda)_{max}$ (Å^{-1})	0.61	0.65	0.616	0.616
Refinement				
No. of reflections	5617	3733	3211	3771
No. of parameters	346	185	204	185
$\Delta\rho_{max}$,$\Delta\rho_{min}$ (e Å^{-3})	0.82, -0.38	0.49, -0.38	0.80, −0.54	0.44, −0.34

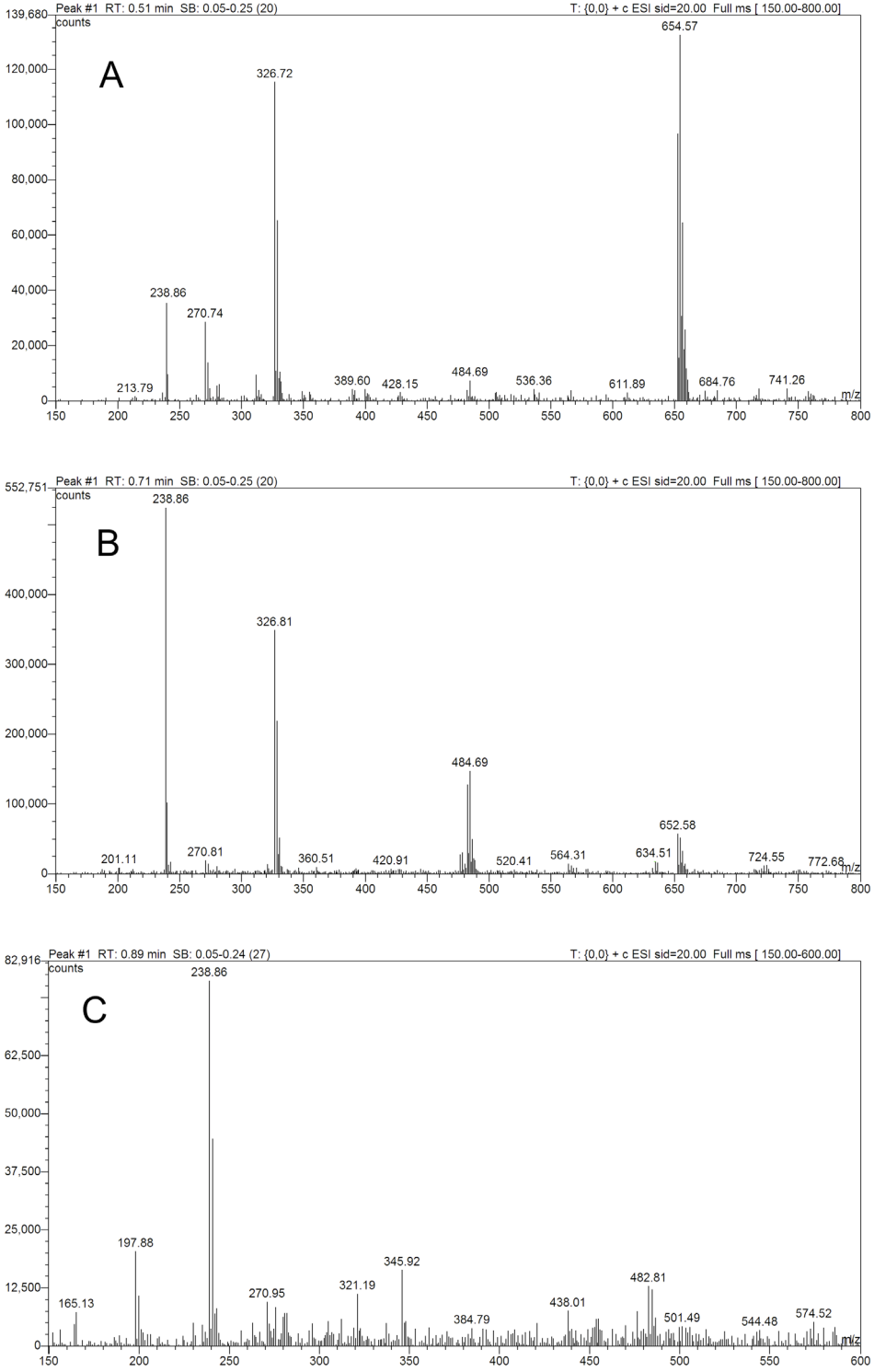

Figure AIV.1. Formation of $[Ni_2(emSmS)_2]$ **(2)** from $[Ni_2(ebSmS)_2]$ **(1)**, as monitored with ESI-MS spectrometry upon irradiation on the toluene solution of $[Ni_2(ebSmS)_2]$ **(1)** at room temperature; (A) 0 hrs, (B) 6 hrs, (C) 12 hrs; *m/z* = 326.72 = $[Ni(ebSmS)+H]^+$, 652.57 = $[\{Ni(ebSmS)\}_2+H]^+$ and 238.86 = $[Ni(emSmS)+H]^+$.

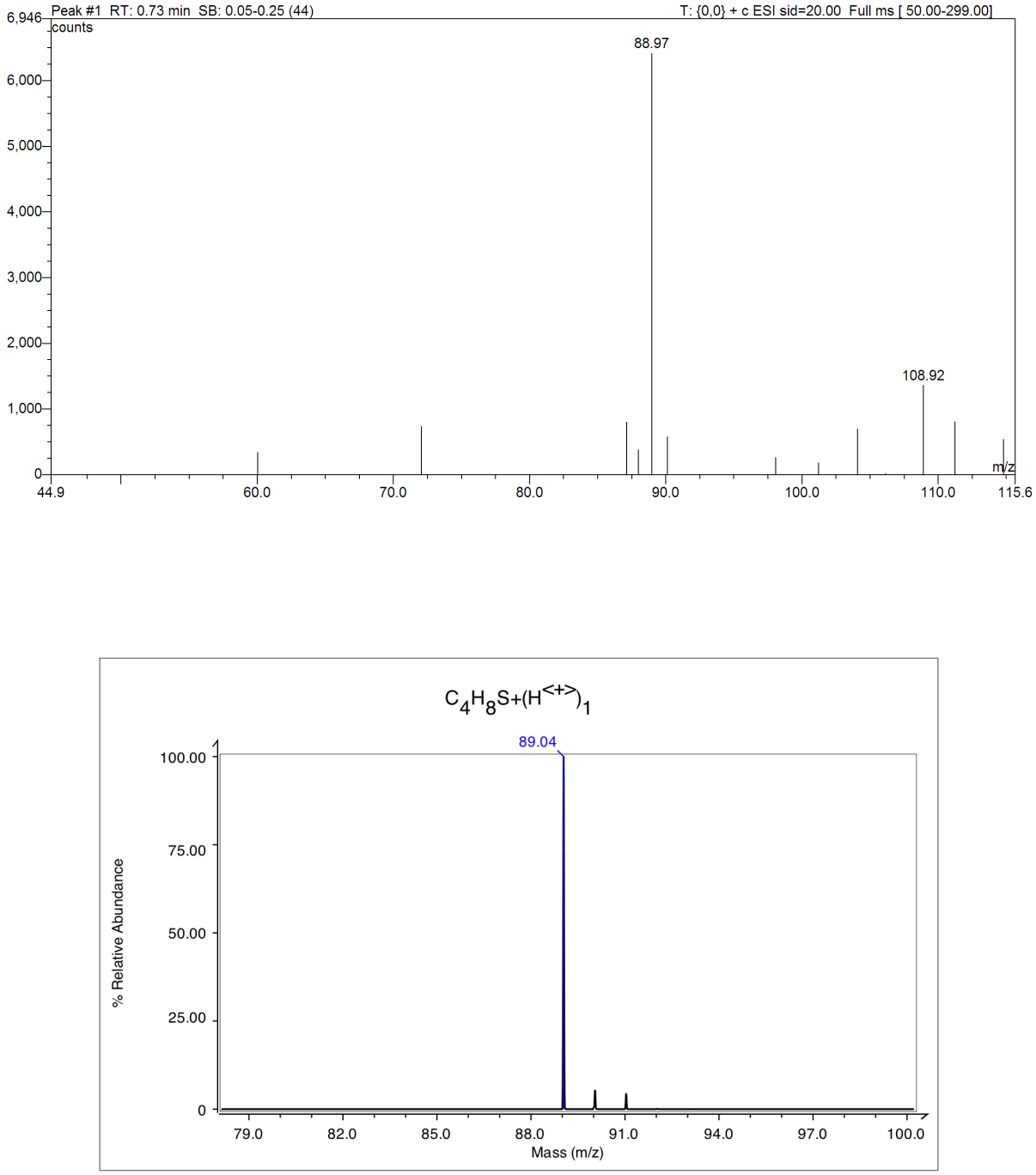

Figure AIV.2. ESI-MS of (poly)isobutylene sulfide in dichloromethane, extracted from the reaction of **(1)** upon irradiation on the toluene solution (top) and the signal simulated for $[C_4H_8S+H]^+$ (bottom).

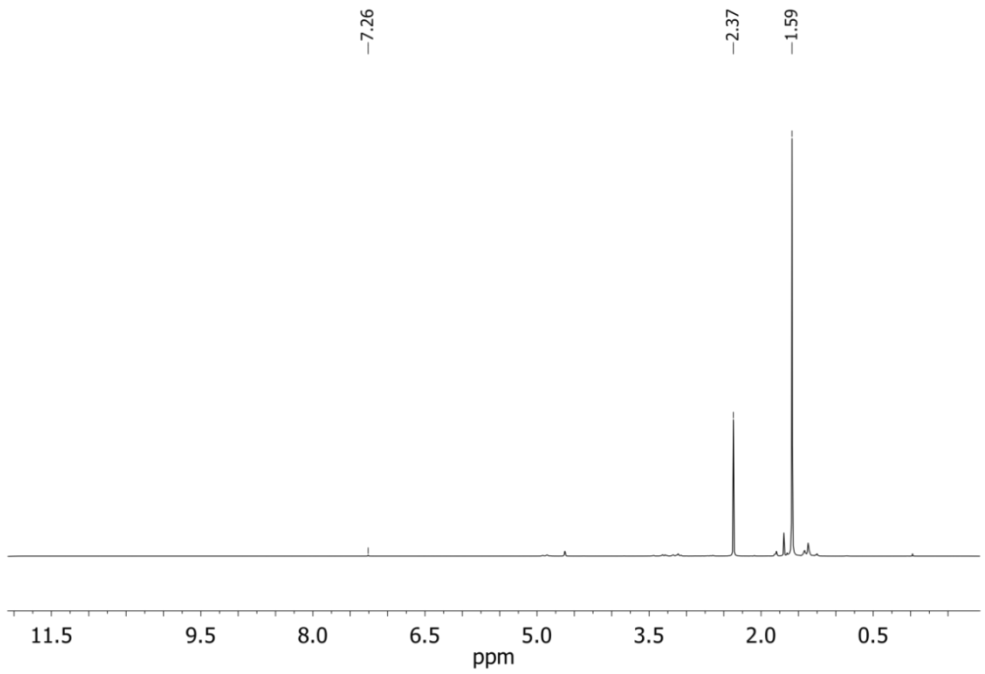

Figure AIV.3. ^{1}H NMR spectrum of isobutylene sulfide isolated after the photolysis of complex (1); recorded using CD_2Cl_2 solution at 298 K.

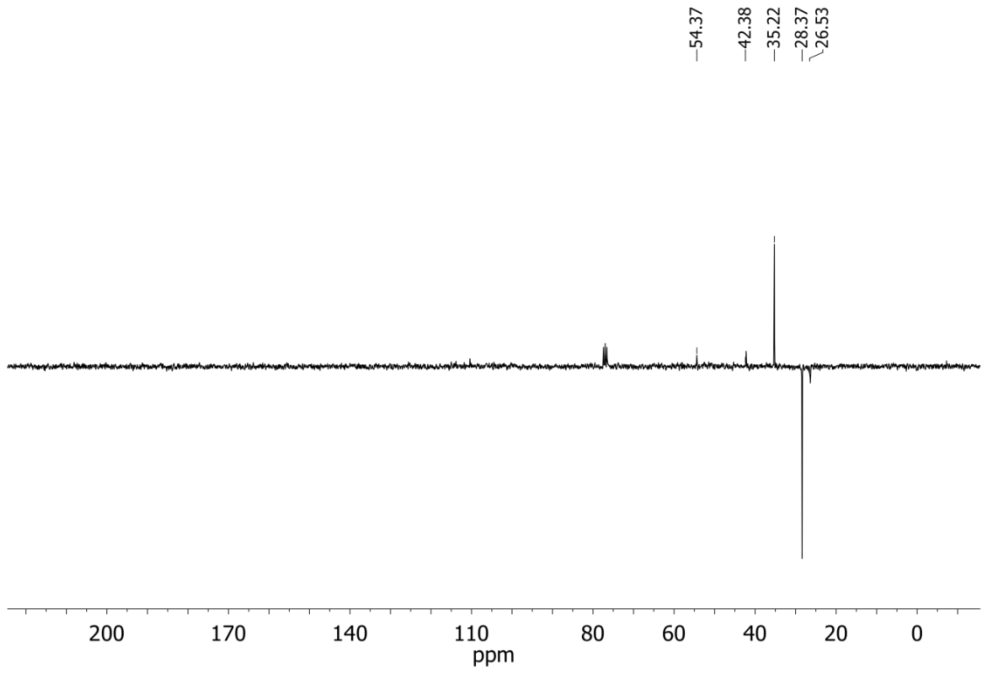

Figure AIV.4. ^{13}C NMR (APT) spectrum of isobutylene sulfide isolated after the photolysis of complex (1); recorded using CD_2Cl_2 solution at 298 K.

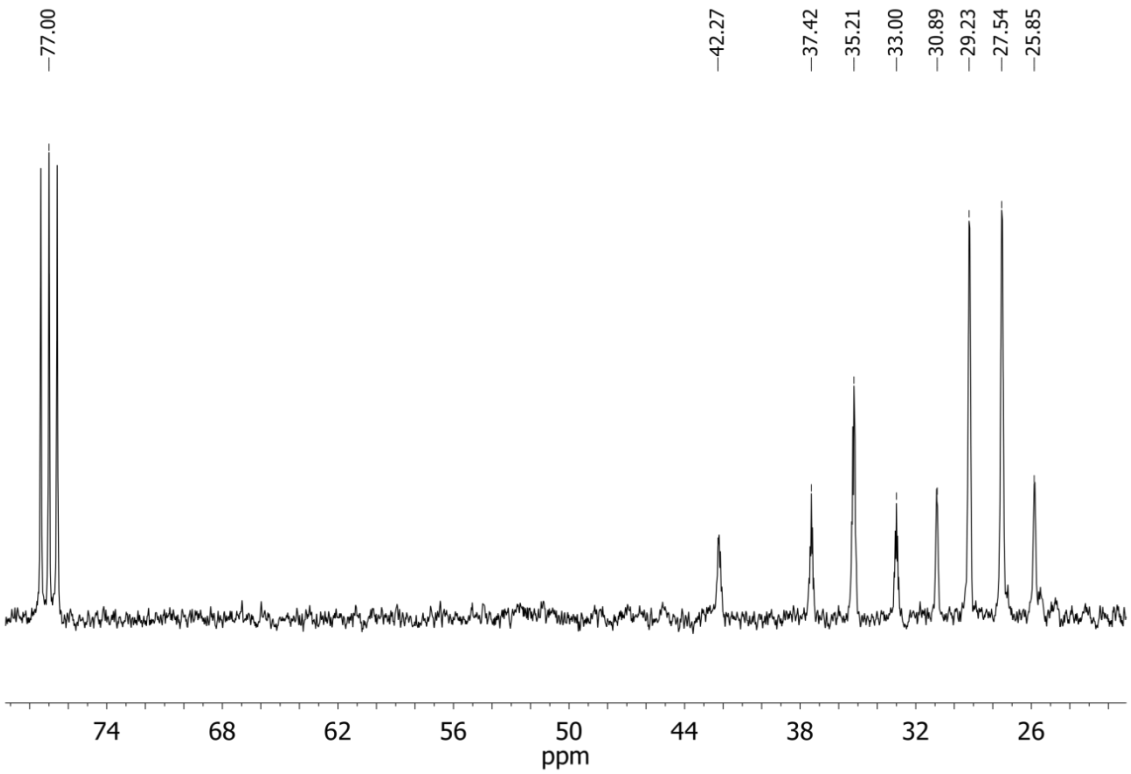

Figure AIV.5. ^{13}C NMR (gated decoupled) spectrum of isobutylene sulfide isolated after photolysis of complex **(1)**, recorded using CD_2Cl_2 solution at 298 K.

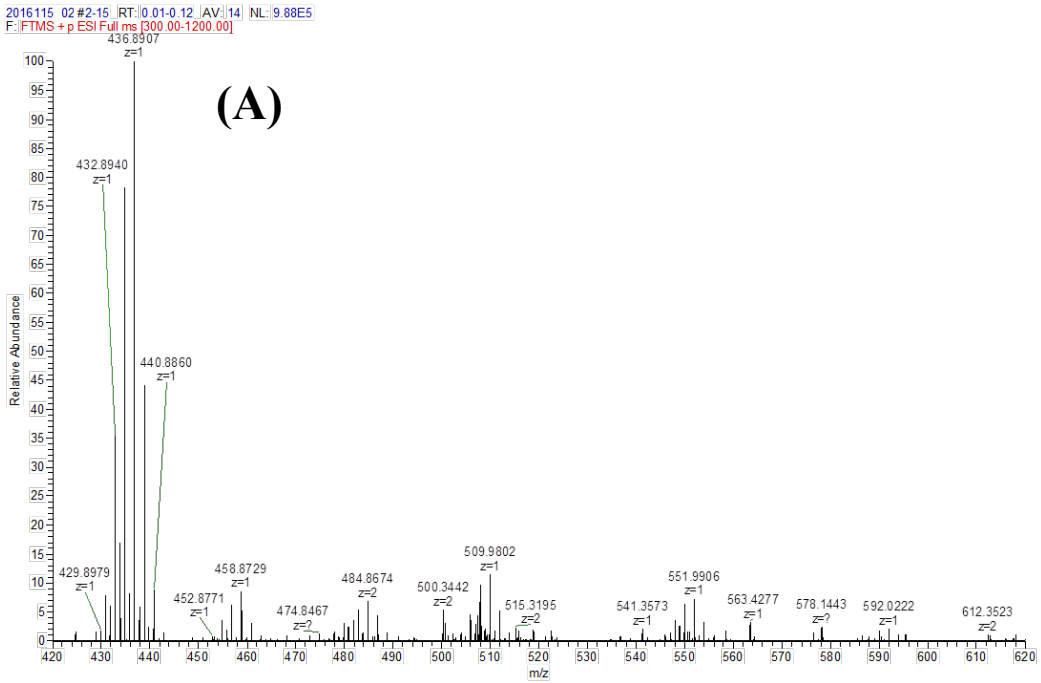

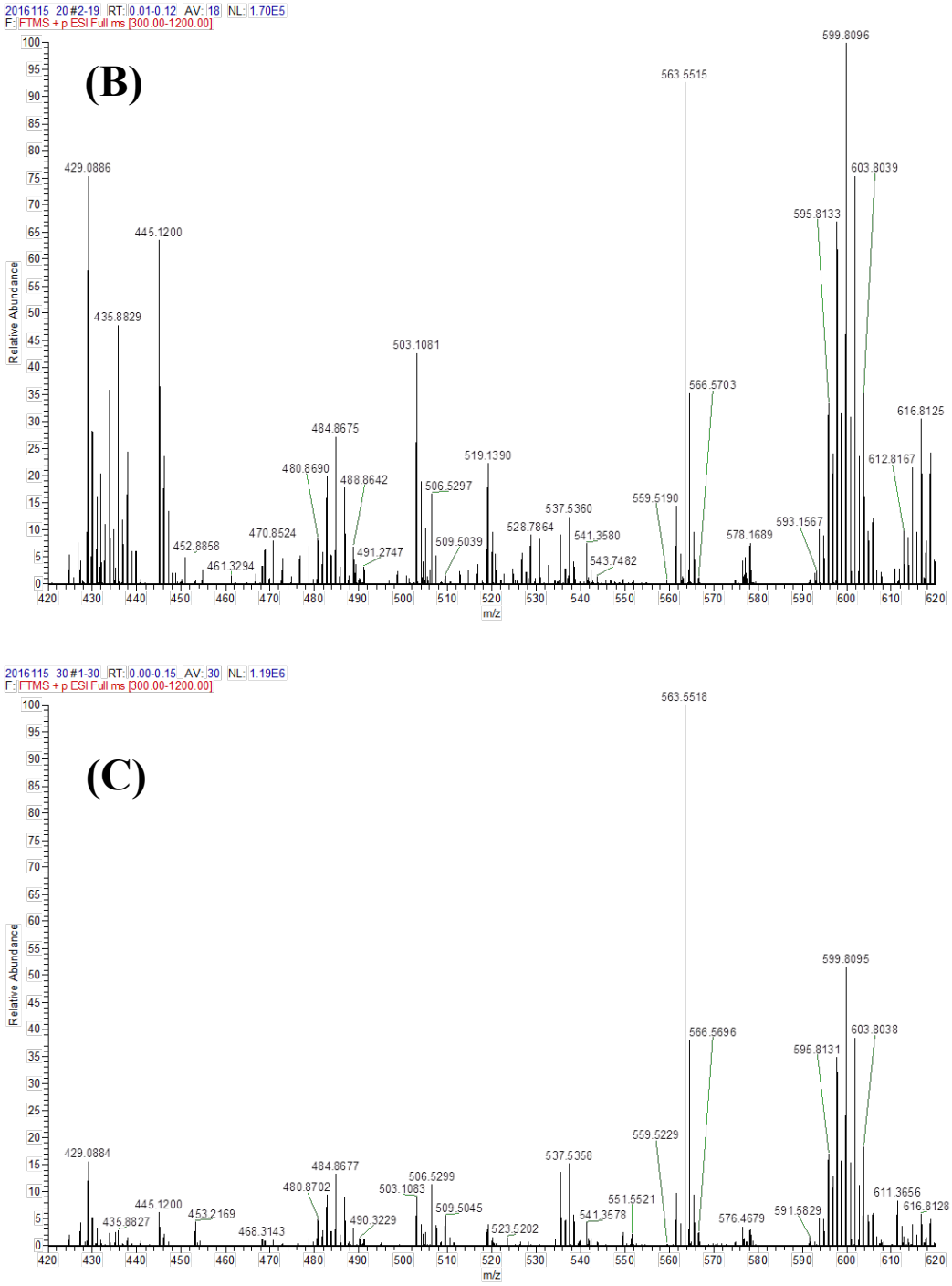

Figure AIV.6. Formation of $[Ni_2(pmSmSe)_2]$ **(4)** from [Ni(pbSmSe)] **(3)**, as monitored with HRMS spectrometry upon irradiation of the dichloromethane solution of [Ni(pbSmSe)] **(3)** at room temperature; (A) 0 hrs, (B) 1 h (C) 2 h *m/z* = 436.8846 = $[Ni(pbSmSe)+H]^+$, *m/z* =599.8111 = $[Ni_2(pmSmSe)_2]$, signals present in the blank from solvent: 509.33 and 563.55.

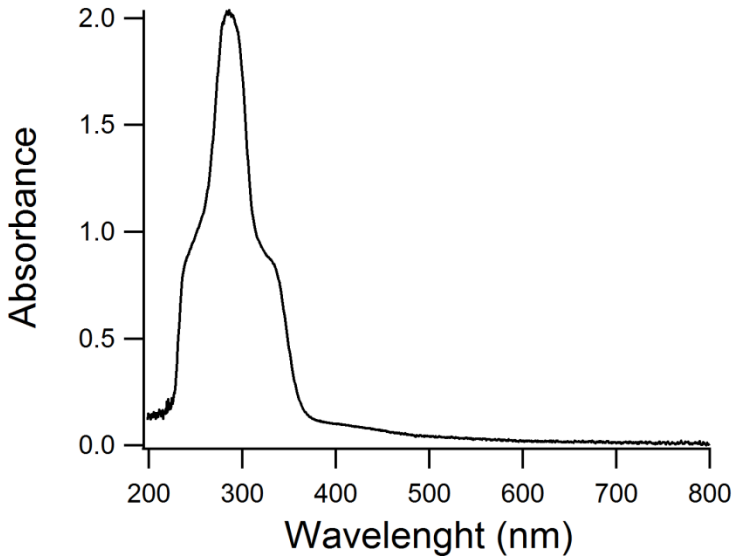

Figure AIV.7. UV-VIS spectrum of complex **(3)** (1 mM) in dichloromethane. The spectrum was recorded with a transmission dipprobe set at a path length of 2 mm.

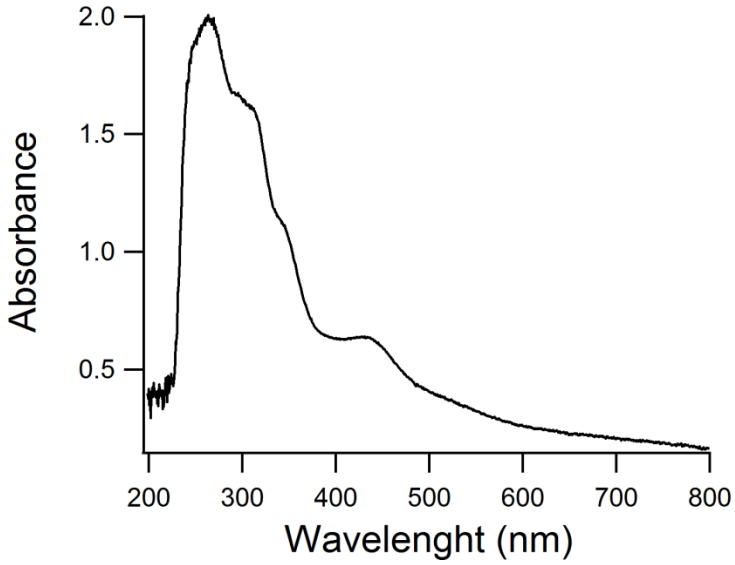

Figure AIV.8. UV-VIS spectrum of complex **(4)** (1 mM) in dichloromethane. The spectrum was recorded with a transmission dipprobe set at a path length of 2 mm.

Appendix V

Supplementary Information on Chapter 5

Table AV.1: Crystal and structure refinement data for complexes **(1)** and **(2)**

Data were collected at 110 K using a SuperNova, Dual, Cu and Mo at zero, Atlas. H-atom parameters were constrained.

	(1)	**(2)**
Crystal data		
Chemical formula	$C_{56}H_{64}N_4Ni_2RuS_8 \cdot 2(F_6P) \cdot 1.437(C_3H_6O)$	$C_{56}H_{64}N_4Ni_2RuS_4Se_4 \cdot 2(F_6P) \cdot 1.387(C_3H_6O)$
M_r	1641.43	1826.21
Crystal system, space group	Triclinic, *P*-1	Triclinic, *P*-1
a, *b*, *c* (Å)	10.0605(3), 17.5378(5), 21.7349(6)	10.1408(2), 18.4675(4), 20.4960(5)
α, β, γ (°)	109.731(3), 96.492(2), 106.004(3)	109.249(2), 98.2255(19), 105.4158(19)
V (Å^3)	3378.57(19)	3379.33(14)
Z	2	2
Radiation type	Cu *K*α	Mo *K*α
μ (mm^{-1})	5.87	3.18
Crystal size (mm)	0.35 × 0.05 × 0.03	0.38 × 0.08 × 0.06

	(1)	(2)
Data collection		
Absorption correction	Analytical *CrysAlis PRO*, Agilent Technologies, Version 1.171.36.32 (release 02-08-2013 CrysAlis171 .NET) (compiled Aug 2 2013,16:46:58) Analytical numeric absorption correction using a multifaceted crystal model based on expressions derived by R.C. Clark & J.S. Reid. (Clark, R. C. & Reid, J. S. (1995). Acta Cryst. A51, 887-897)[1]	Gaussian *CrysAlis PRO*, Agilent Technologies, Version 1.171.36.32 (release 02-08-2013 CrysAlis171 .NET) (compiled Aug 2 2013,16:46:58) Numerical absorption correction based on gaussian integration over a multifaceted crystal model.
T_{min}, T_{max}	0.310, 0.834	0.461, 1.000
No. of measured, independent and observed [$I > 2\sigma(I)$] reflections	32405, 13234, 10915	51473, 15498, 12221
R_{int}	0.033	0.039
$(\sin \theta/\lambda)_{max}$ (Å^{-1})	0.617	0.649
$R[F^2 > 2\sigma(F^2)]$, $wR(F^2)$, S	0.036, 0.093, 1.02	0.035, 0.080, 1.02
No. of reflections	13234	15498
No. of parameters	1333	1044
No. of restraints	1848	1021
$\Delta\rho_{max}$, $\Delta\rho_{min}$ (e Å^{-3})	1.04, -1.20	1.06, -0.74

Computer programs: *CrysAlis PRO*, Agilent Technologies, Version 1.171.36.32 (release 02-08-2013 CrysAlis171 .NET) (compiled Aug 2 2013, 16:46:58), *SHELXS2014*/7 (Sheldrick, 2015), *SHELXS2014*/7 (Sheldrick, 2014), *SHELXL2014*/7 (Sheldrick, 2015), *SHELXL2014*/7 (Sheldrick, 2014), *SHELXTL* v6.10 (Sheldrick, 2008).[2]

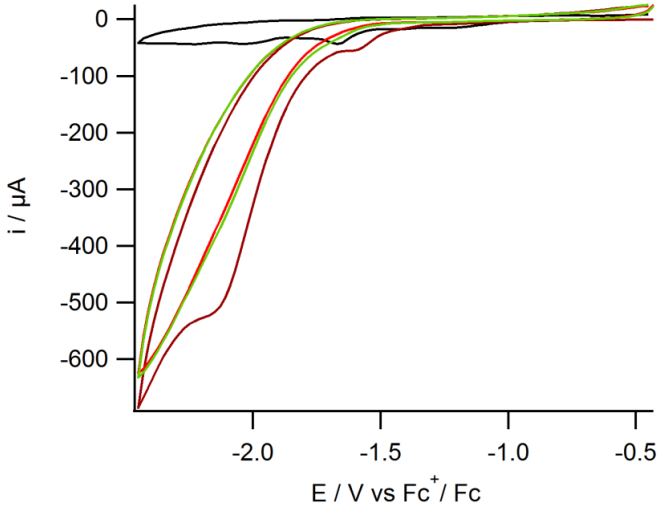

Figure AV.1: Cyclic voltammograms of $[\{Ni(xbSmS)\}_2Ru(phen)_2](PF_6)_2$ (1 mM) in acetonitrile solution containing $TBAPF_6$ (0.1 M) as the supporting electrolyte and using a glassy carbon electrode at 200 mV s^{-1} without acid (black), in the presence of 50 mM acid with three different scans: brown (1st scan), green (2nd scan) and red (3rd scan).

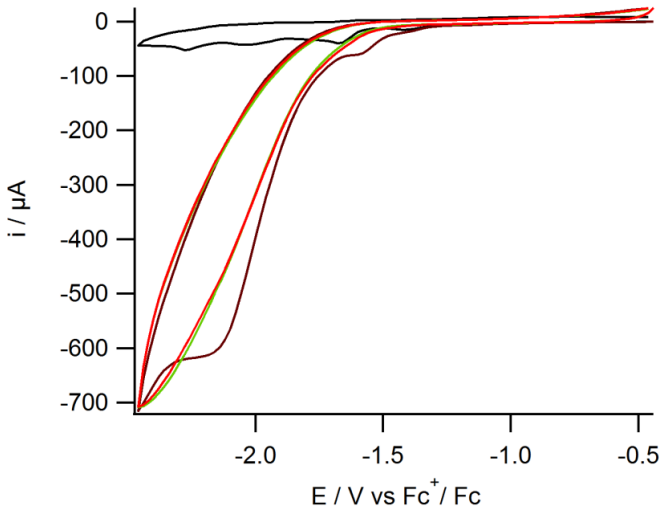

Figure AV.2: Cyclic voltammograms of $[\{Ni(xbSmSe)\}_2Ru(phen)_2](PF_6)_2$ (1 mM) in acetonitrile solution containing $TBAPF_6$ (0.1 M) as the supporting electrolyte and using a glassy carbon working electrode at 200 mV s^{-1} without acid (black), in the presence of 50 mM acid with three different scans: brown (1st scan), green (2nd scan) and red (3rd scan).

References

1. R.C. Clark and J.S. Reid, *Acta Cryst.*, 1995, **A51**, 887.
2. G. M. Sheldrick, *Acta Cryst.,* 2015, **C71**, 3.

Samenvatting

Inleiding

Uit de toenemende mondiale behoefte aan energie kan worden geconcludeerd dat in de toekomst de voorraad fossiele brandstoffen niet zal volstaan om in de behoefte te voorzien. Een mogelijke strategie ter preventie van dit toekomstige energieprobleem is gebaseerd op de ontwikkeling van een waterstofeconomie. Onderzoekers zoeken naar nieuwe en schonere manieren om waterstofgas te produceren en de sleutel tot duurzame waterstofproductie kan wellicht gevonden worden bij de hydrogenases. Hydrogenases zijn in de afgelopen decennia onder de aandacht gekomen van synthetisch chemici vanwege de potentie van deze enzymen voor duurzame waterstofproductie. Door het actieve centrum van de hydrogenases als voorbeeld te nemen, kunnen nieuwe katalysatoren ontwikkeld worden voor efficiënte protonreductie. Drie typen hydrogenases zijn bekend, dit zijn de [FeFe]-, [Fe]- en [NiFe]-hydrogenases.[1] De [NiFeSe]-hydrogenase vormt een subklasse van de [NiFe]-hydrogenases, waarin een van de cysteines (Cys) in het actieve centrum van het enzym is vervangen door een selenocysteine (Sec).[2] Veel gegevens zijn verzameld met betrekking tot de redoxtoestanden en de reactiemechanismen van de reversibele splitsing van diwaterstof in het actieve centrum van de [NiFe]-hydrogenases.[6] In de afgelopen decennia zijn veel structurele en functionele modellen voor het actieve centrum van [NiFe]-hydrogenase gepubliceerd, die actief zijn in de elektro-katalytische reductie van protonen bij overpotentialen zo laag als 50 mV.[3-5] In dit proefschrift wordt de synthese en karakterisering beschreven van structurele en functionele modellen van de nikkel-bevattende enzymen [NiFe]- en [NiFeSe]-hydrogenases. Daarnaast wordt in dit proefschrift ook van een aantal nikkelverbindingen de reactiviteit besproken die mogelijk van belang is voor beter begrip van het werkingsmechanisme van het enzym methyl-coenzyme-M reductase (MCR).

6.1.2 Elektrokatalytische Proton Reductie met een [NiFeSe] Hydrogenase Model

De [NiFeSe]-hydrogenase vormt een subklasse van de [NiFe]-hydrogenases, waarin een van de cysteines (Cys) in het actieve centrum van het enzym is vervangen door een selenocysteine (Sec). Vergeleken met de cysteinehomoloog heeft [NiFeSe]-hydrogenase een hogere katalytische activiteit voor reversibele protonreductie.[2,7,8] In hoofdstuk 2 worden twee nieuwe heterodinucleaire verbindingen als modelsysteem voor hydrogenases beschreven, te weten $[Ni(pbSmSe)FeCpCO]PF_6$ en $[Ni(xbSmSe)FeCpCO]PF_6$, welke gesynthetiseerd zijn uit twee

verschillende nikkelverbindingen in een reactie met een ijzercomplex. Structuurbepalingen door middel van röntgendiffractie hebben aangetoond dat beide [NiFe]-complexen een nickel(II)-centrum bevatten in een vlakvierkante S_2Se_2 omgeving; de twee selenolaatdonoren vormen een brug met het ijzer(II)-ion dat verder gecoördineerd is aan een η^5-cyclopentadienyl- en een koolstofmonoxide-ligand, waardoor structurele gelijkenis met het actieve centrum van de [NiFeSe]-hydrogenase verkregen is. Elektrochemische experimenten laten zien dat alleen het complex $[Ni(pbSmSe)FeCpCO]PF_6$ elektro-katalytische activiteit vertoont voor protonreductie in DMF in de aanwezigheid van azijnzuur bij een potentiaal van –2.1 V vs. Fc^+/Fc. Analyse van de katalytische stroom leverde een schatting op voor k_{obs} van 24 s^{-1}.

6.1.3 Nickel-Ruthenium-gebaseerde Complexen als Biomimetische Modellen van [NiFe] en [NiFeSe] Hydrogenases voor Waterstofevolutie

Veel rutheniumverbindingen zijn actieve katalysatoren voor hydrogenering en waterstof-overdrachtreacties en rutheniumionen vormen doorgaans stabielere complexen dan ijzerionen. Daarnaast zijn Ru(II)-ionen in staat zowel harde als zachte liganden te binden, zoals hydrides en moleculair waterstof, wat rutheniumionen geschikt maakt ter vervanging van het ijzerion in functionele modellen voor [NiFe]-hydrogenase.[9] In hoofdstuk 3 wordt de synthese en karakterisering beschreven van de twee heterodinucleaire nikkel-rutheniumcomplexen $[Ni(xbSmS)RuCp(PPh_3)]PF_6$ en $[Ni(xbSmSe)RuCp(PPh_3)]PF_6$ als modellen voor het actieve centrum van de [NiFe]- en [NiFeSe]-hydrogenases. Structuurbepalingen van deze complexen door middel van röntgendiffractie laten zien dat de twee [NiRu]-complexen isomorf zijn; beide [NiRu]-complexen hebben een nikkel(II)-ion in een vlakvierkante geometrie met twee thioether-donoratomen en twee thiolaat- of selenolaatdonoren die een brug vormen met het ruthenium(II)-ion. Het Ru(II)-ion is verder gecoördineerd aan een η^5-cyclopentadienyl- en een trifenylfosfaanligand. Beide complexen katalyseren de waterstof-evolutiereactie in de aanwezigheid van azijnzuur in een acetonitril-oplossing bij een potentiaal van circa −2.20 V vs. Fc^+/Fc met overpotentialen van 810 en 830 mV, en kunnen derhalve gezien worden als functionele modellen van de [NiFe]- en [NiFeSe]-hydrogenases.

6.1.4 Dealkylering door verbreken van C-S en Ni-S bindingen relevant voor het mechanisme van methyl-coenzyme M reductase (MCR)

Nickel-thiolaatverbindingen genieten veel aandacht onder onderzoekers in de bioinorganische en organometaalchemie; deze verbindingen zijn belangrijk in de context van structurele en/of functionele modellen van enzymen. In hoofdstuk 4 wordt de synthese beschreven van het

thiouronium-tussenproduct van het nieuwe tetradentate dithioether-dithiolaat-ligand, alsook van het overeenkomstige selenouronium-tussenproduct van het tetradentate dithioether-diselenolaat-ligand. De nieuwe complexen $[Ni_2(ebSmS)_2]$ en [Ni(pbSmSe)] zijn geïsoleerd en gekarakteriseerd, maar deze verbindingen bleken lichtgevoelig te zijn en te ontleden na bestraling met licht. De snelheid van de dealkyleringsreactie van de verbindingen was verschillend, en kan worden gerelateerd aan het verschil in atoomstraal van zwavel en selenium, alsook aan de verschillen in flexibiliteit van de koolstofbrug tussen de twee thioether-donoratomen in de tetradentaat liganden. De verbinding [Ni(ebSmSe)] bleek het meest reactief te zijn; deze verbinding kon niet worden geïsoleerd, maar hiervan kon alleen het ontledingsproduct geïsoleerd en gekarakteriseerd worden. De resultaten zijn mogelijk relevant voor een beter begrip van het mechanisme van methyl-coenzyme-M reductase, alsook voor de ontwikkeling van katalysatoren voor hydrodesulfurisatie.

6.1.5 Synthese en karakterisering van trinucleaire [NiRu] complexen voor elektrokatalytische proton reductie

In hoofdstuk 5 wordt de synthese en karakterisering beschreven van twee nieuwe trinucleaire $[Ni_2Ru]$-complexen die gevormd zijn uit een NiS_4- of NiS_2Se_2-complex. Structuurbepalingen met behulp van röntgendiffractie hebben aangetoond dat de trinucleaire complexen in $[\{Ni(xbSmS)\}_2Ru(phen)_2](PF_6)_2$ en $[\{Ni(xbSmSe)\}_2Ru(phen)_2](PF_6)_2$ twee vlakvierkante nikkel(II)-ionen bevatten die via een bruggend thiolaat- of selenolaatdonor gebonden zijn in cis-posities van het octaëdrische ruthenium(II)-ion. Elektro-katalytische protonreductie vindt plaats voor beide complexen in acetonitril na toevoeging van azijnzuur bij een potentiaal van −2.1 V vs. Fc^+/Fc met faradaische efficienties van 65%.

Referenties

1. H. Ogata, W. Lubitz and Y. Higuchi, *Dalton Trans.* 2009, 7577.
2. C. Wombwell and E. Reisner, *Chem. Eur. J.* 2015, **21**, 8096.
3. M. Fontecave and V. Artero, *C. R. Chim.* 2011, **14**, 362.
4. S. Canaguier, M. Field, Y. Oudart, J. Pécaut, M. Fontecave and V. Artero, *Chem. Commun.* 2010, **46**, 5876.
5. S. Canaguier, V. Artero and M. Fontecave, *Dalton Trans* 2008, 315.
6. S. Kaur-Ghumaan and M. Stein, *Dalton Trans*, 2014, **43**, 9392.
7. L. De Gioia, *Bioinorganic Fundamentals and Applications: Metals in Natural Living Systems and Metals in Toxicology and Medicine,* Elsevier, 2013, Vol. 3.
8. E. Garcin, X. Vernede, E. Hatchikian, A. Volbeda, M. Frey and J. Fontecilla-Camps, *Structure* 1999, **7**, 557.
9. T. R. Simmons, G. Berggren, M. Bacchi, M. Fontecave and V. Artero, *Coord. Chem. Rev.*, 2014, **271**, 127.

List of Publications

- 'Electrocatalytic Proton Reduction by a Model for [NiFeSe] Hydrogenases'
  G. Gezer, D. Durán Jiménez, M. A. Siegler, and E. Bouwman, ***Dalton Trans.*****,** 2017, 46, 7506.

- 'Improved Solubility of Celecoxib by Inclusion in SBA-15 Mesoporous Silica: Drug Loading in Different Solvents and Release.

  Z. S. Eren, S. Tuncer, **G. Gezer,** L. T. Yildirim, S. Banerjee and A. Yilmaz, ***Microporous Mesoporous Mater.,*** 2016, 235, 211.

- 'Nickel-Ruthenium-Based Complexes as Biomimetic Models of [NiFe] and [NiFeSe] Hydrogenases for Dihydrogen Evolution'

  G. Gezer, S. Verbeek, M. A. Siegler, and E. Bouwman. *Submitted.*

- 'Dealkylation through C–S and Ni–S bond cleavage relevant to the mechanism of methyl-coenzyme M reductase (MCR)'

  G. Gezer, R. Angamuthu, W. Roorda, M. A. Siegler, M. Lutz, A. L. Spek and E. Bouwman. *In preparation.*

- 'Synthesis and Characterization of Trinuclear [NiRu] Complexes for Electrocatalytic Proton Reduction'

  G. Gezer, D. Durán Jiménez, M.A. Siegler, and E. Bouwman. *Submitted.*

Curriculum Vitea

Gamze Gezer was born in Corlu, Turkey on October 25th in 1989. In 2007, she graduated from Hasan Sabriye Gumus Anatolian High School. In that year, she started her BSc studies in Chemistry at the Middle East Technical University (METU). During her undergraduate studies in 2009, she started a minor degree in Chemical Reaction Engineering at the same university. In 2012 she graduated from METU with a BSc degree in Chemistry and a minor degree in chemical reaction engineering.

Gamze continued at METU for her MSc degree in inorganic chemistry under the supervision of Prof. Dr. Aysen Yilmaz, studying the surface functionalization of SBA-15 particles for celecoxib delivery. After obtaining her MSc degree in 2013, she started her PhD studies at Leiden University under the supervision of Prof. Dr. E. Bouwman. She supervised a number of BSc and MSc students and was involved in the supervision of a number of organic chemistry practical courses for first-year students. Furthermore, she participated in the Leiden University PhD courses 'Communication in Science', 'On being a Scientist', 'Time Management' and 'Effective Communication'.

Parts of the results reported in this thesis were presented at conferences:

- Advanced Metal-Organic Chemistry and Catalysis summer school, The Netherlands, 2014 (poster)
- Netherlands' Catalysis and Chemistry Conference, The Netherlands, 2014 (poster), 2017 (oral)
- NWO Chains Conference, The Netherlands, 2016 (poster)
- International Coordination Chemistry Conference, France, 2016 (poster)